NASA TECHNICAL MEMORANDUM

NASA TM X-3128

NASA TM X-3128

EXPERIMENTAL AERODYNAMIC CHARACTERISTICS FOR A CYLINDRICAL BODY OF REVOLUTION WITH VARIOUS NOSES AT ANGLES OF ATTACK FROM 0° TO 58° AND MACH NUMBERS FROM 0.6 TO 2.0

Leland H. Jorgensen and Edgar R. Nelson

Ames Research Center

Moffett Field, Calif. 94035

NATIONAL AERONAUTICS AND SPACE ADMINISTRATION • WASHINGTON, D. C. • DECEMBER 1974

1. Report No. NASA TM X-3128	2. Government Accession No.	3. Recipient's Catalog No.
4. Title and Subtitle EXPERIMENTAL AERODYNAMIC CHARACTERISTICS FOR A CYLINDRICAL BODY OF REVOLUTION WITH VARIOUS NOSES AT ANGLES OF ATTACK FROM 0° TO 58° AND MACH NUMBERS FROM 0.6 TO 2.0		5. Report Date December 1974 6. Performing Organization Code
7. Author(s) Leland H. Jorgensen and Edgar R. Nelson		8. Performing Organization Report No. A-5746
9. Performing Organization Name and Address NASA Ames Research Center, Moffett Field, Calif. 94035 and ARO, Inc., Moffett Field, Calif. 94035		10. Work Unit No. 505-06-81 11. Contract or Grant No.
12. Sponsoring Agency Name and Address National Aeronautics and Space Administration Washington, D. C. 20546		13. Type of Report and Period Covered Technical Memorandum 14. Sponsoring Agency Code
15. Supplementary Notes		

16. Abstract

For a body of revolution, an experimental investigation was conducted in the Ames 6- by 6-Foot Wind Tunnel to determine the effect on the aerodynamic characteristics of forebody geometry, a grit ring around the nose, Reynolds number, Mach number, and angle of attack. Aerodynamic force and moment characteristics were measured for a cylindrical body (cylinder fineness ratio of 7) with tangent ogive noses of fineness ratio 2.5, 3.0, 3.5, and 5.0. In addition, the cylindrical body was tested with an ogive nose having a rounded tip and an ogive nose with two different nose strake arrangements.

The various configurations were tested at Mach numbers of 0.6, 0.9, 1.2, 1.5, and 2.0 at angles of attack from 0° to about 58°. The Reynolds numbers, based on base diameter, were 2.2×10^5, 4.3×10^5, and 6.5×10^5 at $M = 0.6$ and 0.9 and 3.8×10^5 at $M = 1.2$, 1.5, and 2.0.

The data demonstrate that the aerodynamic characteristics for a body of revolution can be significantly affected by changes in nose fineness ratio, nose bluntness, Reynolds number, Mach number, and, of course, angle of attack. Nose strakes increased the normal forces but had little effect on the side forces that developed at subsonic Mach numbers for α greater than about 25°. A grit ring around the nose had little or no effect on the aerodynamic characteristics.

17. Key Words (Suggested by Author(s)) High angle-of-attack aerodynamics Body of revolution Nose fineness ratio	18. Distribution Statement Unclassified – Unlimited Cat. 01

19. Security Classif. (of this report)	20. Security Classif. (of this page)	21. No. of Pages	22. Price*
Unclassified	Unclassified	91	$4.75

*For sale by the National Technical Information Service, Springfield, Virginia 22151

NOMENCLATURE

All forces and moments are referred to the body axis coordinate system. Because the data are computer plotted, both the conventional symbol and the plot symbol are given.

Symbol	Plot Symbol	Definition
A_r		reference area = body base area = 34.26 cm^2 (5.31 in.^{2})
C_A	CA	axial-force coefficient = $C_{A_{bal}} - C_{A_{base}}$
$C_{A_{bal}}$		balance axial-force coefficient, $\frac{F_A}{qA_r}$
$C_{A_{base}}$		base-pressure force coefficient, $\frac{(p - p_{base})}{q}$
C_m		pitching-moment coefficient about balance center 4d from body base, $\frac{\text{pitching moment}}{qA_rX}$
C_{m_R}		resultant moment coefficient, $C_m \cos \phi + C_n \sin \phi$
C_N	CN	normal-force coefficient, $\frac{F_N}{qA_r}$
C_n	CYN	yawing-moment coefficient about balance center 4d from body base, $\frac{\text{yawing moment}}{qA_rX}$
C_R		resultant force coefficient, $(C_N^2 + C_Y^2)^{1/2}$
C_Y	CY	side-force coefficient, $\frac{F_Y}{qA_r}$
d		body base diameter = reference length = 6.60 cm (2.60 in.)
F_A, F_N, F_Y		axial, normal, and side force, respectively
ℓ_N		nose length
M	MACH	free-stream Mach number
p		free-stream static pressure
p_{base}		base pressure

q		free-stream dynamic pressure
$\frac{Re}{L}$		unit Reynolds number, million/m
Re	RE	Reynolds number based on d
X		reference length = d = 6.60 cm (2.60 in.)
$\frac{x_{ac_N}}{d}$	XACN/D	distance (in diameters) from body base to aerodynamic force center in normal-force plane, $\left(\frac{C_m}{C_N} + \frac{x_m}{X}\right)$
$\frac{x_{ac_Y}}{d}$		distance (in diameters) from body base to aerodynamic force center in side-force plane, $\left(\frac{C_n}{C_Y} + \frac{x_m}{X}\right)$
$\frac{x_{ac_R}}{d}$	XACR/D	distance (in diameters) from body base to resultant aerodynamic force center, $\left(\frac{C_{m_R}}{C_R} + \frac{x_m}{X}\right)$
x_m		distance from body base to balance moment reference = $4d$ = 26.42 cm (10.40 in.)
α	ALPHA	angle of attack, deg
ϕ	PHI	angle between normal force and resultant force (clockwise rotation is positive when looking along the axis from the body base to the nose), deg

Configuration Code

Symbol	Plot Symbol	Component	Fineness Ratio
C_1	C1	circular cylinder	7
N_1	N1	tangent ogive nose	3
N_2	N2	tangent ogive nose	3.5
N_3	N3	tangent ogive nose	5
N_4	N4	tangent ogive nose with rounded tip	3

N_5	N5	tangent ogive nose with tip strakes	3
N_6	N6	tangent ogive nose with side strakes	3
N_7	N7	tangent ogive nose	2.5
G	G	transition strip around nose (0.249-cm-diam glass spheres, 0.159 cm wide, and 3.81 cm aft of nose apex)	

EXPERIMENTAL AERODYNAMIC CHARACTERISTICS FOR A CYLINDRICAL BODY OF REVOLUTION WITH VARIOUS NOSES AT ANGLES OF ATTACK FROM 0° TO 58° AND MACH NUMBERS FROM 0.6 TO 2.0

Leland H. Jorgensen and Edgar R. Nelson*

Ames Research Center

SUMMARY

For a body of revolution, an experimental investigation was conducted in the Ames 6- by 6-Foot Wind Tunnel to determine the effect on the aerodynamic characteristics of forebody geometry, a grit ring around the nose, Reynolds number, Mach number, and angle of attack. Aerodynamic force and moment characteristics were measured for a cylindrical body (cylinder fineness ratio of 7) with tangent ogive noses of fineness ratio 2.5, 3.0, 3.5, and 5.0. In addition, the cylindrical body was tested with an ogive nose having a rounded tip and an ogive nose with two different nose strake arrangements.

The various configurations were tested at Mach numbers of 0.6, 0.9, 1.2, 1.5, and 2.0 at angles of attack from 0° to about 58°. The Reynolds numbers, based on base diameter, were 2.2×10^5, 4.3×10^5, and 6.5×10^5 at $M = 0.6$ and 0.9 and 3.8×10^5 at $M = 1.2$, 1.5, and 2.0.

The data demonstrate that the aerodynamic characteristics for a body of revolution can be significantly affected by changes in nose fineness ratio, nose bluntness, Reynolds number, Mach number, and, of course, angle of attack. Nose strakes increased the normal forces but had little effect on the side forces that developed at subsonic Mach numbers for α greater than about 25°. A grit ring around the nose had little or no effect on the aerodynamic characteristics.

INTRODUCTION

The importance of high angle-of-attack aerodynamics is increasing because of the demand for greater maneuverability of missiles and military aircraft (both manned and remotely piloted). Some recent introductory investigations in this field are reported in references 1 to 8. However, there is great need to enlarge the relatively small data base for basic bodies alone and in combination with strakes, wings, and tails at subsonic, transonic, and supersonic Mach numbers.

To help enlarge the data base for basic bodies alone, an investigation was conducted to measure the aerodynamic force and moment characteristics for a cylindrical body of revolution (cylinder fineness ratio of 7) with tangent ogive noses of fineness ratio 2.5 to 5.0. In addition, the

---

*Project Engineer, ARO, Inc., Moffett Field, Calif. 94035.

cylindrical body was tested with an ogive nose having a rounded tip and an ogive nose with two different strake arrangements.

In this investigation, the cylindrical body was tested with the various noses in the Ames 6- by 6-Foot Wind Tunnel at Mach numbers of 0.6, 0.9, 1.2, 1.5, and 2.0. The Reynolds numbers, based on model base diameter, were 2.2×10^5, 4.3×10^5, and 6.5×10^5 at the subsonic Mach numbers and 3.8×10^5 at the supersonic Mach numbers. Six-component static aerodynamic force and moment coefficients were measured for angles of attack from 0° to 58°.

This report presents the basic data that show the effects on the aerodynamic characteristics of nose fineness ratio, nose tip rounding, nose strakes, Reynolds number, and Mach number over the angle-of-attack range.

TEST FACILITY

The experimental investigation was conducted in the Ames 6- by 6-Foot Wind Tunnel, a variable pressure, continuous flow, closed return type facility. The nozzle ahead of the test section consists of an asymmetric sliding block that permits a continuous variation of Mach number from 0.6 to 2.3. The test section has a perforated floor and ceiling to remove boundary layer for transonic testing.

MODELS AND BALANCE

The model components are shown in figure 1(a) and the configurations tested in figure 1(b). All test models had a combination of one of seven noses with a circular-cylinder aftersection. The cylinder (C_1), 7 diameters long, was attached to the desired nose (N_1 through N_7). Noses N_1, N_2, N_3, and N_7 were all circular-arc tangent ogives ranging in length from 2.5 to 5 diameters. Noses N_4, N_5, and N_6 were also circular-arc tangent ogives but with some modifications. N_4 was formed by rounding the tip of a fineness-ratio 3.5 ogive to give a resulting fineness ratio of 3. N_5 was a fineness-ratio 3 ogive with side strakes near the tip, and N_6 was a similar ogive but with side strakes extending over the entire nose length. In figure 1(b), planform views of all configurations tested are identified by the code used throughout this report.

All model parts were constructed of stainless steel, and all models were sting mounted through the base on a six-component, strain-gage "Task" balance. The balance force center was located inside the cylindrical body 4 diameters forward of the base.

TESTS AND DATA REDUCTION

All configuration arrangements shown in figure 1(b) were tested at angles of attack from 0° to 58° on the two model-support setups shown in figure 2. One setup (fig. 2(a)) was used to test the models for $\alpha = 0°$ to about 27°, and the other (fig. 2(b)) was used for $\alpha = 27°$ to 58°.

The models were tested at the following Mach numbers and Reynolds numbers:

M	$Re \times 10^{-6}$ (m)	$Re \times 10^{-6}$ (ft)	$Re \times 10^{-5}$ (based on d)
0.6, 0.9	3.28	1.0	2.2
0.6, 0.9	6.56	2.0	4.3
0.6, 0.9	9.84	3.0	6.5
1.2, 1.5, 2.0	5.74	1.75	3.8

Several runs were made with a boundary-layer transition strip around the noses of bodies N_1C_1 and N_3C_1. This strip consisted of 0.249-cm-diam glass spheres, 0.159 cm wide and located 3.81 cm aft of the nose apex.

Six-component aerodynamic force and moment data were measured at each test condition, and all data were reduced to coefficient form and referred to the body axis coordinate system. The average base pressure from four base pressure tubes (at the sides, top, and bottom of the base) was used to compute the base drag, which was subtracted from the total axial-force balance measurements so that the data presented are for forces ahead of the body base. Rolling-moment coefficients were generally negligible and are omitted. Normal-force aerodynamic centers were computed from the normal-force and pitching-moment coefficients and are presented in lieu of the pitching-moment coefficients.

RESULTS AND DISCUSSION

Experimental results (figs. 3 through 27) show the effects of nose fineness ratio, nose tip rounding, nose strakes, grit ring around the nose, Reynolds number, and Mach number. Each one of these effects is discussed briefly with the aid of plots of C_N, x_{ac_N}/d, C_Y, C_Y/C_N, and C_n versus α for $\alpha = 0°$ to $60°$. Plots of C_A versus α are also presented but are not discussed. Because the models were sting supported from the rear, the C_A data probably include some effects of support interference.

Effect of Nose Fineness Ratio

Data that show the effect of nose fineness ratio on the aerodynamic characteristics are presented in figures 3 through 7 for $M = 0.6$ to 2.0. The data are for the highest test Reynolds numbers, $Re = 6.5 \times 10^5$ at $M = 0.6$ and 0.9 (figs. 3 and 4) and $Re = 3.8 \times 10^5$ at $M = 1.2$, 1.5, and 2.0 (figs. 5, 6, and 7).

An increase in nose fineness ratio from 2.5 to 5.0 can cause significant changes in the aerodynamic characteristics. As expected, the normal-force coefficient generally increases with an increase in nose fineness ratio at all Mach numbers, and the aerodynamic force center in the normal-force plane moves forward. There are, however, some angles of attack where the changes are negligible, especially at subsonic Mach numbers.

Probably the most interesting result is the effect of nose fineness ratio on the development of side force and yawing moment with increase in angle of attack above about 25°. As shown in figures 3 and 4 for the subsonic Mach numbers of 0.6 and 0.9, the side-force and yawing-moment coefficients become rather large for the body cylinder with noses whose fineness ratios are 3.5 and 5.0 (configurations N_2C_1 and N_3C_1). In fact, for some angles of attack, the side forces become as large as 30 or 40 percent of the normal forces (see plots of C_Y/C_N vs. α). When the nose fineness ratio is 3.0 or less (configurations N_1C_1 and N_7C_1), the side-force and yawing-moment coefficients became essentially zero throughout the α range.

This side-force phenomenon appears to be associated primarily with subsonic flow; the side-force and yawing-moment coefficients greatly diminish at supersonic Mach numbers. They are small at $M = 1.2$ (fig. 5) and completely disappear at $M = 1.5$ (fig. 6) and $M = 2.0$ (fig. 7).

Based on the results from this investigation and from other sources (e.g., refs. 1, 2, 7, and 8), two conclusions become evident. First, the magnitudes of the maximum side-force and yawing-moment coefficients generally increase with an increase in the nose fineness ratio. Second, the magnitudes appear to decrease with an increase in Mach number.

When large side forces and yawing moments develop, the position on the body of the resultant aerodynamic force center can shift significantly. The angle ϕ between the normal force and resultant force can increase, and the resultant force center can move along the longitudinal axis away from the usual normal force center. In figures 8 and 9, the aerodynamic centers are given for the cylinder with fineness ratio 3 and 5 noses (N_1C_1 and N_3C_1) at $M = 0.6$ and 0.9. For the configuration with the fineness ratio 5 nose (N_3C_1), the resultant force is moved around the body about 17° ($\phi = -17°$) from the normal force at $\alpha = 40°$ and $M = 0.6$ (see fig. 8). With an increase in Mach number to $M = 0.9$, the displacement angle was less ($\phi = -12°$ as shown in fig. 9). Also, at $\alpha = 40°$, the aerodynamic center for the resultant force, x_{ac_R}/d, is moved forward of that for the normal force, x_{ac_N}/d (compare values of x_{ac_R}/d and x_{ac_N}/d in figs. 8 and 9).

Effect of Nose Tip Rounding

In figures 10 through 14, data are presented for the body cylinder (C_1) with the fineness ratio 3.5 ogive nose (N_2) and with the fineness ratio 3.5 ogive nose whose tip was cut back by rounding to give a fineness ratio of 3 (N_4). Also shown for comparison are data for the cylinder (C_1) combined with the fineness ratio 3 sharp ogive nose (N_1).

Generally, the nose tip rounding has little effect on the variation of C_N, x_{ac_N}/d, and C_A with α. However, the tip rounding appears to significantly decrease the side-force and yawing-moment coefficients that appear at $M = 0.6$ and 0.9 for α greater than about 25° (compare results for N_2C_1 and N_4C_1 in figs. 10 and 11). Even though rounding off the tip of the fineness ratio 3.5 nose to give a fineness ratio of 3 appears to be beneficial in reducing side force and yawing moment, the beneficial effect is no greater than that obtained from merely using the fineness ratio 3 sharp ogive nose (compare results for N_4C_1 and N_1C_1 in figs. 10 and 11).

Effect of Nose Strakes

In figures 15 through 19, data are presented which show the effect of nose strakes on the aerodynamic characteristics. Data are compared for the cylinder (C_1) combined with the fineness ratio 3 ogive nose (N_1) and the cylinder combined with fineness ratio 3 noses having side strakes (N_5 and N_6).

As expected, the nose strakes provide additional normal force and move the aerodynamic force centers forward. The configuration with the tip strake, N_5C_1, develops some undesirable side force at $M = 0.6$, but generally the side forces and yawing moments are very small or zero for the other configurations (N_1C_1 and N_6C_1) which are compared with N_5C_1.

Effect of Grit Ring Around Nose

In figures 20 through 22, data are presented which show the effect of a ring of grit around the noses of configurations N_1C_1 and N_3C_1 at $M = 0.6$, 0.9, and 1.2. This ring consisted of 0.25-cm-diam glass spheres, 0.16 cm wide, and located 3.8 cm aft of the nose tip.

The effect of the grit ring was generally small for all conditions investigated. At $M = 0.6$, the variation of C_Y (CY) and C_n (CYN) with α was changed with the grit ring in place, but the maximum magnitudes of the side-force and yawing-moment coefficients were about the same (see fig. 20).

Effect of Reynolds Number

In figures 23 through 26, data are presented which show the effect of Reynolds number for configurations N_1C_1 and N_3C_1 at $M = 0.6$ and 0.9. The Reynolds numbers are 2.2×10^5, 4.3×10^5, and 6.5×10^5 based on body base diameter.

For both body configurations, there is a significant effect of Reynolds number on the variation of C_N and x_{ac_N}/d with α at $M = 0.6$. Generally, C_N decreases with increasing Re (see figs. 23 and 25). The effect at $M = 0.9$, however, is much smaller (see figs. 24 and 25). At first observation, it might be surprising that there would be this effect at $M = 0.6$ but not so much at $M = 0.9$ for such a small range of Reynolds numbers. The explanation probably can be made on the basis of crossflow theory (e.g., ref. 4). The theory tells us that, for crossflow Mach numbers ($M \sin\alpha$) less than critical (about 0.4), a change in crossflow Reynolds number ($Re \sin\alpha$) from about 2×10^5 to 5×10^5 can cause a significant decrease in crossflow drag coefficient and hence normal force. In the present investigation, for $M = 0.6$ the crossflow Mach numbers were subcritical over most of the α range, and the crossflow Reynolds numbers ranged from subcritical (less than about 2×10^5 throughout all of the α range for $Re = 2.2\times10^5$) to supercritical (greater than about 2×10^5 throughout most of the α range for $Re = 6.5\times10^5$). For this situation, crossflow theory would predict a decrease in C_N at high α with increase in Reynolds numbers from 2.2×10^5 to 6.5×10^5. Crossflow theory, however, would predict little or no effect at $M = 0.9$, since the crossflow Mach number would be supercritical for α greater than about 30°.

The effect of Reynolds number on side-force and yawing-moment coefficients appears to be signficant only for the body with the high fineness ratio nose (N_3C_1) at $M = 0.6$ (fig. 25). At present there is no explanation for this effect.

Effect of Mach Number

In figure 27, data are presented which show the effect of Mach number on the aerodynamic characteristics for configuration N_3C_1 (the fineness ratio 5 ogive nose attached to the cylinder). For the data at $M = 0.6$ and 0.9, the Reynolds number is 6.5×10^5, and for the data at $M = 1.2$, 1.5, and 2.0, the Reynolds number is 3.8×10^5.

At the higher angles of attack, the values of C_N increase with M from $M = 0.6$ to 1.2 or 1.5; then there is possibly a little decrease with further increase in M. This trend is generally in accord with that which would be predicted from crossflow theory (ref. 4) for bodies of revolution.

The side-force and yawing-moment plots clearly demonstrate that the side-force phenomenon at α greater than about 25° is essentially associated with subsonic Mach numbers. The results show that the maximum side-force coefficient was measured at about $\alpha = 40°$, and it was as large as about 30 percent of the normal-force coefficient at $M = 0.6$.

CONCLUSIONS

1. An increase in nose fineness ratio caused significant changes in the aerodynamic characteristics. Normal-force coefficient generally increased, and the aerodynamic normal-force center moved forward. For noses with fineness ratios greater than 3, large side-force and yawing-moment coefficients developed at subsonic Mach numbers for angles of attack above about 25°.

2. The large side-force and yawing-moment coefficients that developed at subsonic Mach numbers greatly decreased and disappeared with increase in Mach number into the supersonic flow regime.

3. Nose-tip rounding significantly decreased the side-force and yawing moment coefficients for a body with a sharp-nosed ogive of fineness ratio 3.5. However, the beneficial decrease was no greater than that obtained by merely using a sharp-nosed ogive nose of the same fineness ratio (fineness ratio 3) as that for the resulting blunted nose.

4. Nose strakes provided some additional normal force and moved the aerodynamic force centers forward, but they had little effect on the side forces and yawing moments for the body with the fineness ratio 3 nose. Unfortunately, they were not investigated on the body with the fineness ratio 5 nose, the nose that developed the largest side forces.

5. A grit ring around the fineness ratio 5 nose failed to diminish the undesirable side forces and yawing moments associated with this configuration.

6. The normal-force, aerodynamic-center, and side-force characteristics were all significantly affected by change in Reynolds number at $M = 0.6$. The effect of Reynolds number, however, decreased with increase in Mach number to $M = 0.9$.

Ames Research Center
National Aeronautics and Space Administration
Moffett Field, Calif. 94035, September 20, 1974

REFERENCES

1. Pick, George S.: Side Force on Ogive-Cylinder Bodies at High Angles of Attack in Transonic Flow. Journal of Spacecraft and Rockets, vol. 9, no. 6, June 1972, pp. 389–390.

2. Clark, William H.; Peoples, John R.; and Briggs, M. Michael: Occurrence and Inhibition of Large Yawing Moments During High Incidence Flight of Slender Missile Configurations. AIAA Second Atmospheric Flight Mechanics Conference, Palo Alto, Calif., Sept. 11–13, 1972 (AIAA Paper 72-968).

3. Coe, Paul L., Jr.: Chambers, Joseph R.; and Letko, William: Asymmetric Lateral-Directional Characteristics of Pointed Bodies of Revolution at High Angles of Attack. NASA TN D-7095, 1972.

4. Jorgensen, Leland H.: Prediction of Static Aerodynamic Characteristics for Space-Shuttle-Like and Other Bodies at Angles of Attack from 0° to 180°. NASA TN D-6996, 1973.

5. Jorgensen, Leland H.: Estimation of Aerodynamics for Slender Bodies Alone and With Lifting Surfaces at α's from 0° to 90°. AIAA Journal, vol. 11, no. 3, March 1973, pp. 409–412.

6. Jorgensen, Leland H.: A Method for Estimating Static Aerodynamic Characteristics for Slender Bodies of Circular and Noncircular Cross Section Alone and With Lifting Surfaces at Angles of Attack from 0° to 90°. NASA TN D-7228, 1973.

7. Fleeman, E. L.; and Nelson, R. C.: Aerodynamic Forces and Moments on a Slender Body with a Jet Plume for Angles of Attack up to 180 Degrees. AIAA 12th Aerospace Sciences Meeting, Wash., D.C., Jan. 30– Feb. 1, 1974 (AIAA Paper 74-110).

8. Keener, Earl R.; and Chapman, Gary T.: Onset of Aerodynamic Side Forces at Zero Sideslip on Symmetric Forebodies at High Angles of Attack. AIAA Mechanics and Control of Flight Conference, Anaheim, Calif., Aug. 5–7, 1974 (AIAA Paper 74-770).

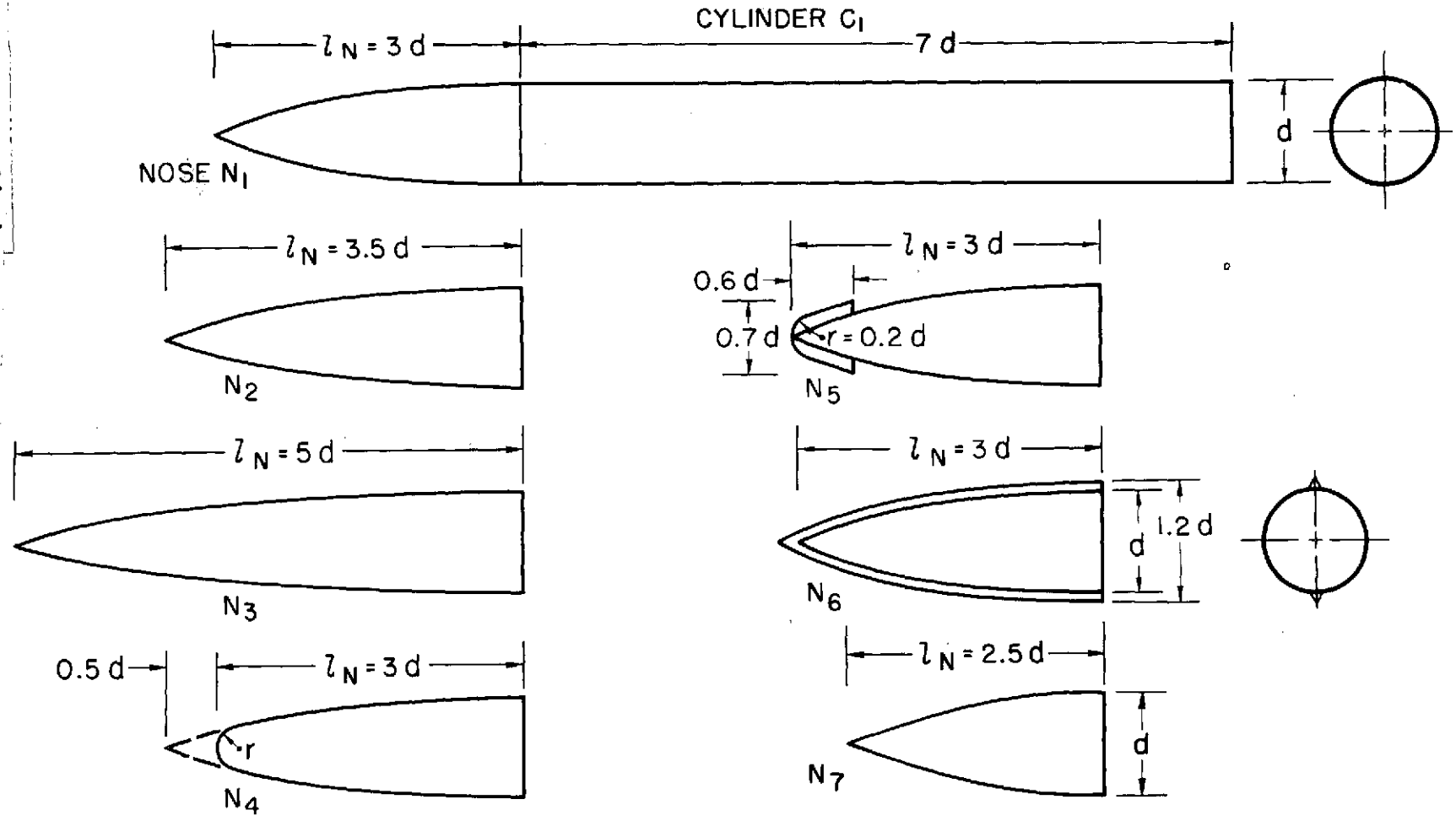

(a) Model components with $d = 6.6$ cm (2.6 in.).

Figure 1.– Model components and planform views of configurations tested.

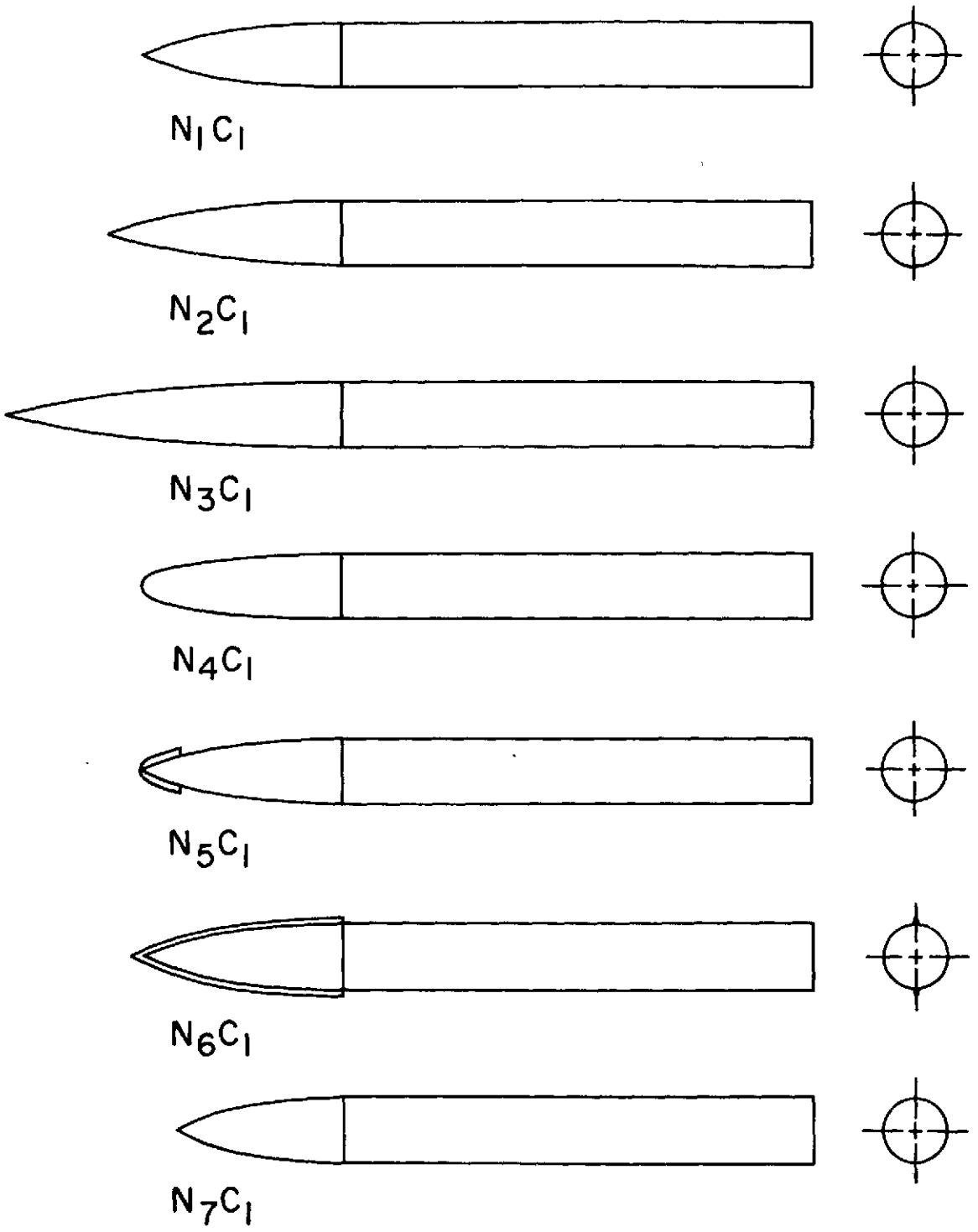

(b) Planform views of configurations tested.

Figure 1.– Concluded.

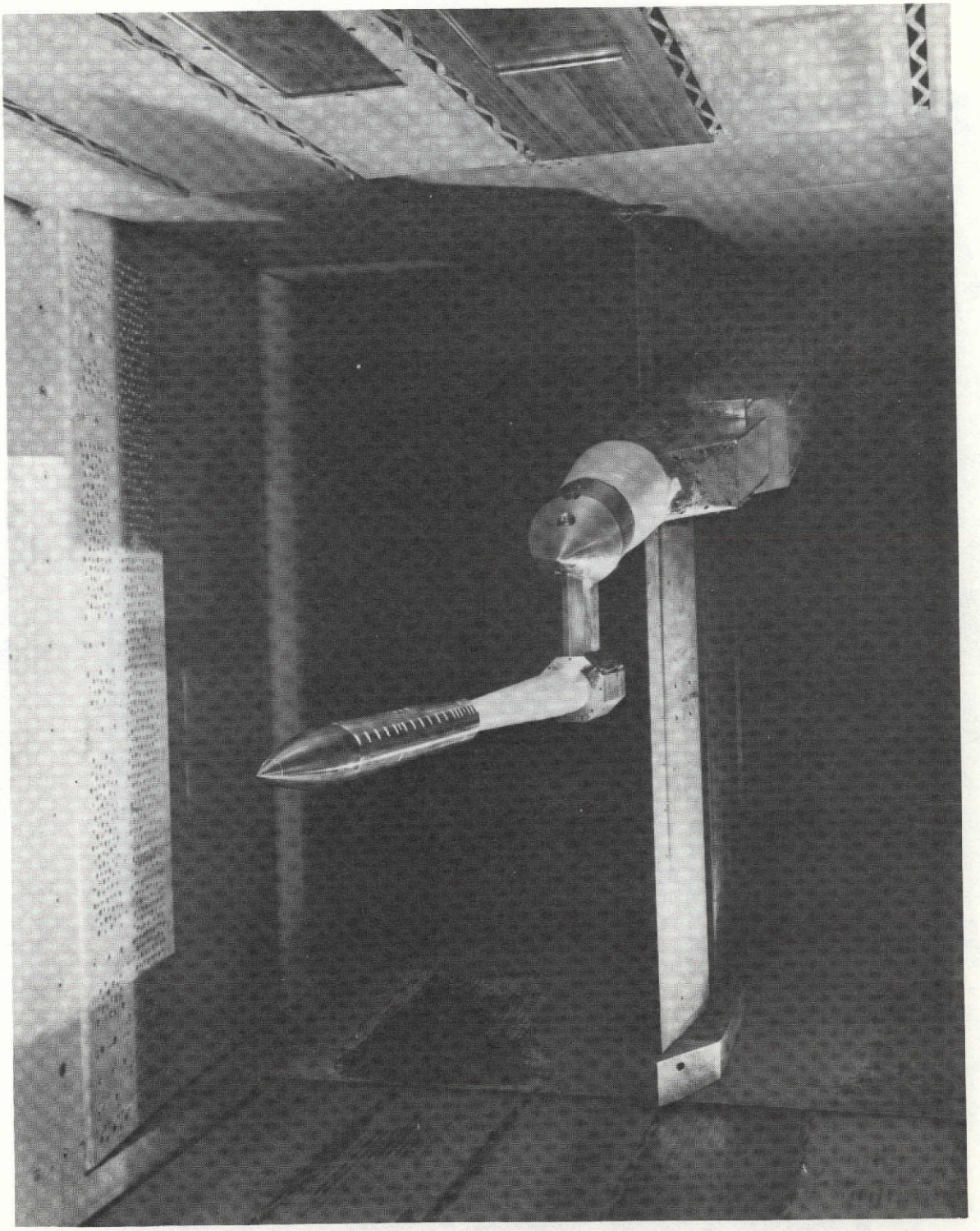

(a) Test model ($N_1 C_1$ with grit nose ring) on support setup for $\alpha = 0°$ to about 27°.

Figure 2.– Typical model-support setups in the Ames 6- by 6-Foot Wind Tunnel.

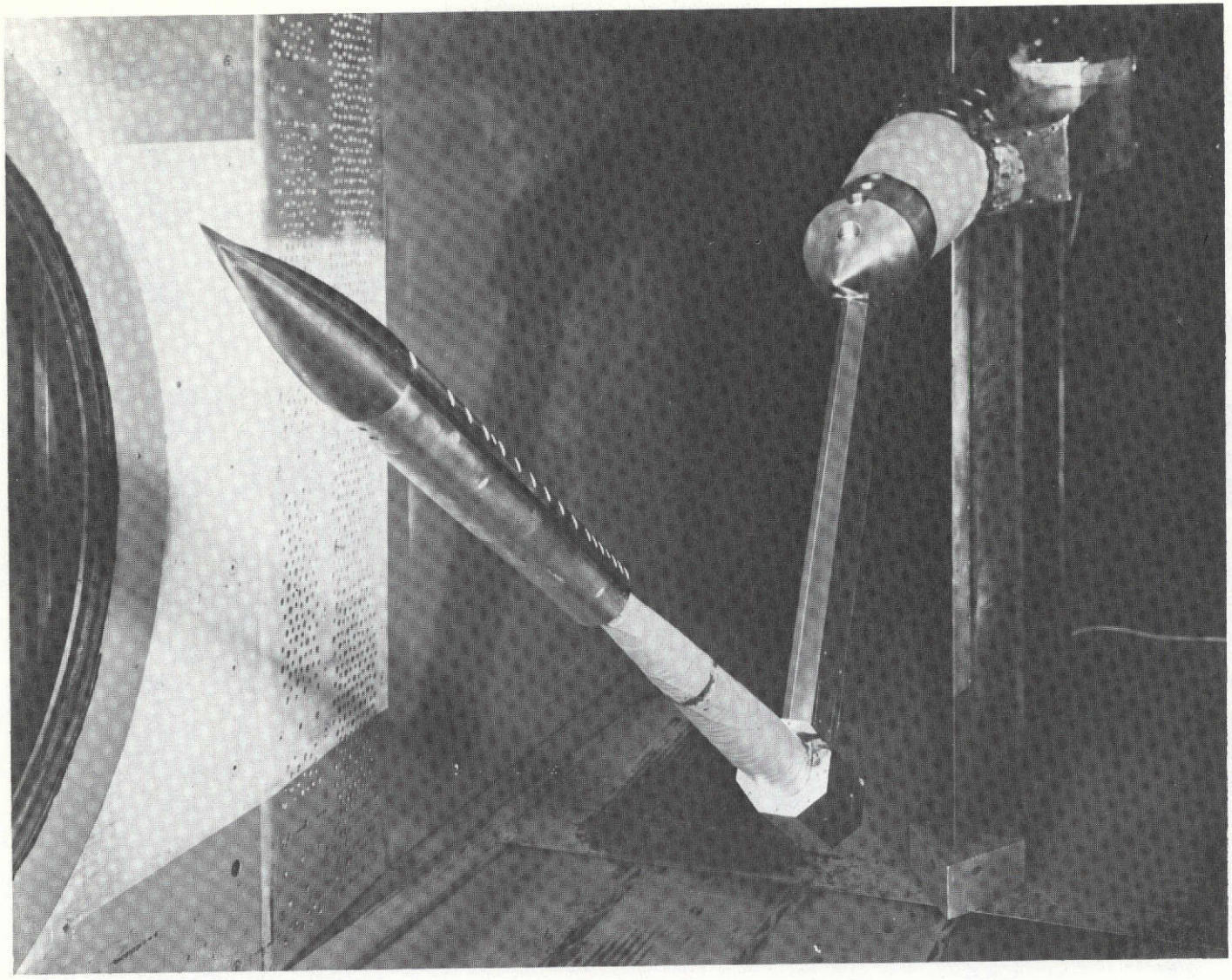

(b) Test model (N_6C_1) on support setup for $\alpha = 27°$ to $58°$.

Figure 2.– Continued.

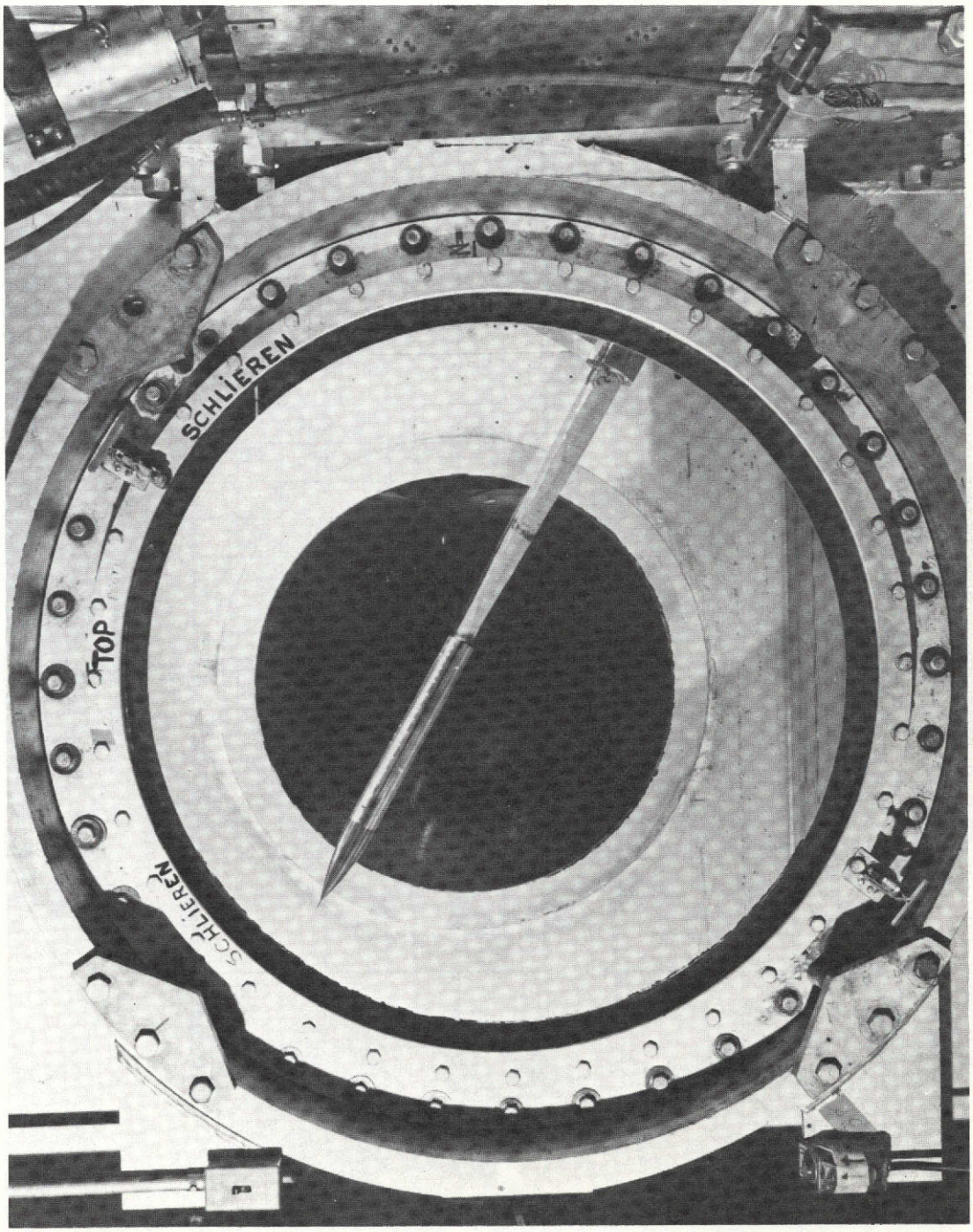

(c) Side view of test model (N_6C_1) viewed through tunnel window.

Figure 2.– Concluded.

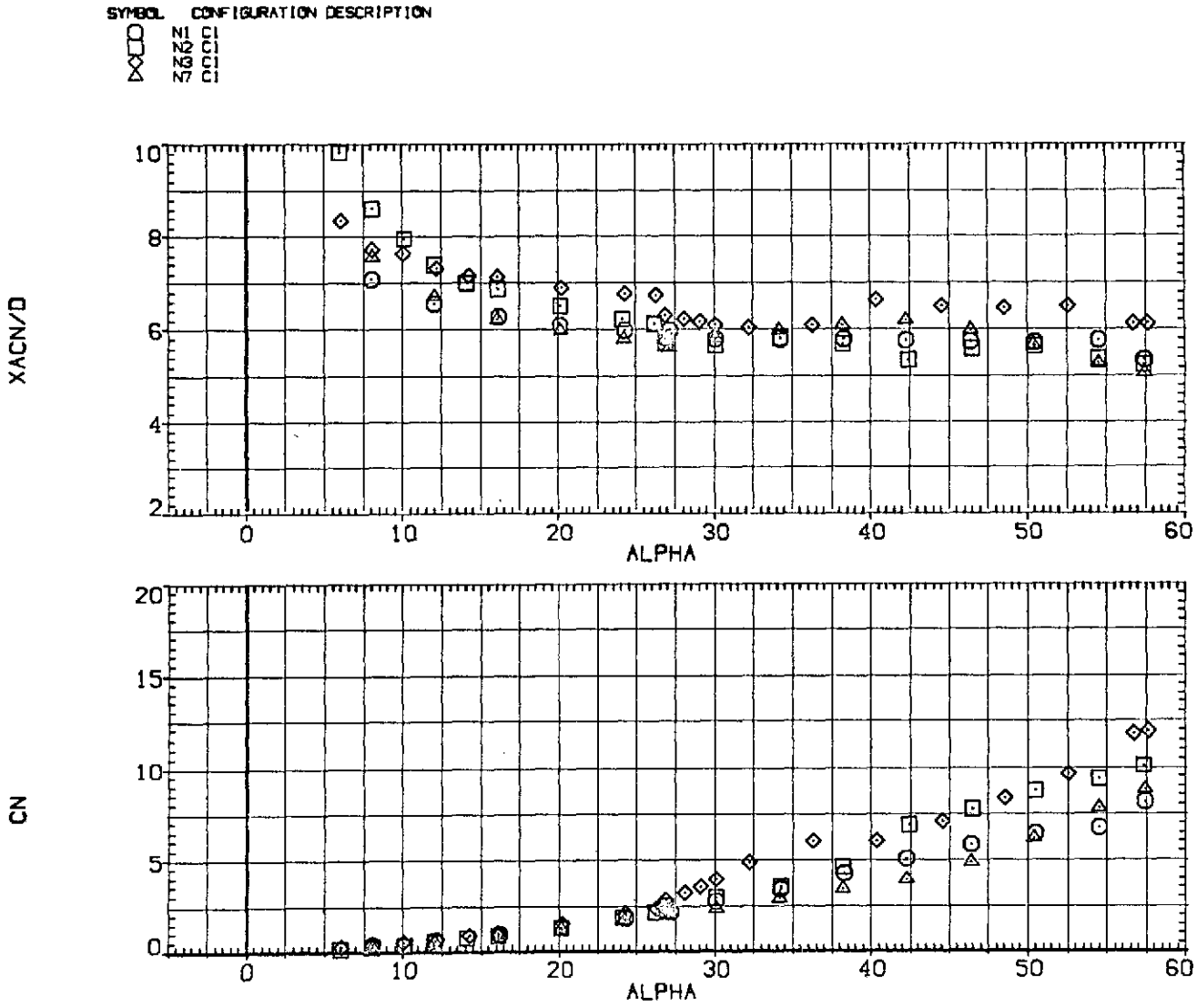

(a) x_{ac_N}/d and C_N versus α.

Figure 3.– Effect of nose fineness ratio; $M = 0.6$, $Re = 6.5 \times 10^5$.

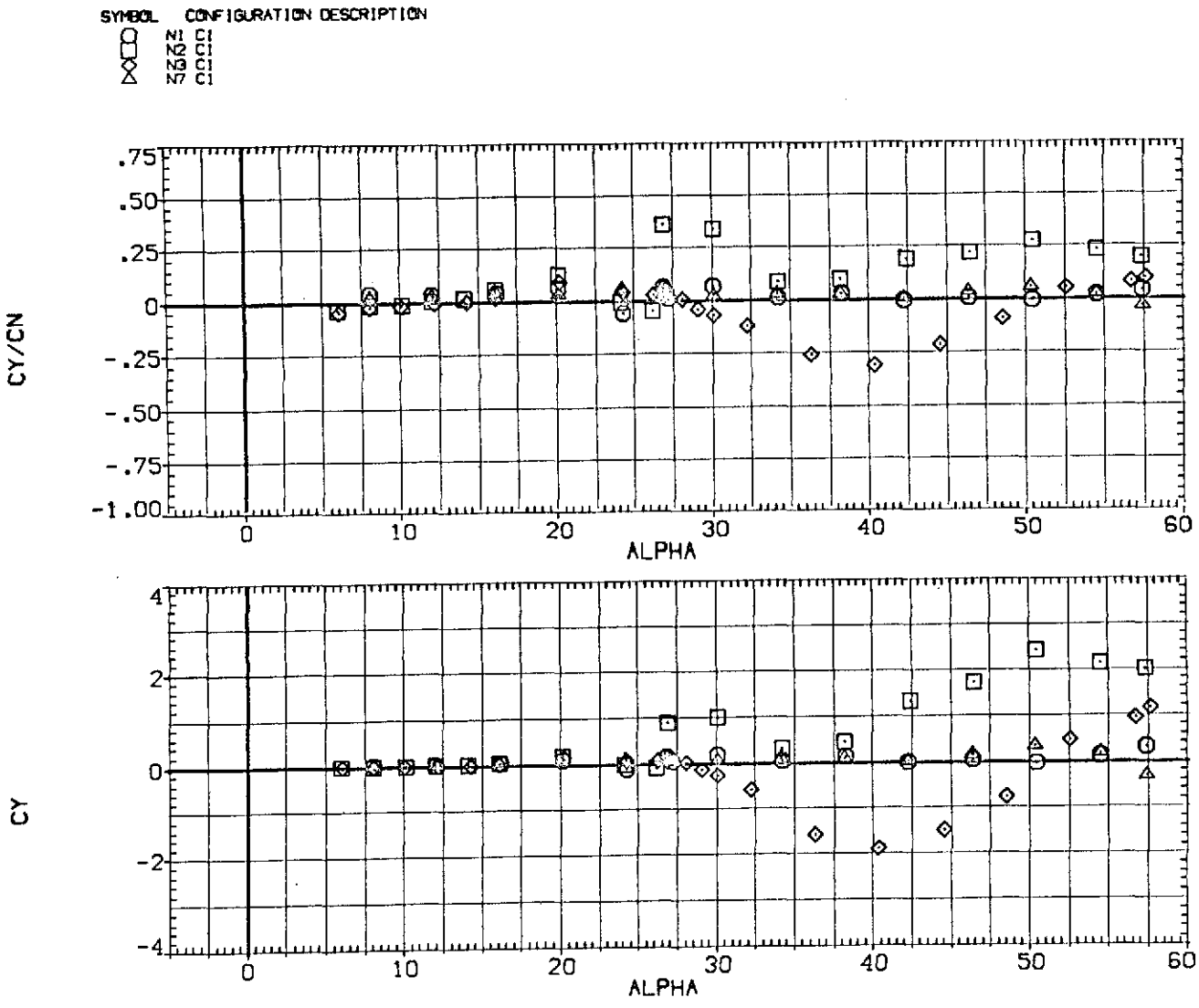

(b) C_Y/C_N and C_Y versus α.

Figure 3.– Continued.

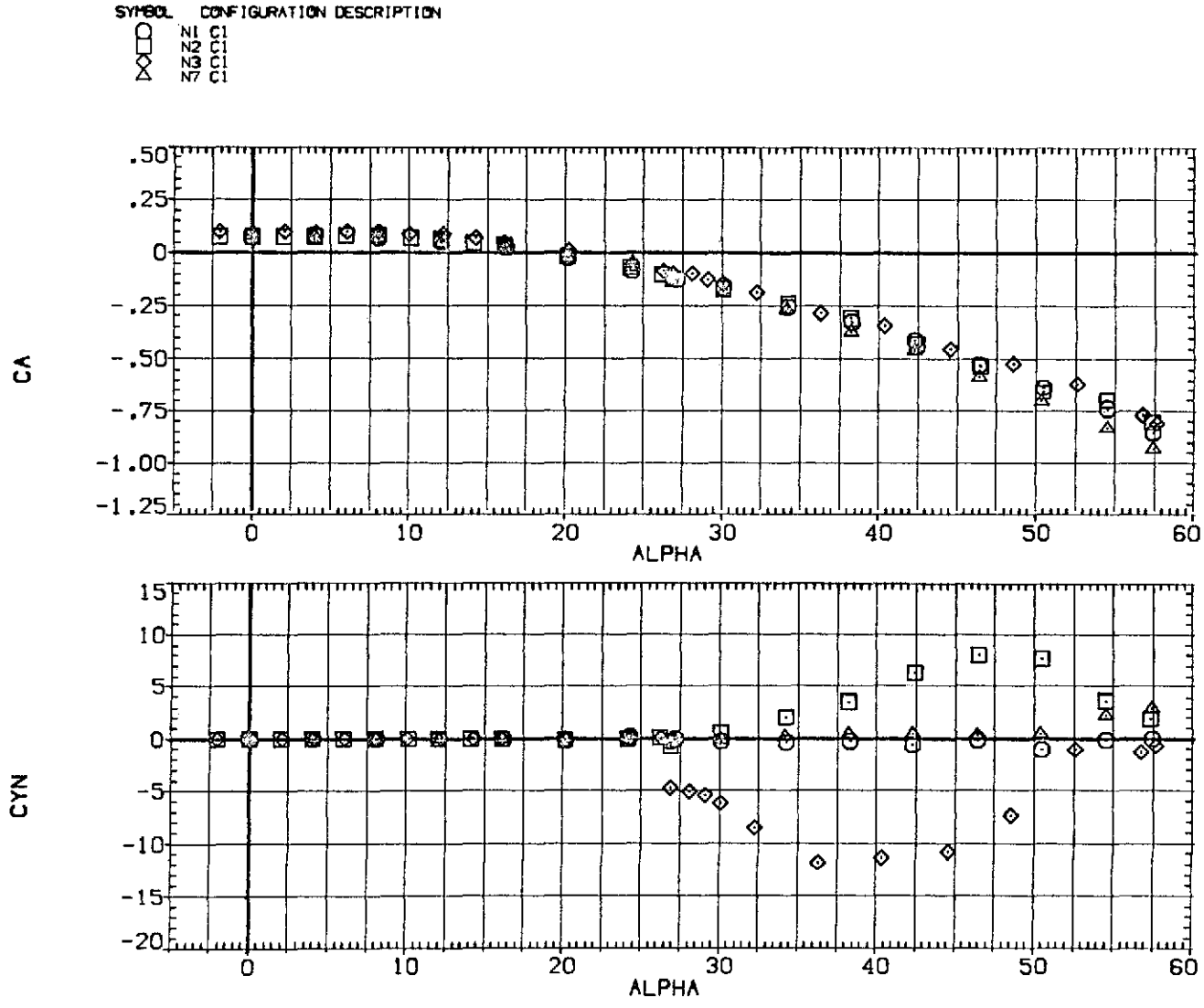

(c) C_A and C_n versus α.

Figure 3.– Concluded.

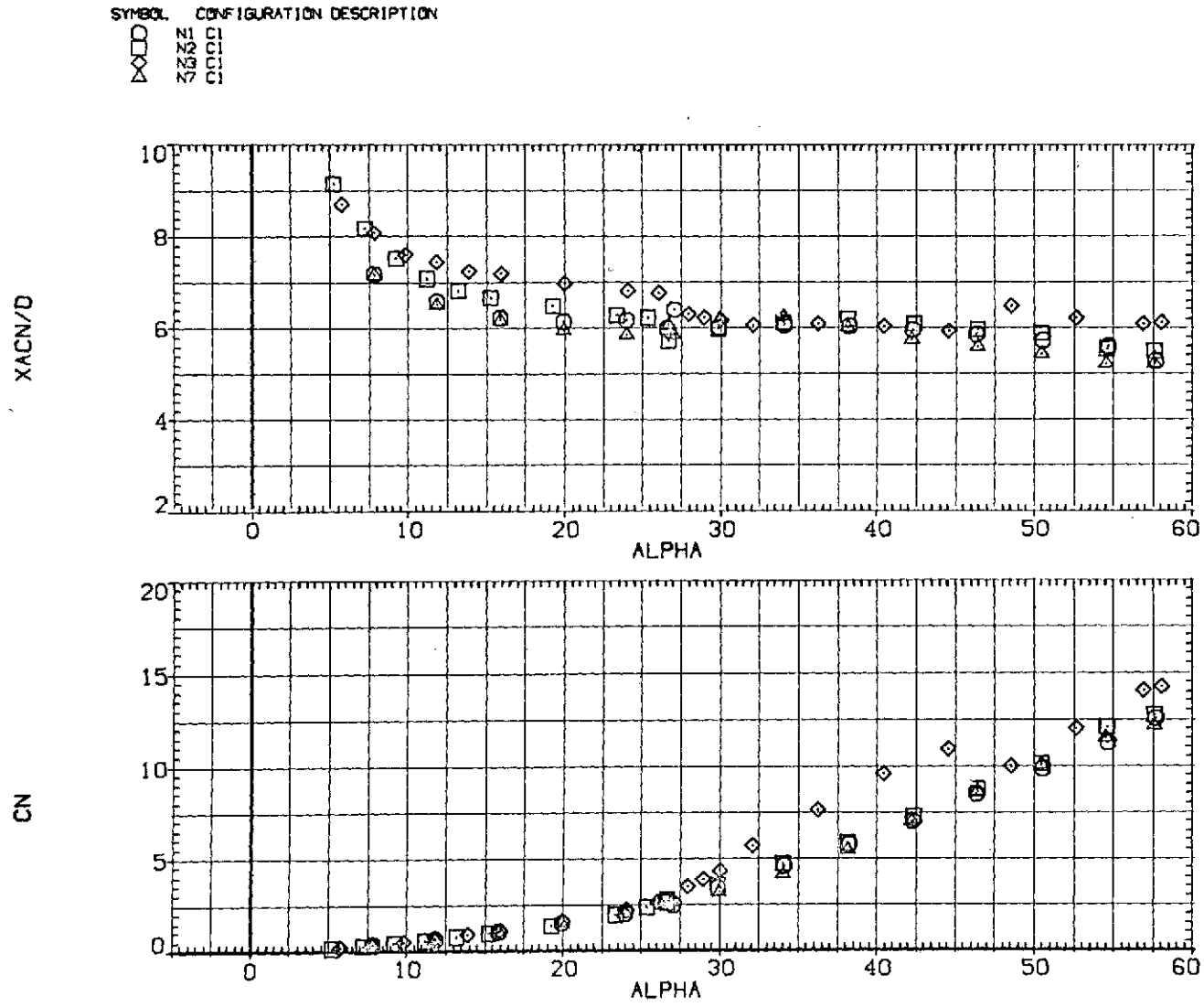

(a) x_{ac_N}/d and C_N versus α.

Figure 4.-- Effect of nose fineness ratio; $M = 0.9$, $Re = 6.5 \times 10^5$.

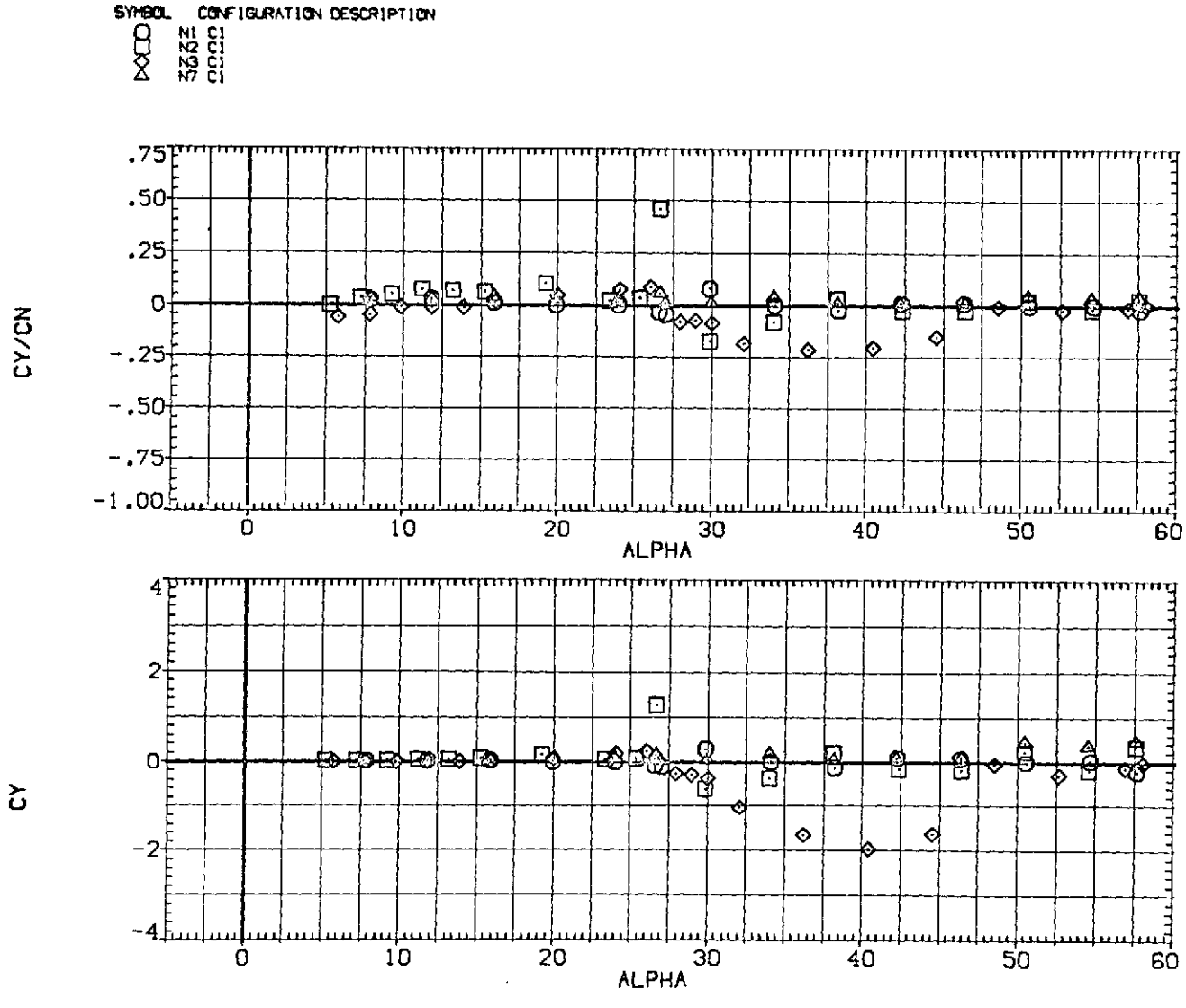

(b) C_Y/C_N and C_Y versus α.

Figure 4.– Continued.

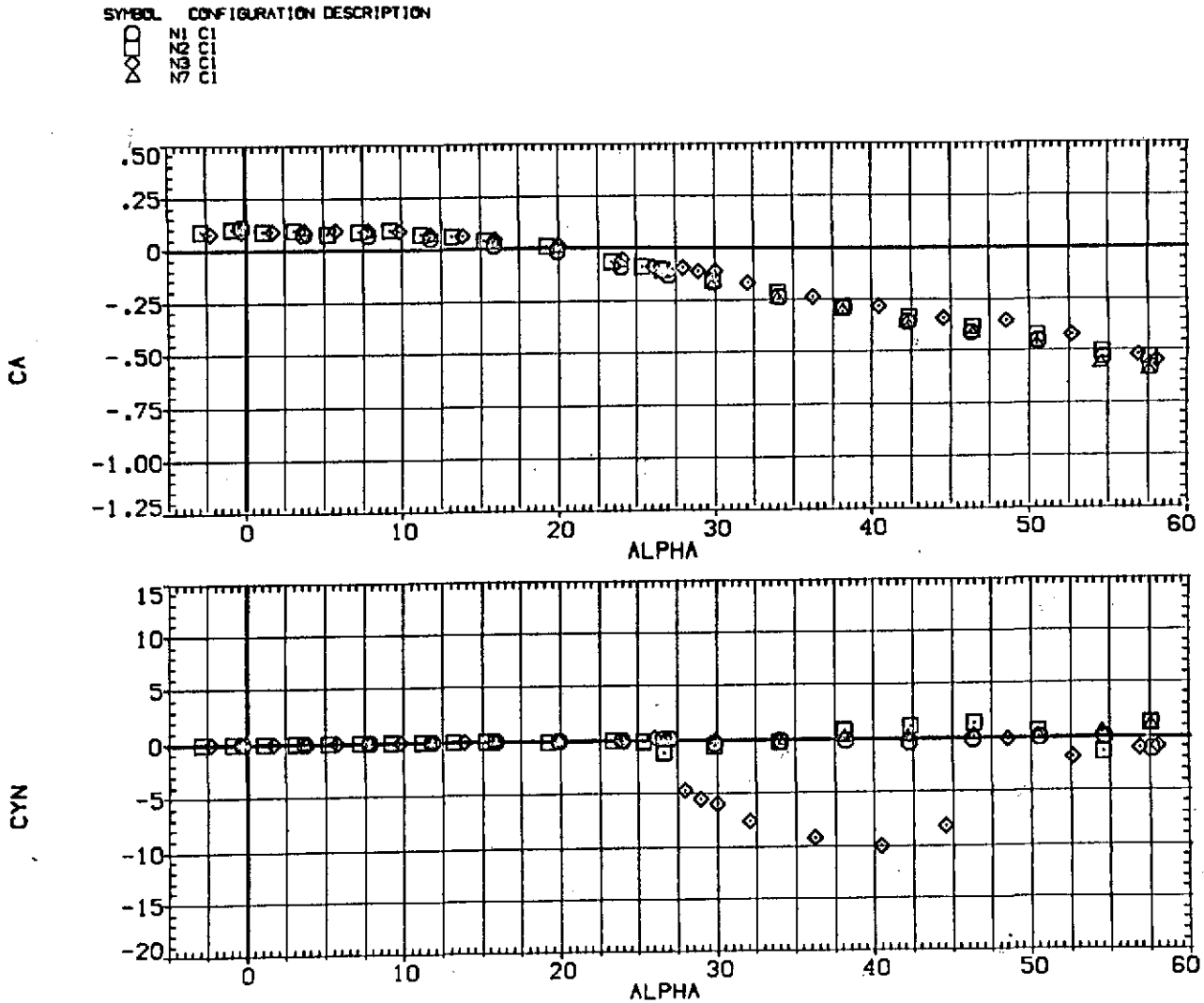

(c) C_A and C_n versus α.

Figure 4.-- Concluded.

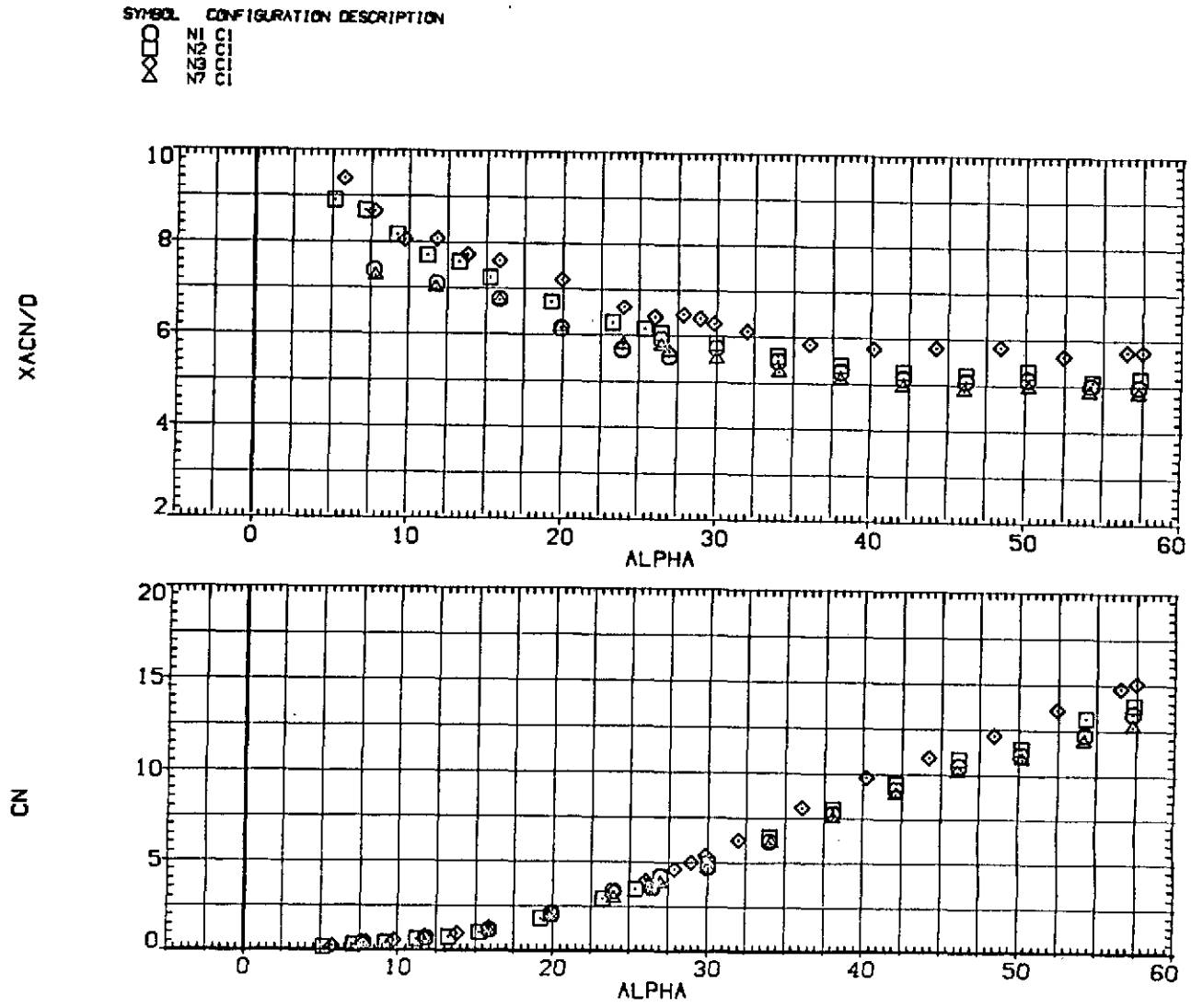

(a) x_{ac_N}/d and C_N versus α.

Figure 5.– Effect of nose fineness ratio; $M = 1.2$, $Re = 3.8 \times 10^5$.

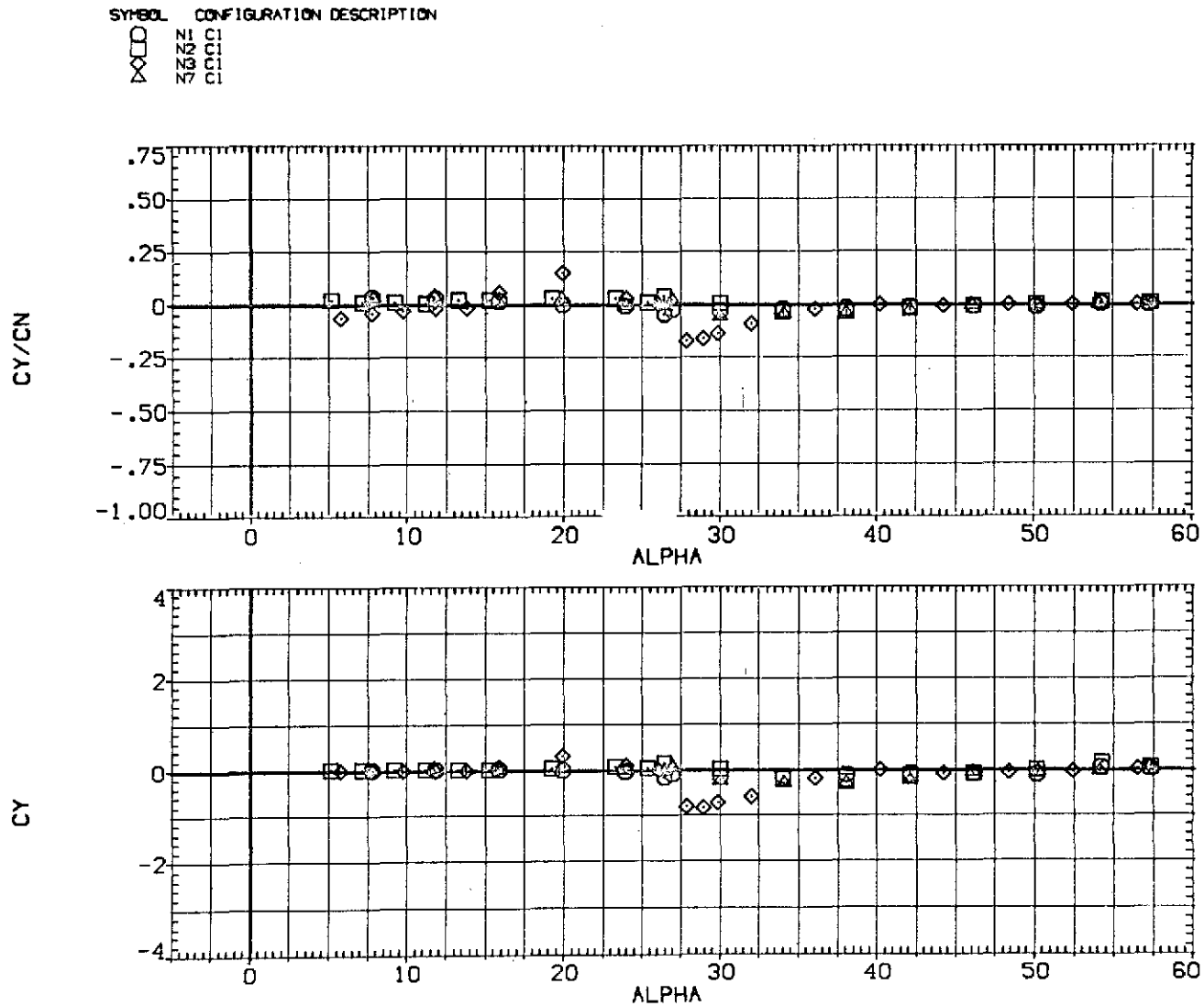

(b) C_Y/C_N and C_Y versus α.

Figure 5.– Continued.

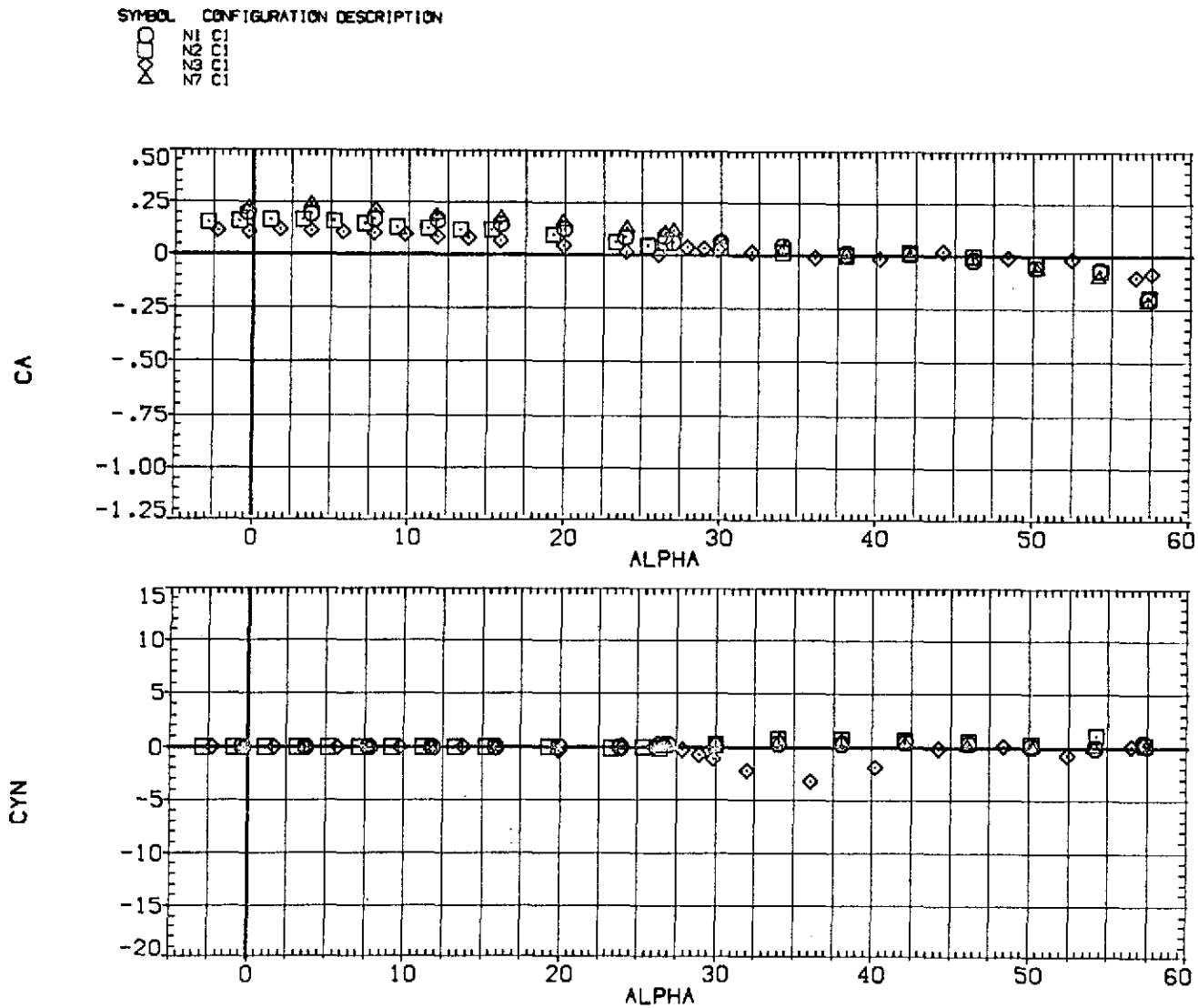

(c) C_A and C_n versus α.

Figure 5.– Concluded.

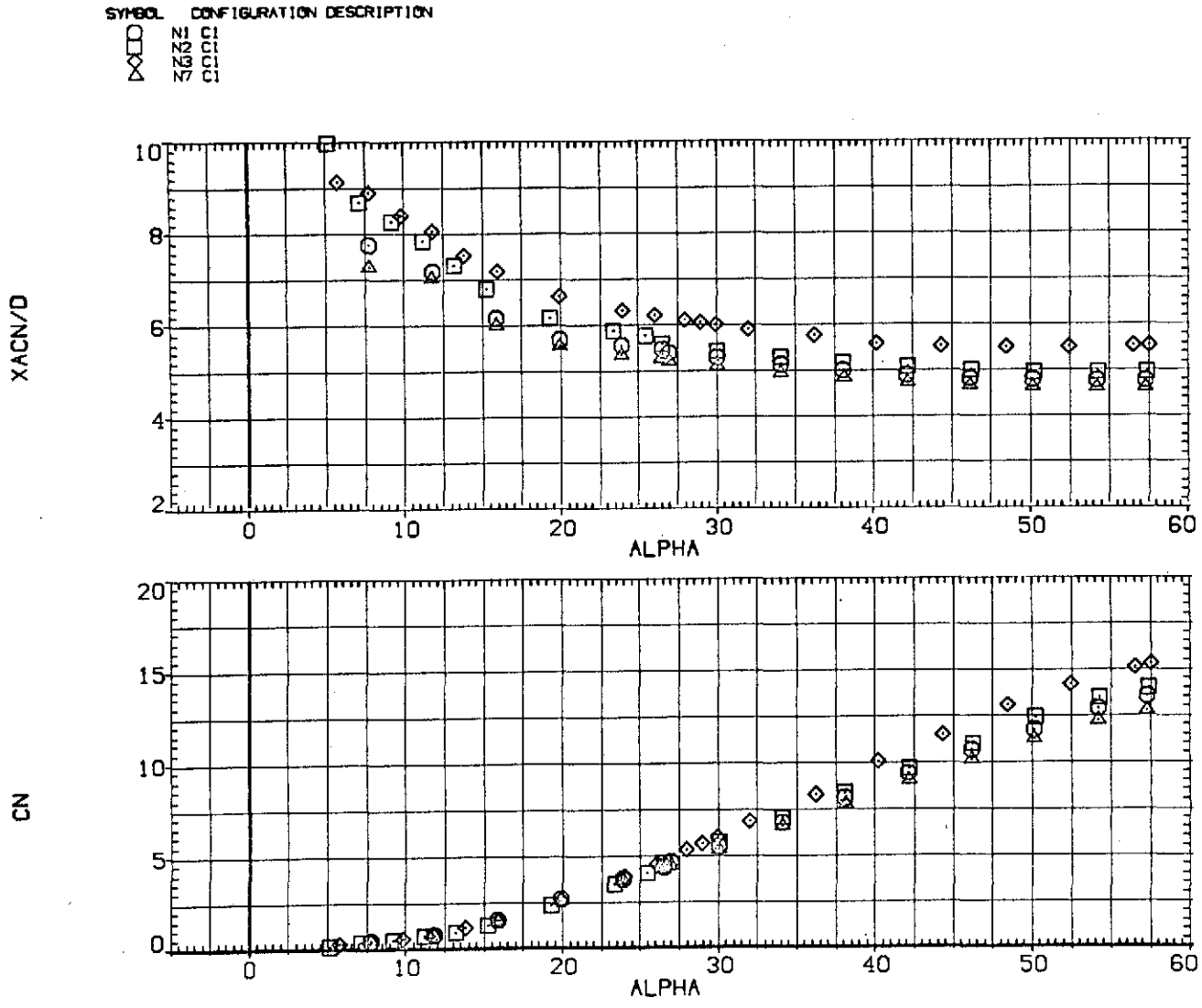

(a) x_{ac_N}/d and C_N versus α.

Figure 6.– Effect of nose fineness ratio; $M = 1.5$, $Re = 3.8 \times 10^5$.

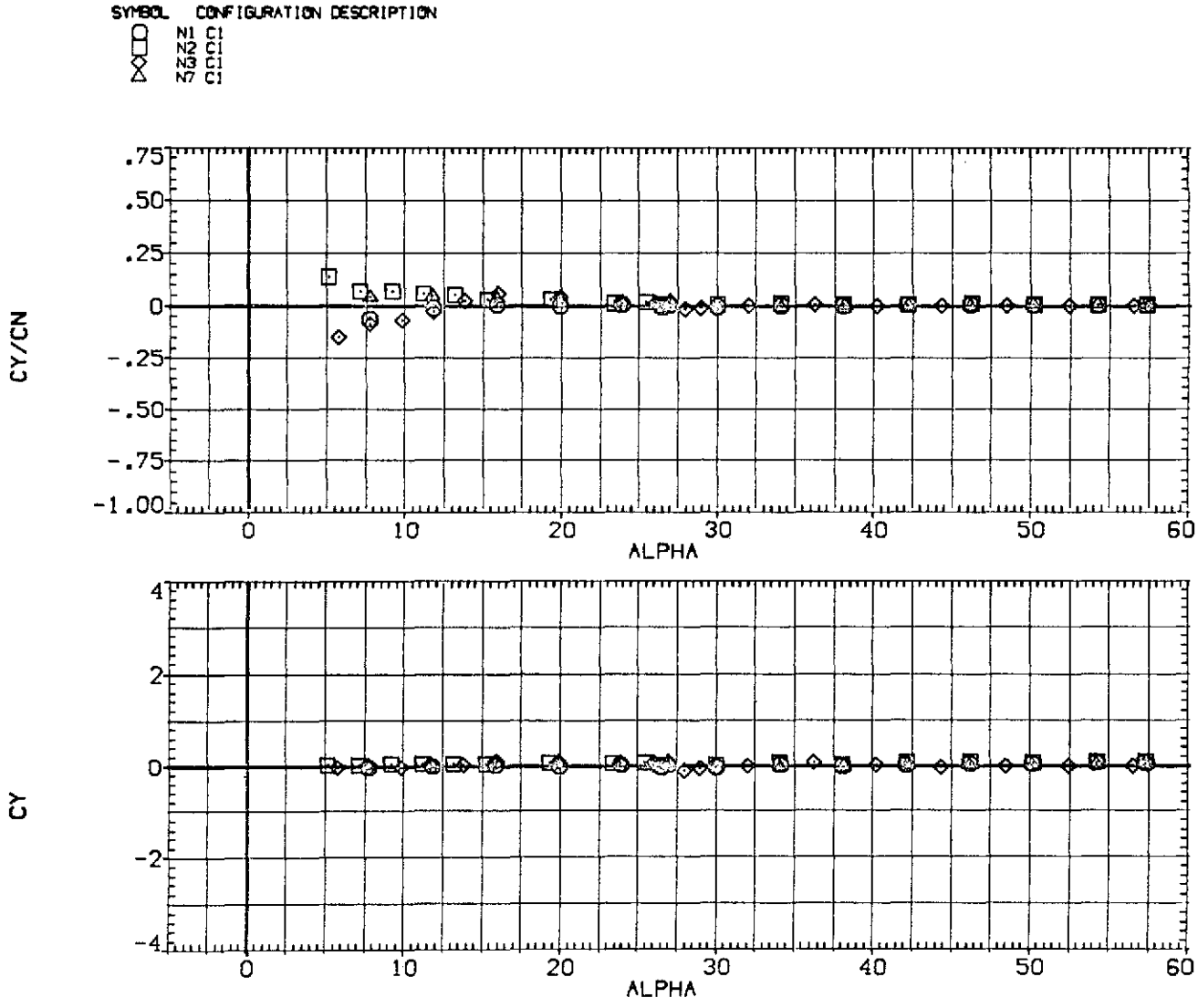

(b) C_Y/C_N and C_Y versus α.

Figure 6.– Continued.

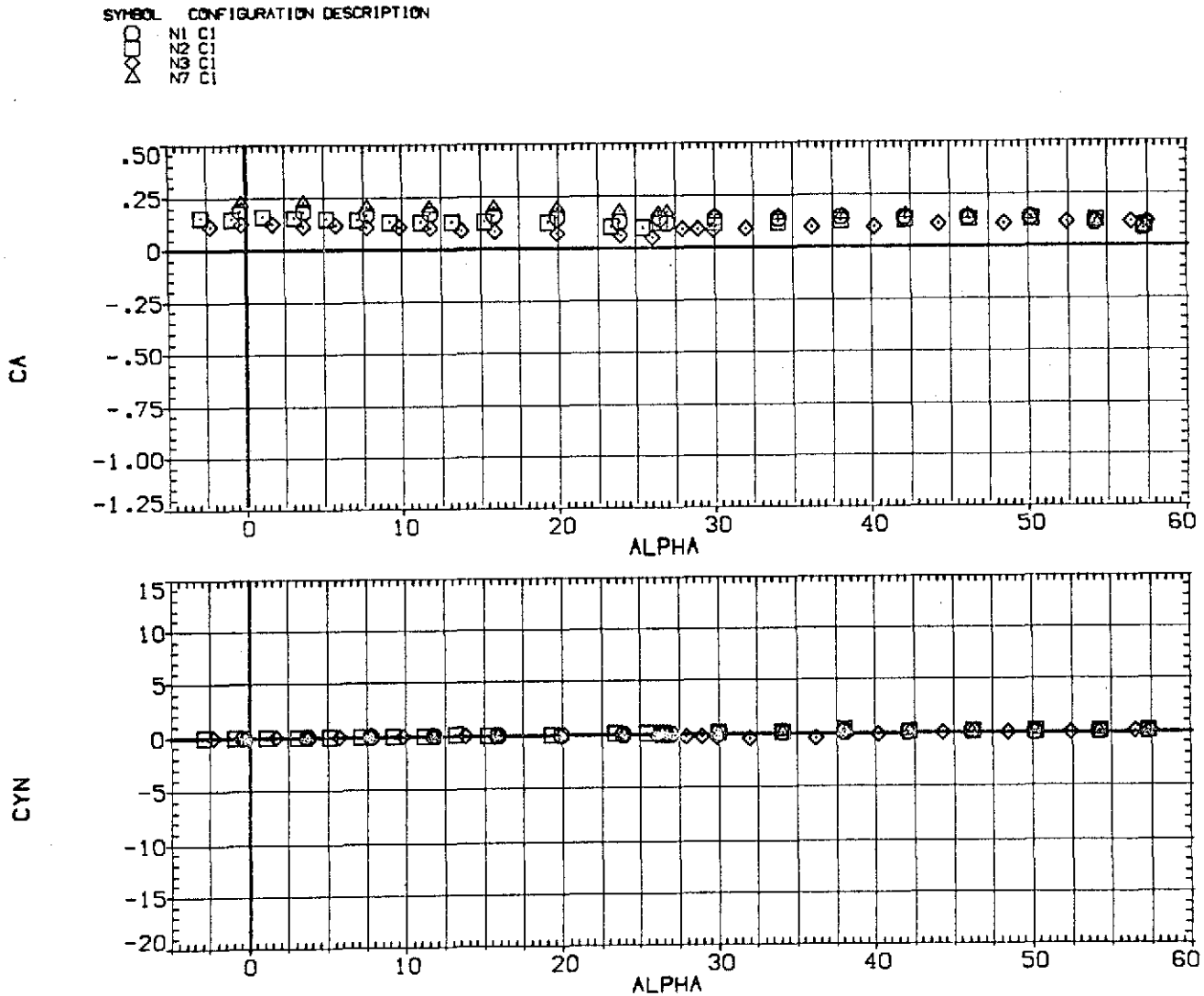

(c) C_A and C_n versus α.

Figure 6.– Concluded.

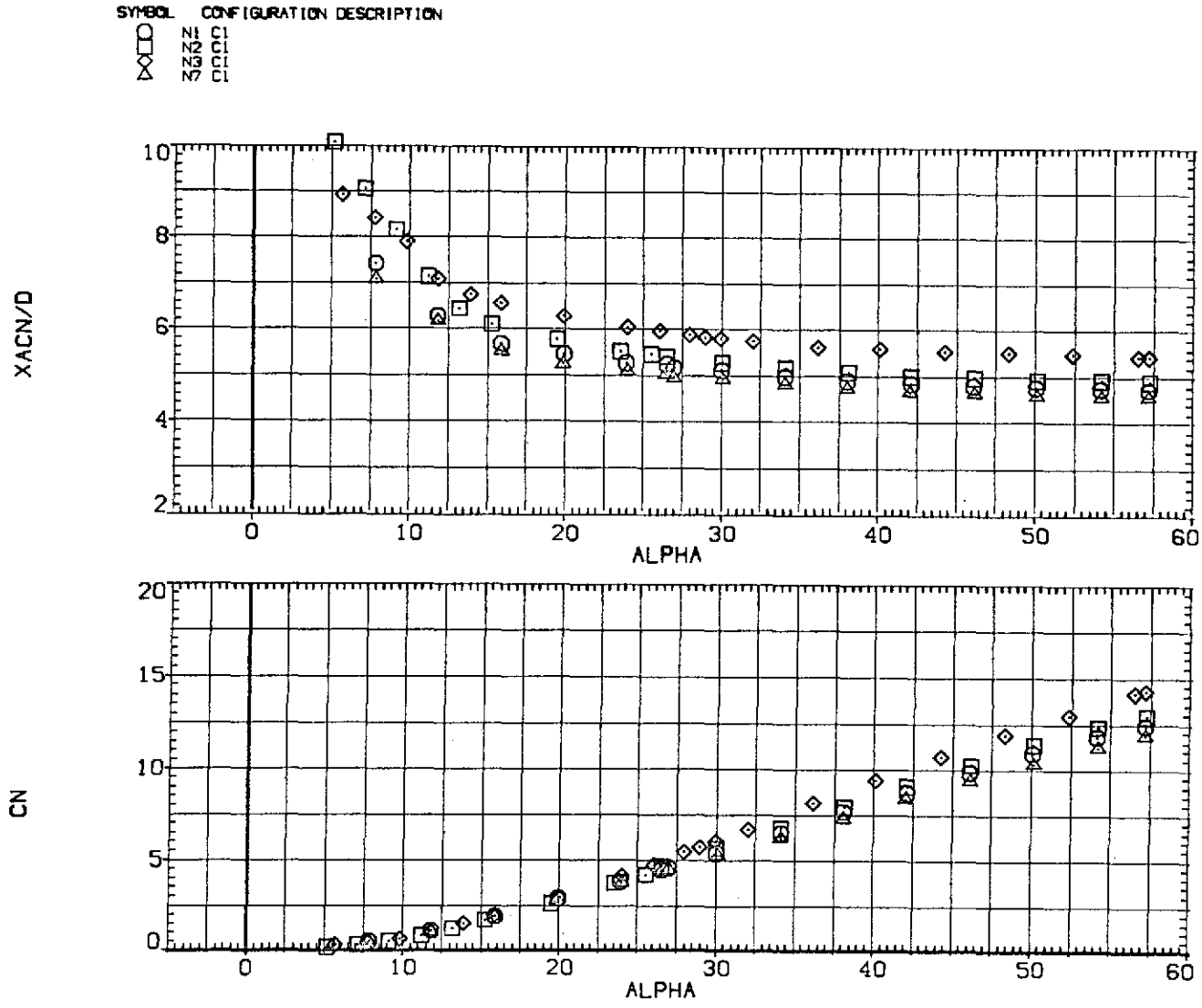

(a) x_{ac_N}/d and C_N versus α.

Figure 7.– Effect of nose fineness ratio; $M = 2.0$, $Re = 3.8 \times 10^5$.

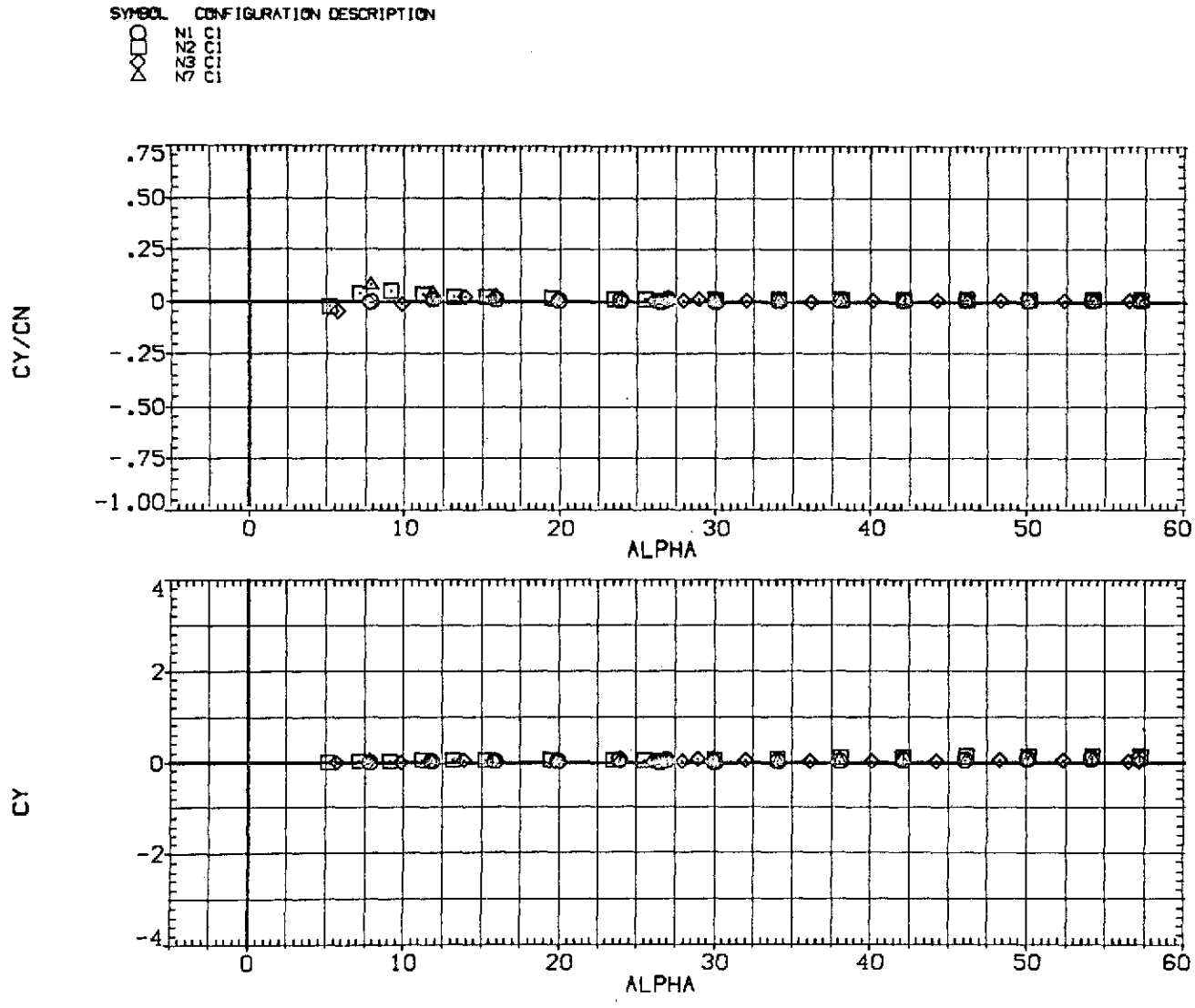

(b) C_Y/C_N and C_Y versus α.

Figure 7.– Continued.

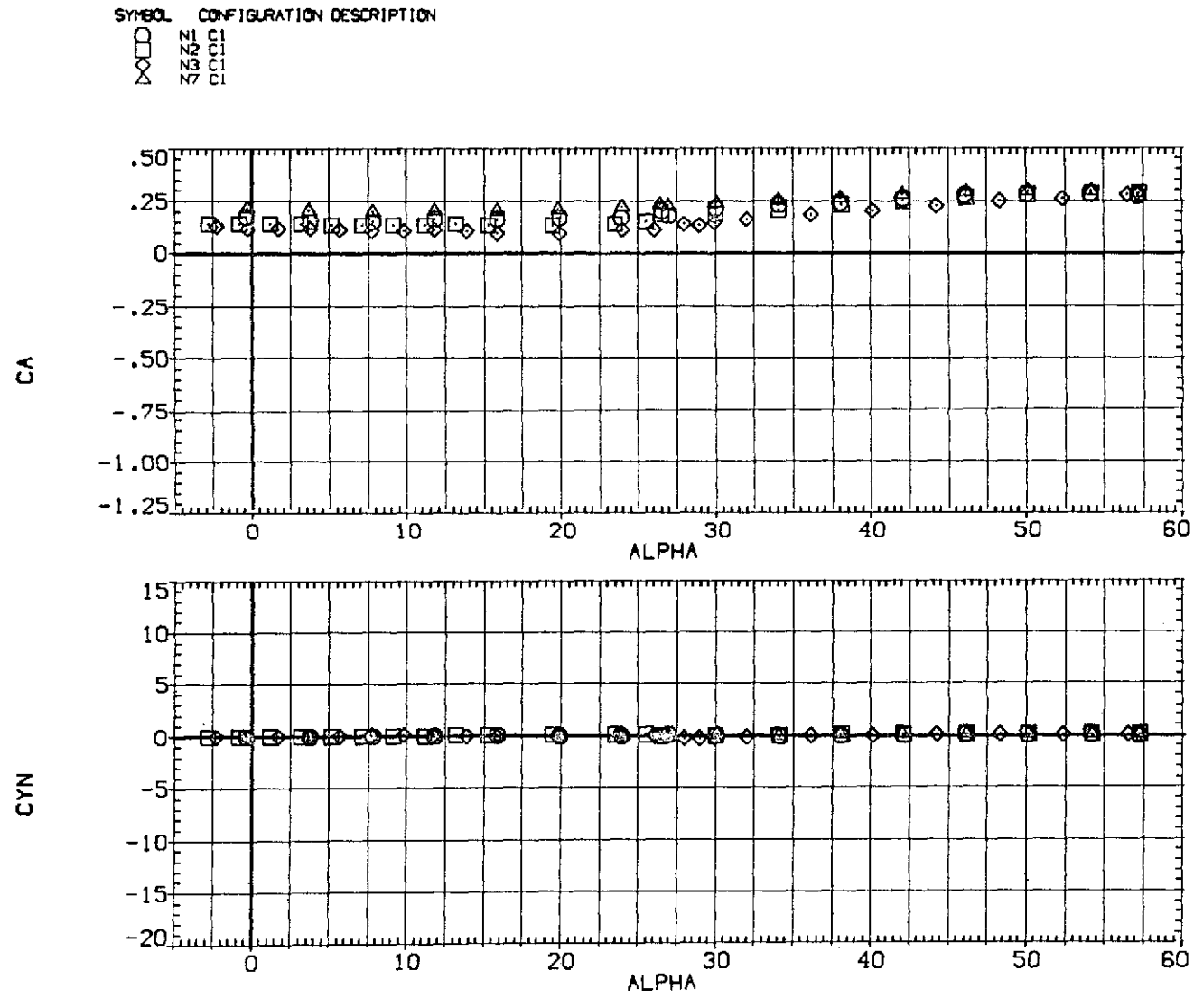

(c) C_A and C_n versus α.

Figure 7.– Concluded.

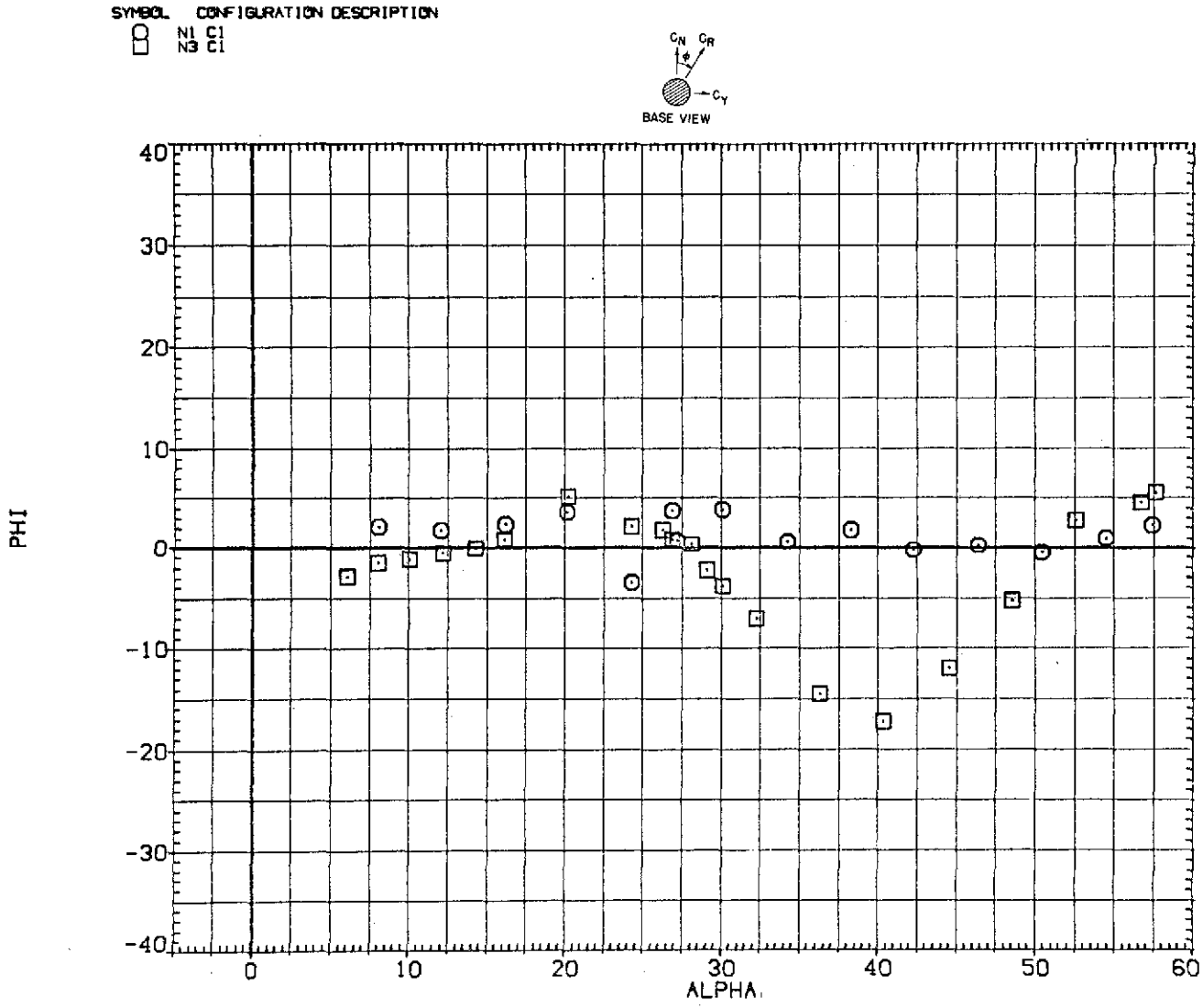

(a) ϕ versus α.

Figure 8.– Effect of nose fineness ratio on aerodynamic centers; $M = 0.6$, $Re = 6.5 \times 10^5$.

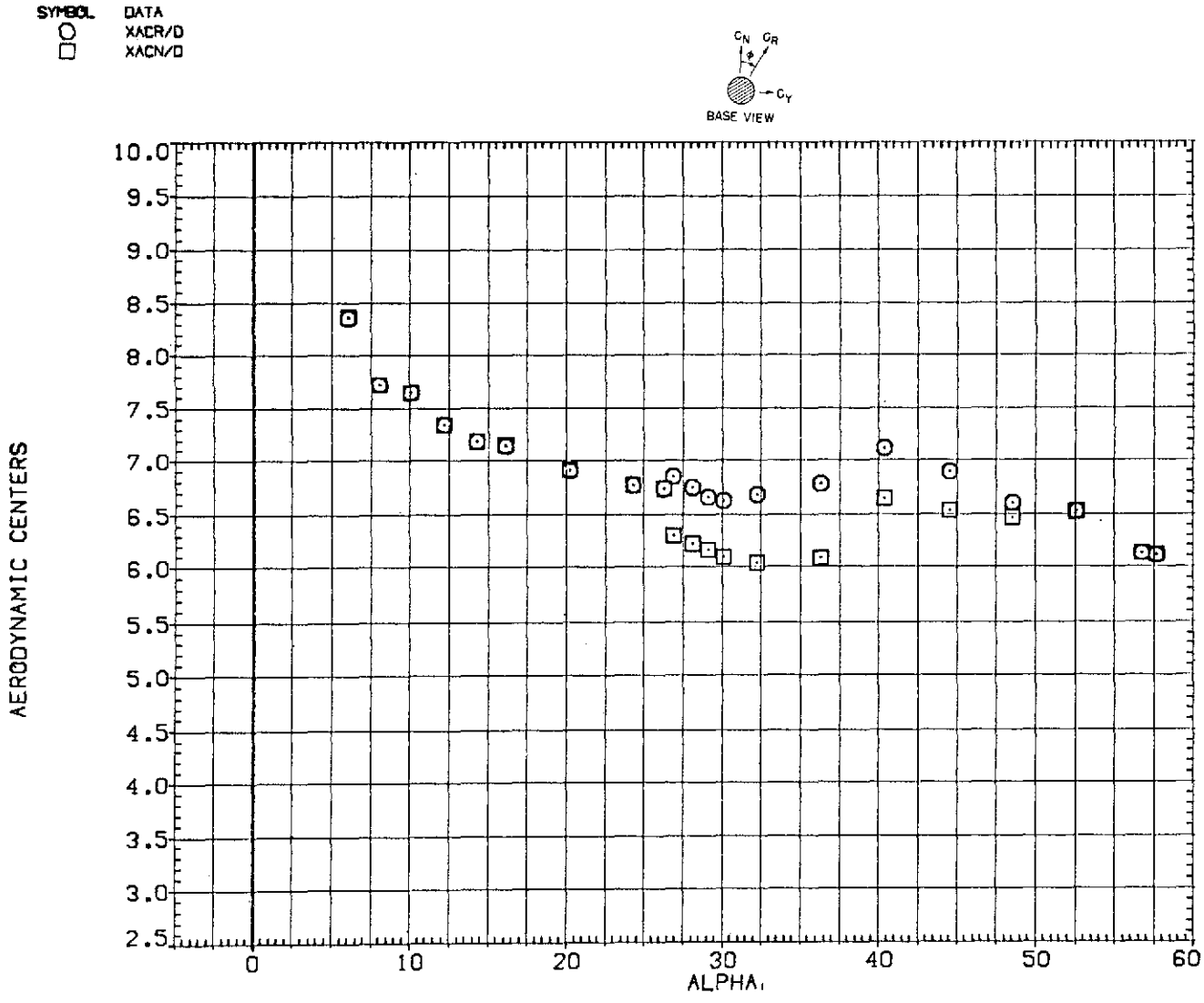

(b) Aerodynamic centers versus α for $N_3 C_1$.

Figure 8.– Concluded.

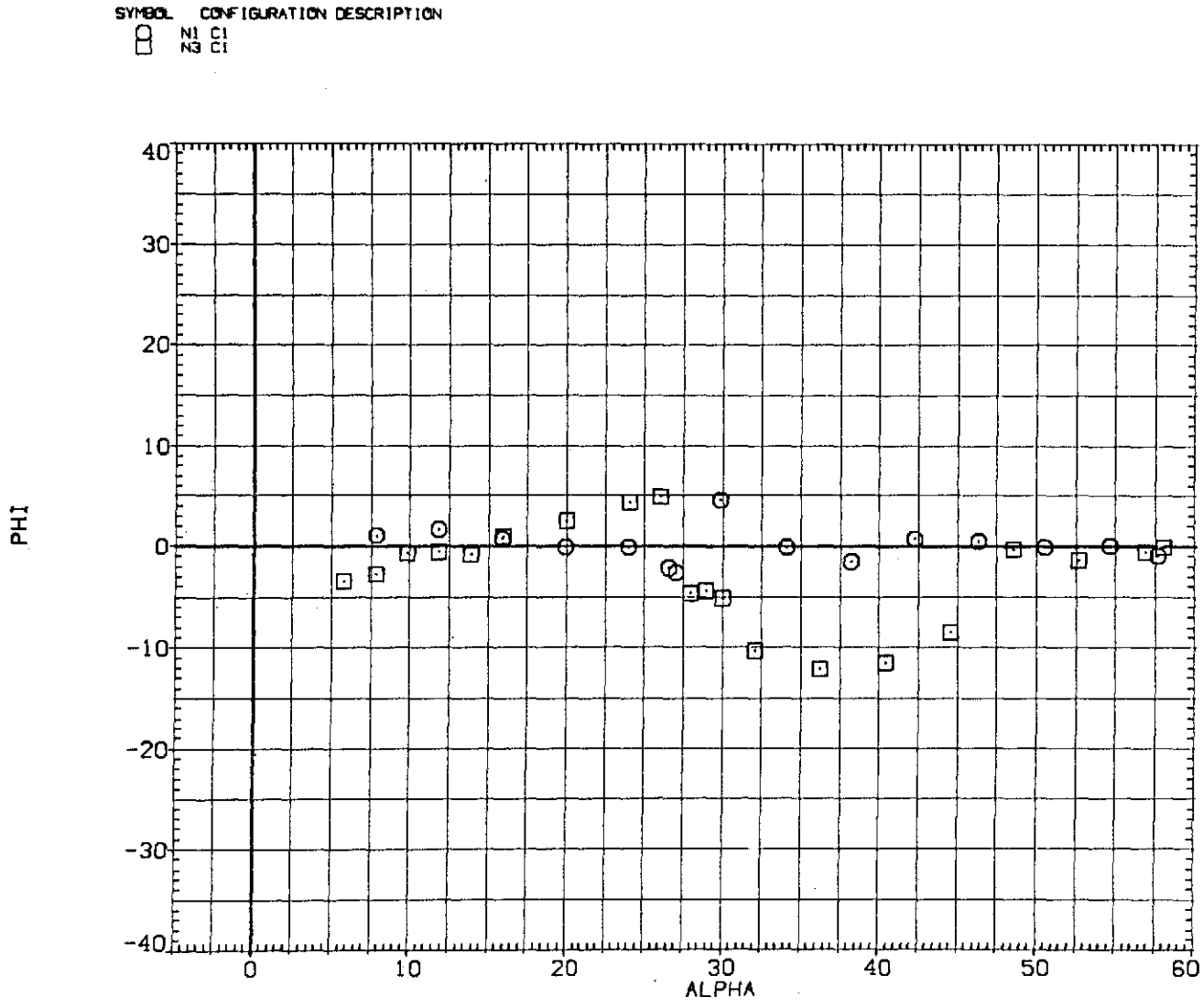

(a) ϕ versus α.

Figure 9.-- Effect of nose fineness ratio on aerodynamic centers; $M = 0.9$, $Re = 6.5 \times 10^5$.

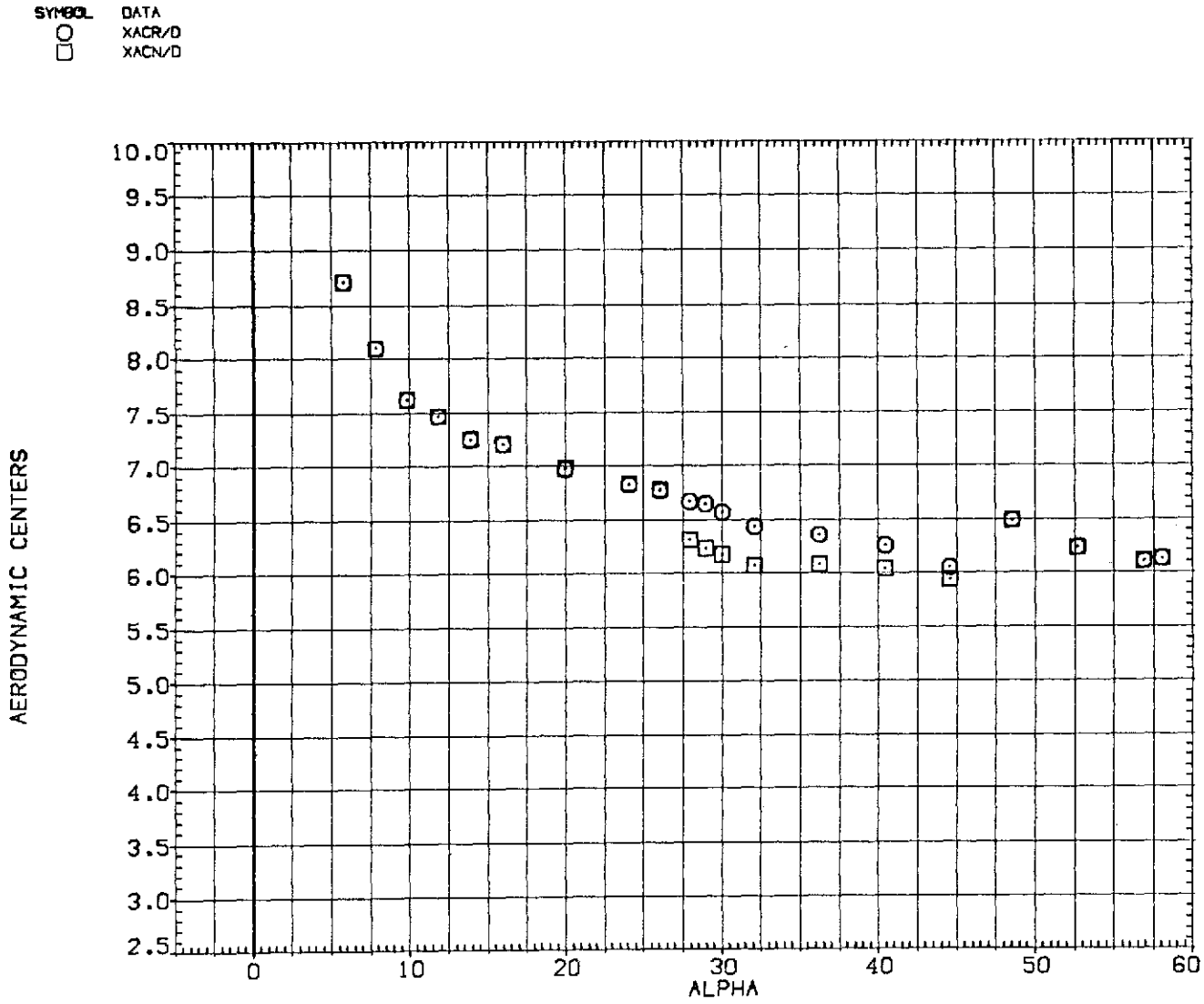

(b) Aerodynamic centers versus α for $N_3 C_1$.

Figure 9.– Concluded.

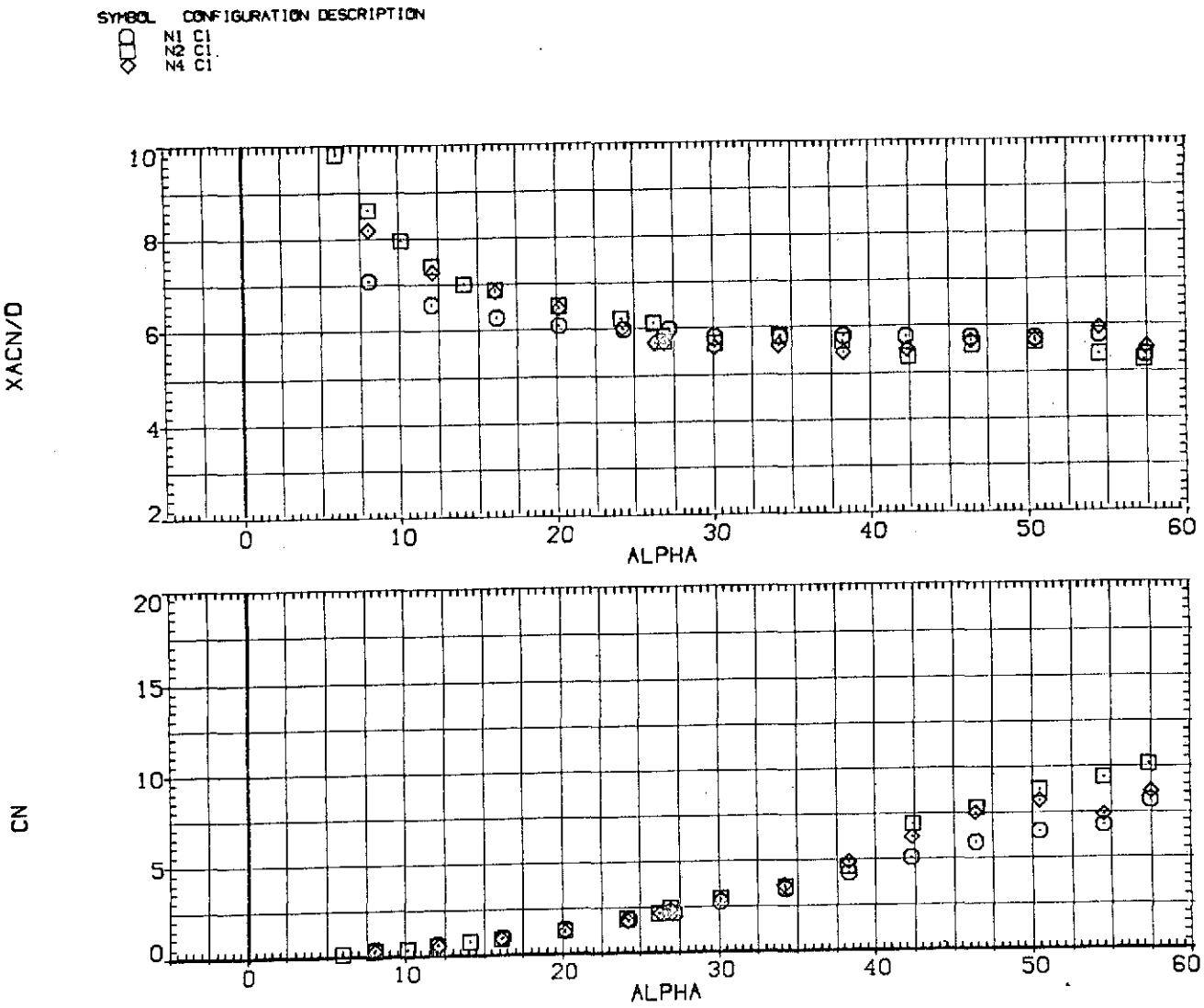

(a) x_{ac_N}/d and C_N versus α.

Figure 10.– Effect of nose-tip rounding; $M = 0.6$, $Re = 6.5 \times 10^5$.

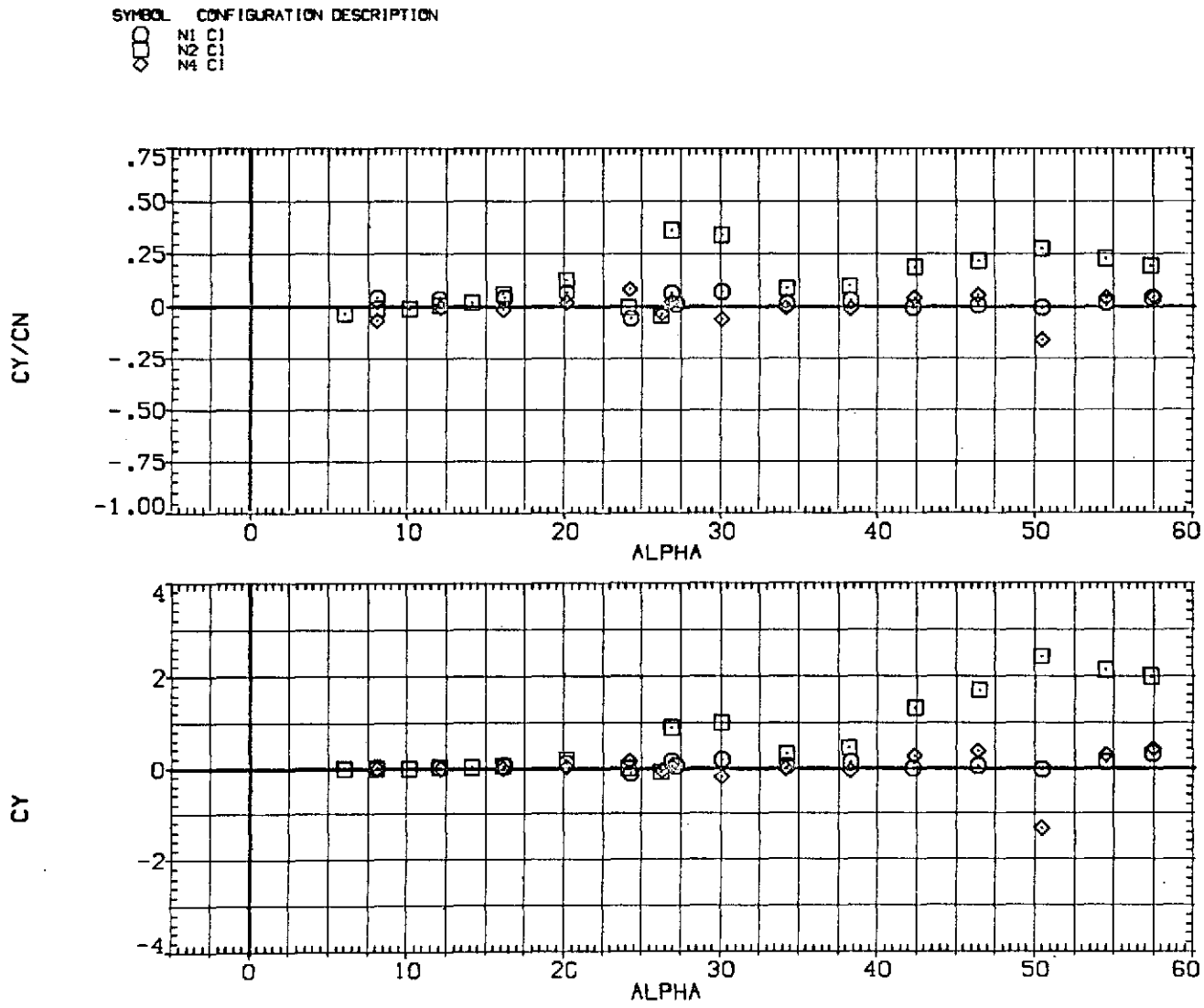

(b) C_Y/C_N and C_Y versus α.

Figure 10.– Continued.

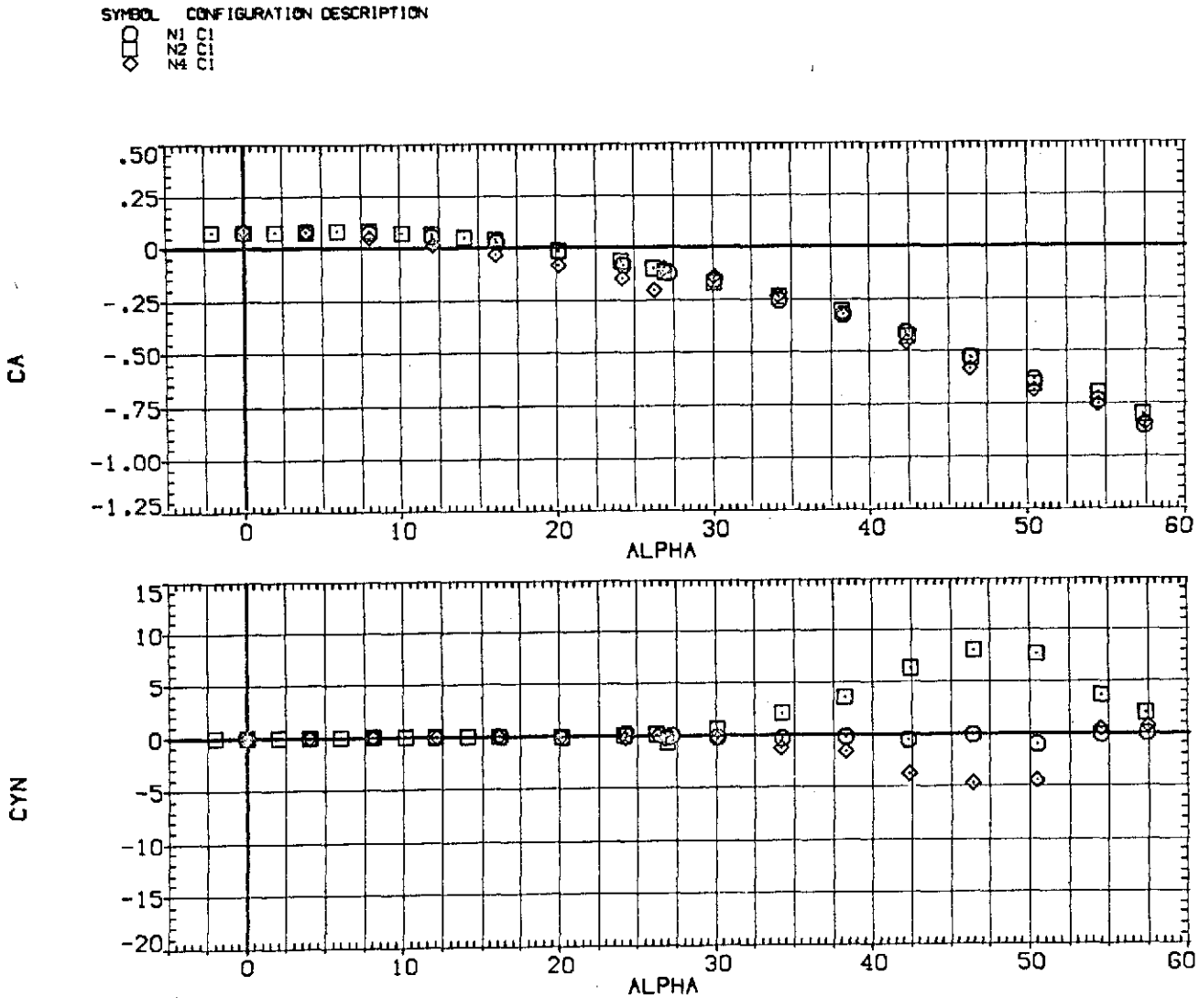

(c) C_A and C_n versus α.

Figure 10.– Concluded.

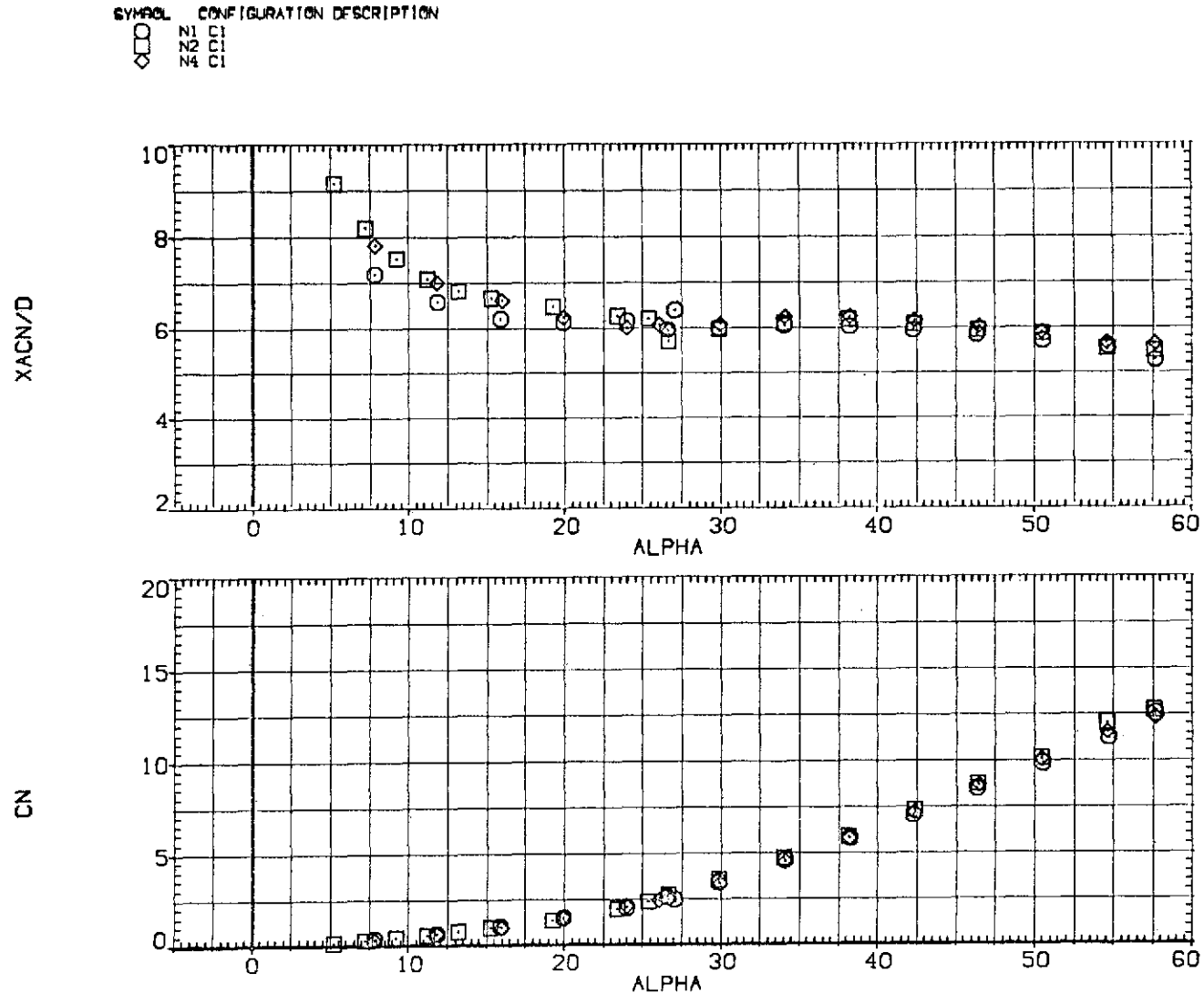

(a) x_{ac_N}/d and C_N versus α.

Figure 11.– Effect of nose-tip rounding; $M = 0.9$, $Re = 6.5 \times 10^5$.

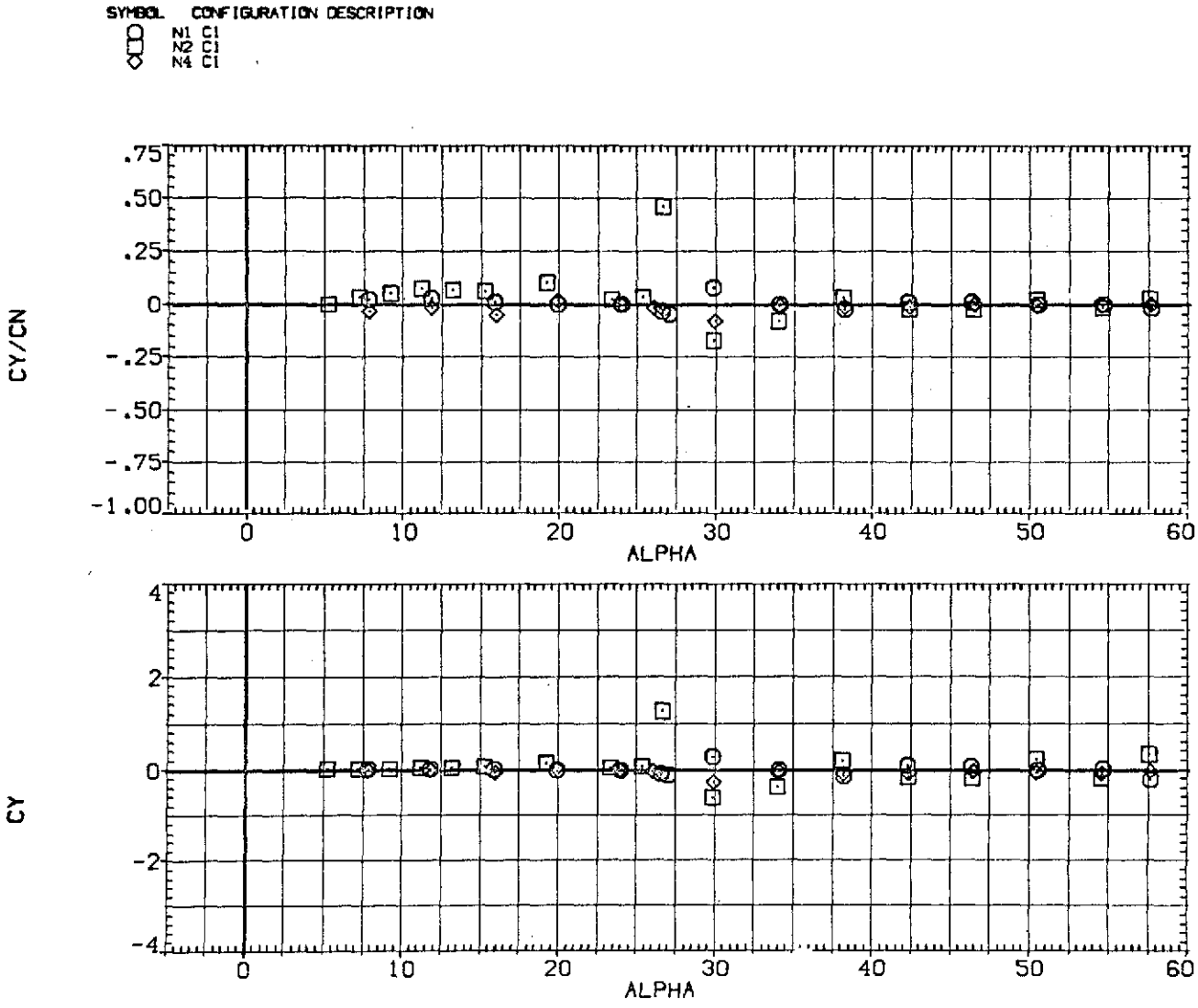

(b) C_Y/C_N and C_Y versus α.

Figure 11.– Continued.

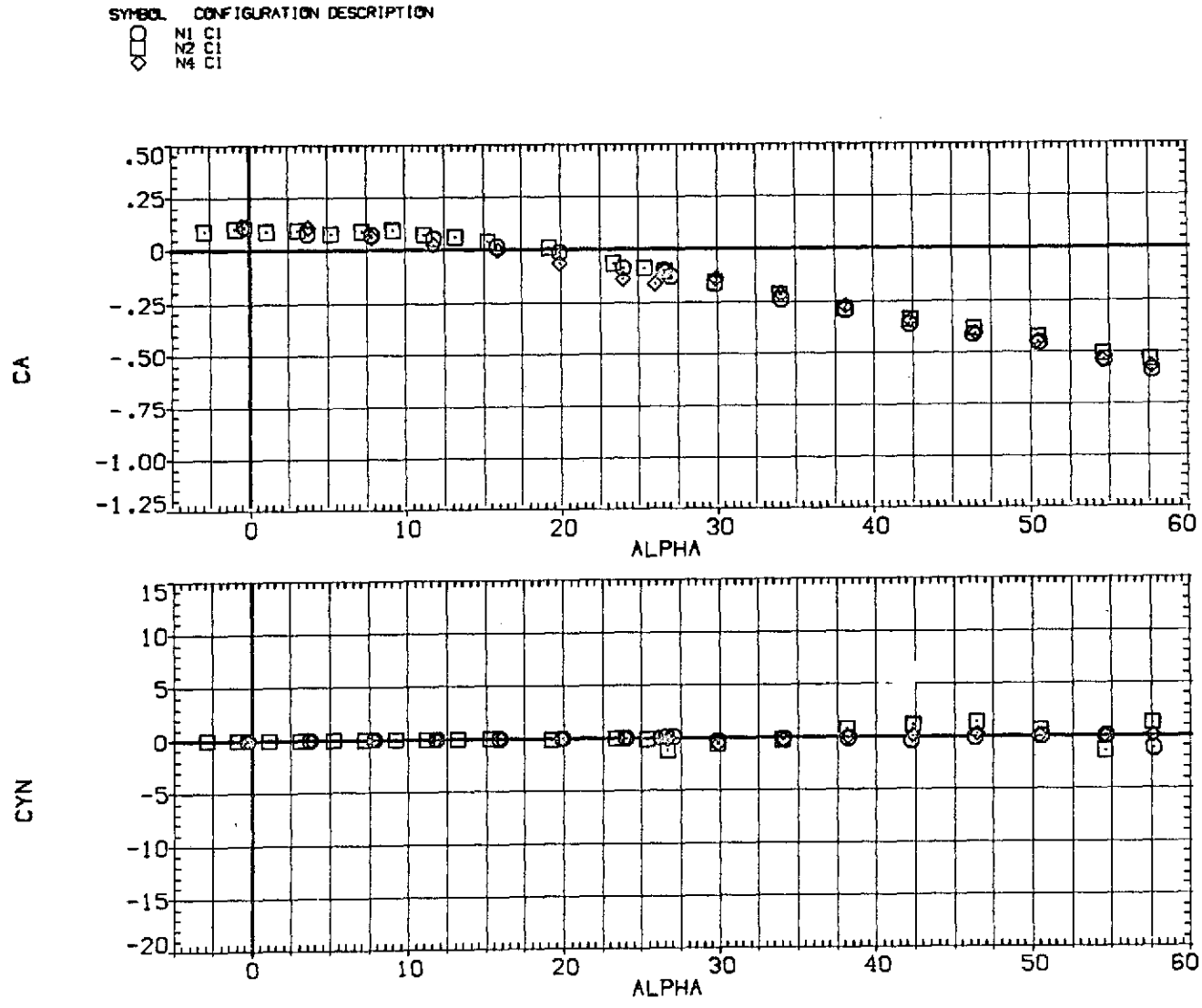

(c) C_A and C_n versus α.

Figure 11.— Concluded.

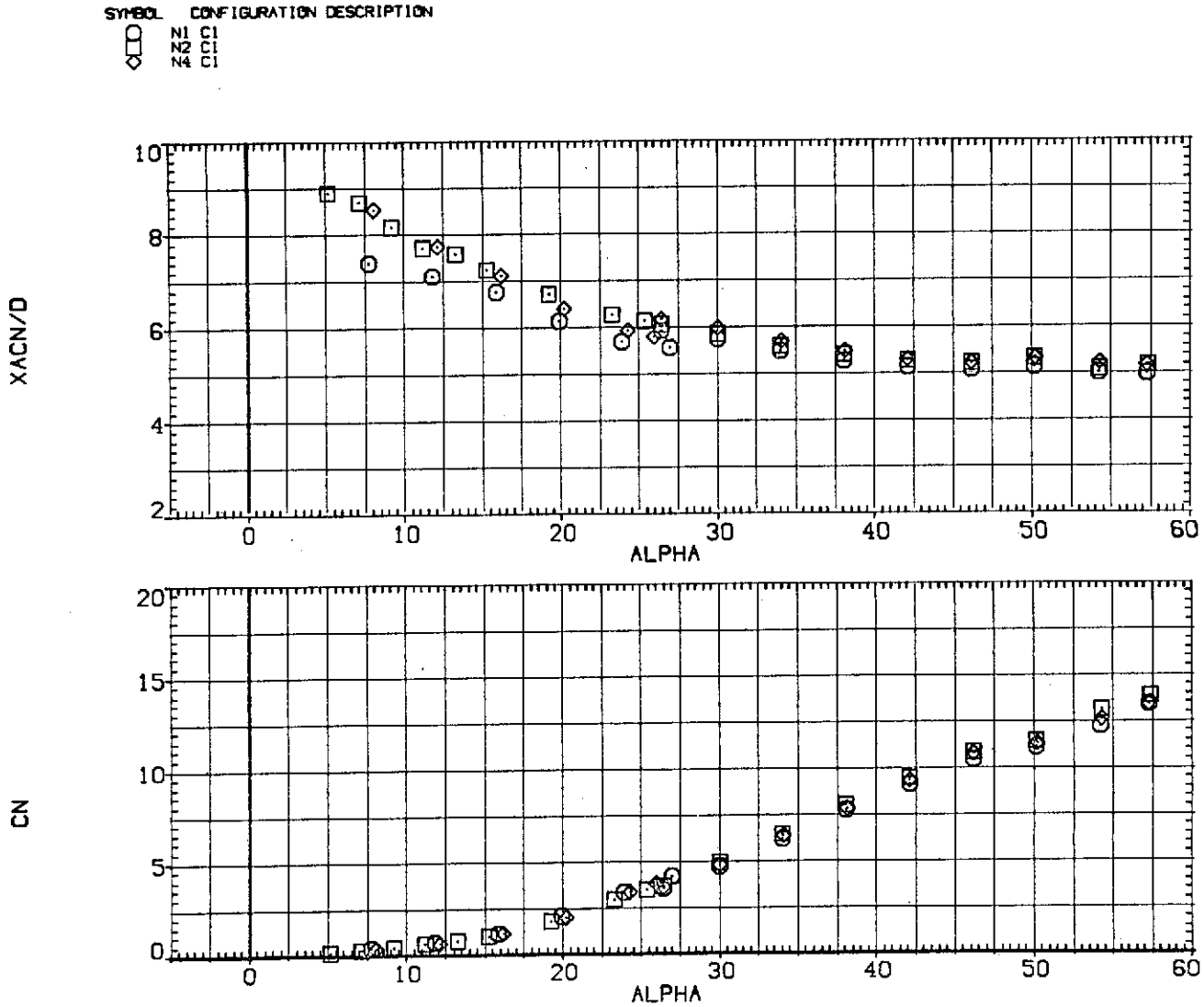

(a) x_{ac_N}/d and C_N versus α.

Figure 12.– Effect of nose-tip rounding; $M = 1.2$, $Re = 3.8 \times 10^5$.

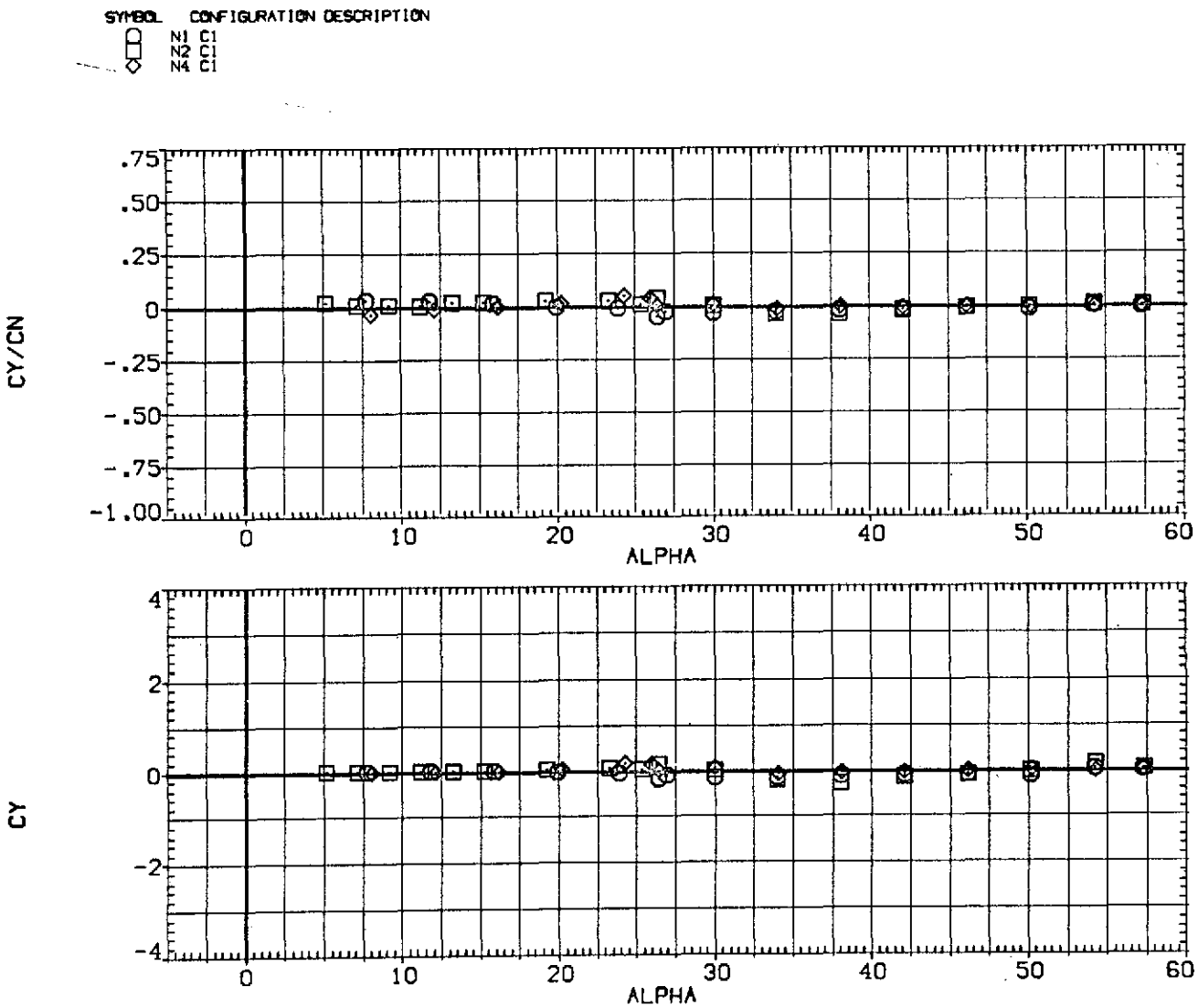

(b) C_Y/C_N and C_Y versus α.

Figure 12.– Continued.

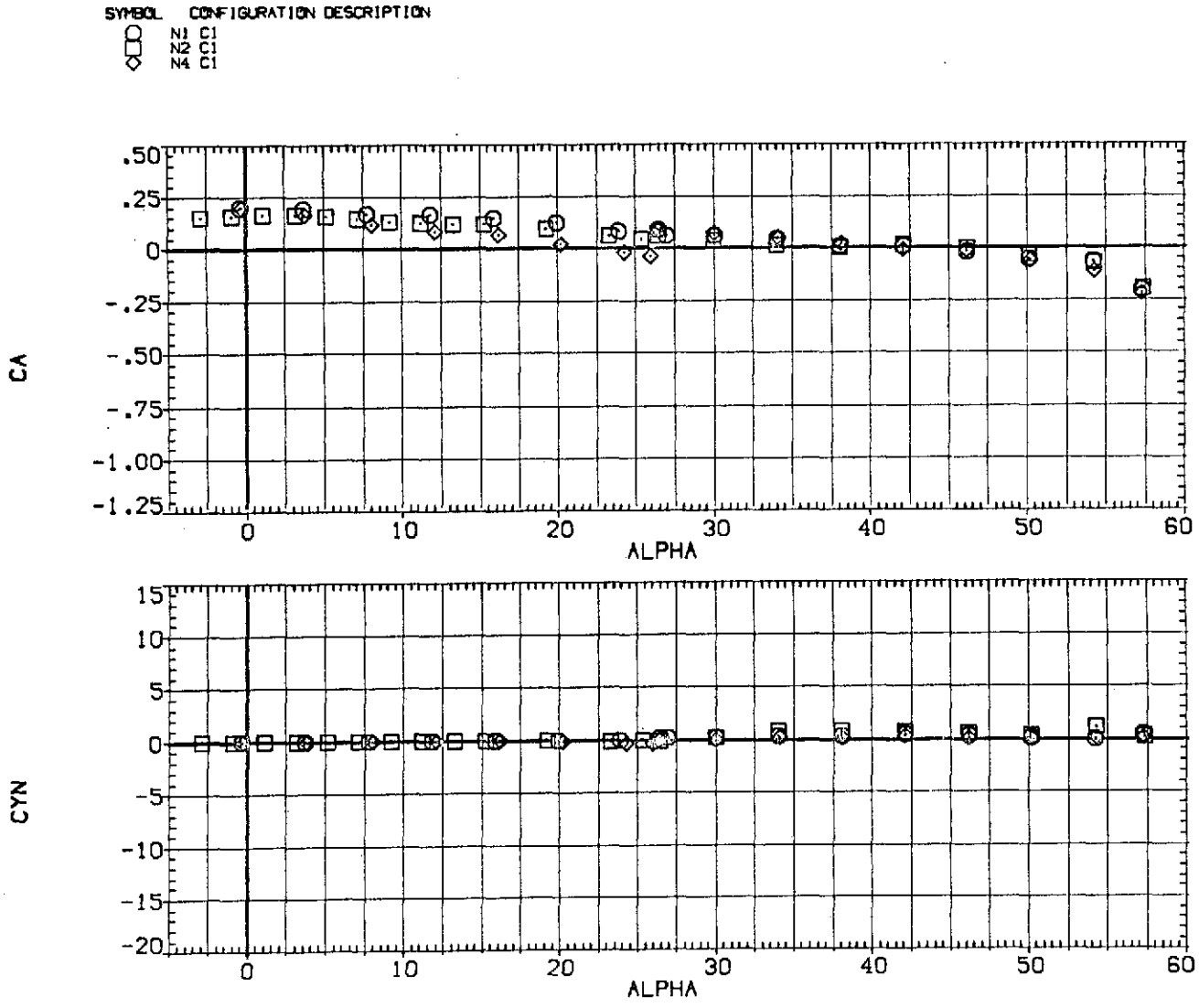

(c) C_A and C_n versus α.

Figure 12.– Concluded.

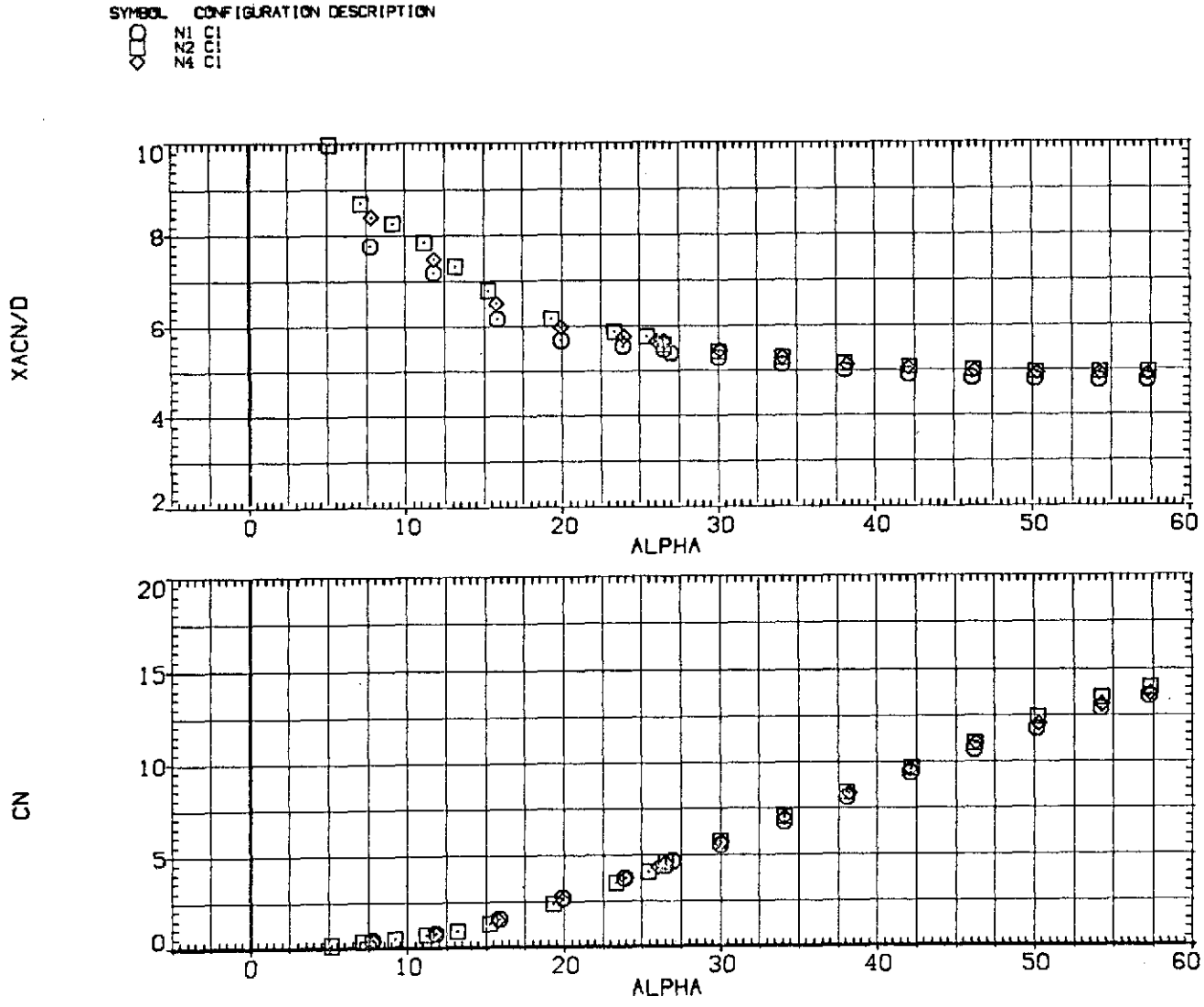

(a) x_{ac_N}/d and C_N versus α.

Figure 13.– Effect of nose-tip rounding; $M = 1.5$, $Re = 3.8 \times 10^5$.

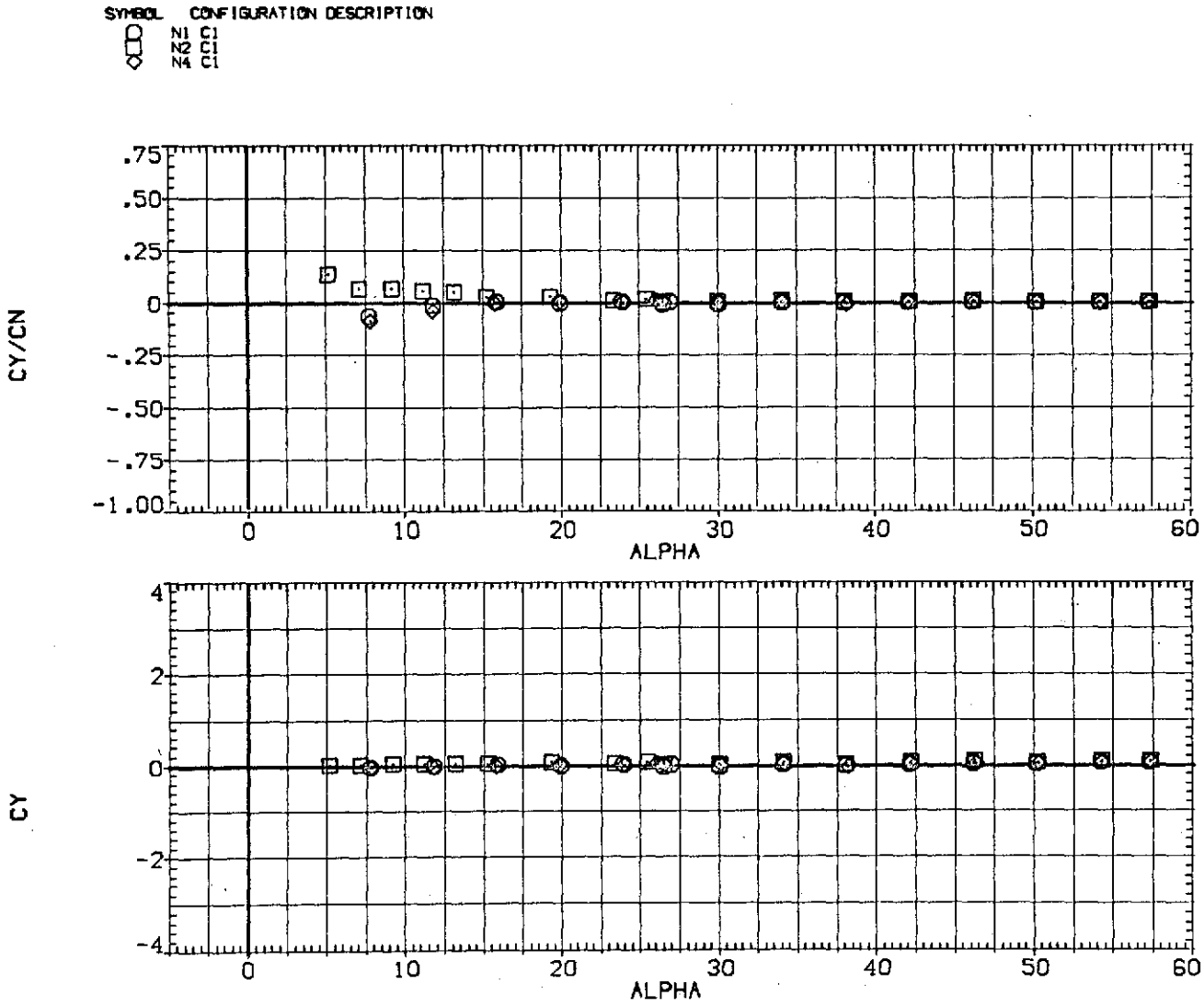

(b) C_Y/C_N and C_Y versus α.

Figure 13.– Continued.

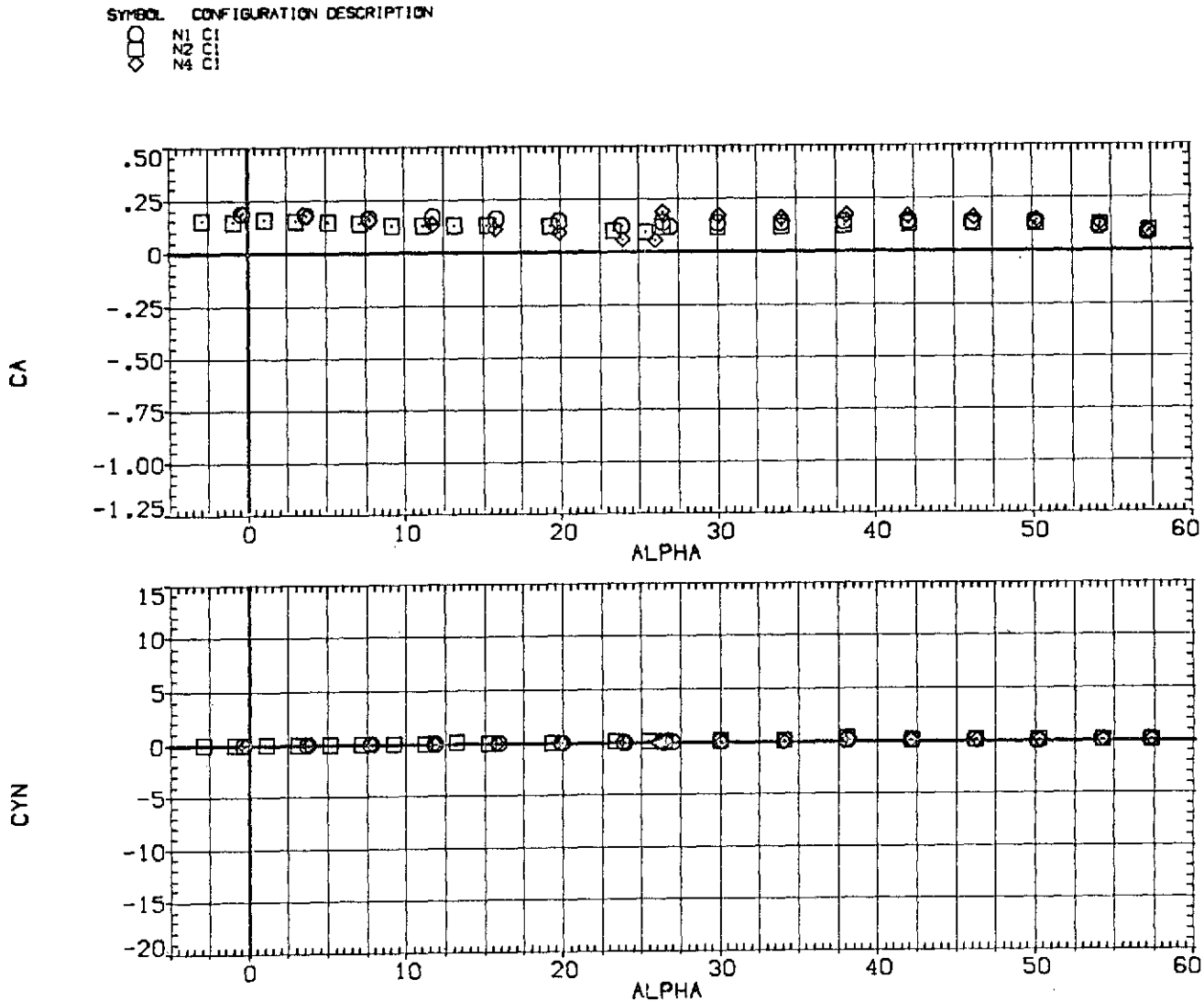

(c) C_A and C_n versus α.

Figure 13.– Concluded.

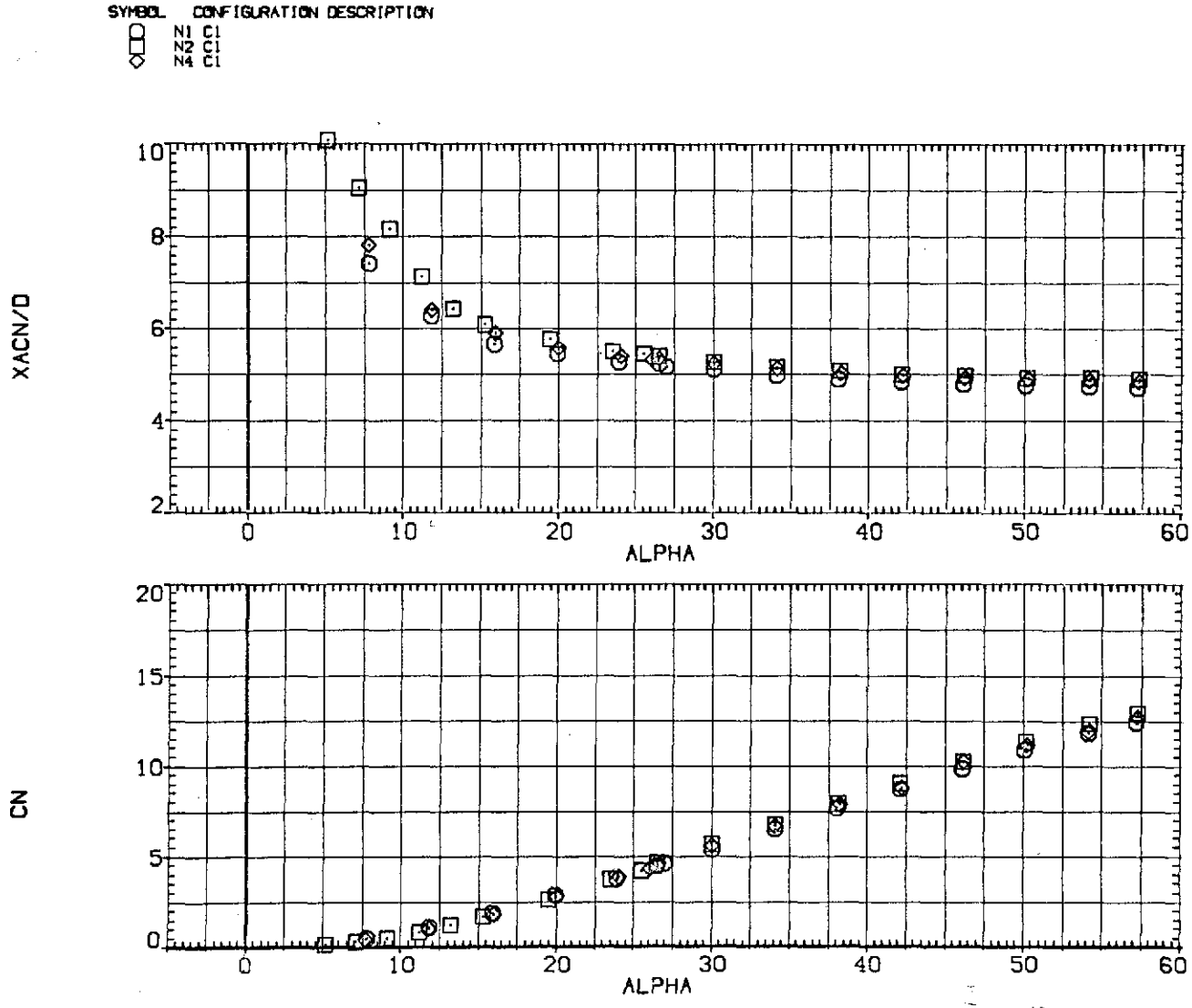

(a) x_{ac_N}/d and C_N versus α.

Figure 14.– Effect of nose-tip rounding; $M = 2.0$, $Re = 3.8 \times 10^5$.

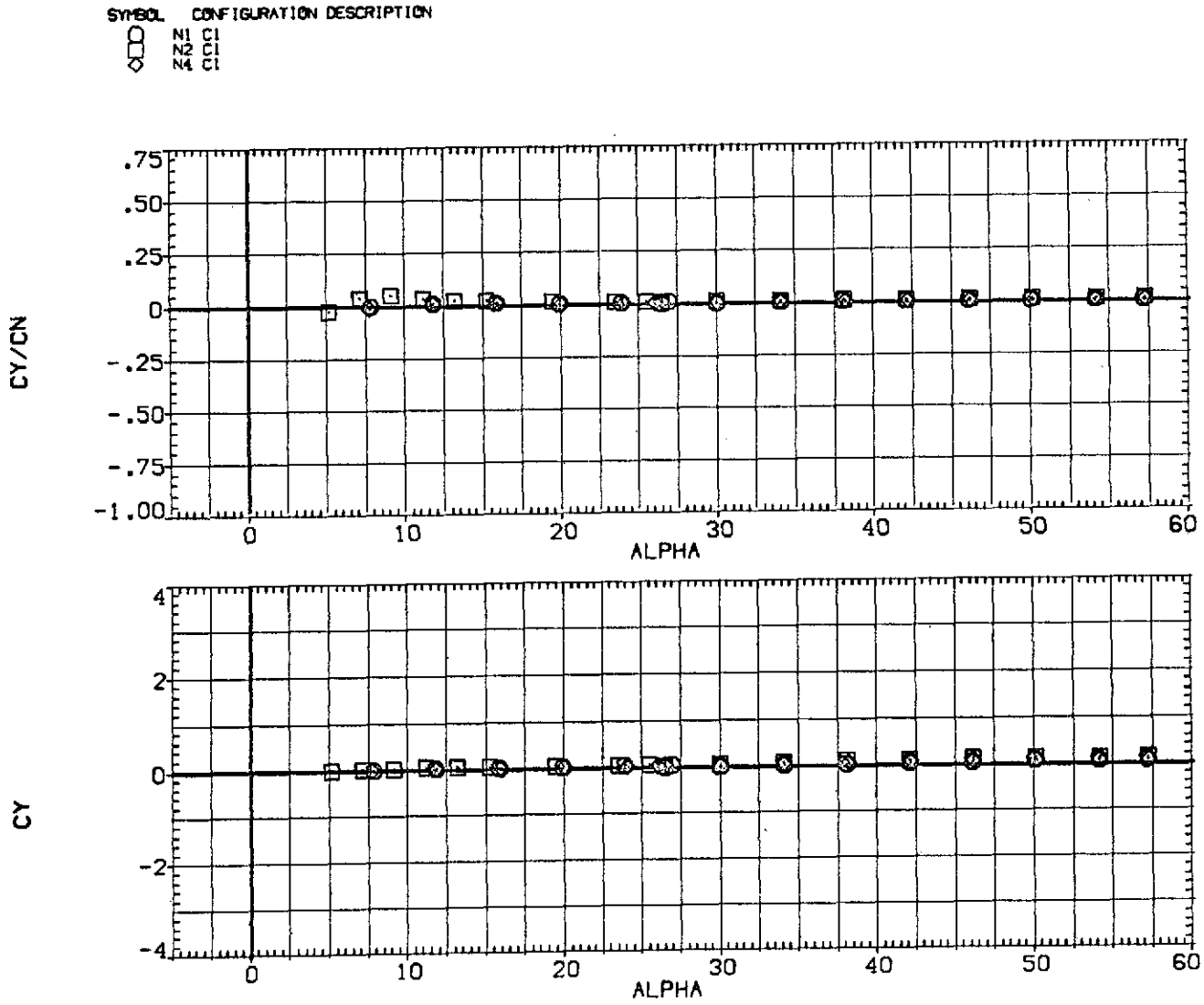

(b) C_Y/C_N and C_Y versus α.

Figure 14.-- Continued.

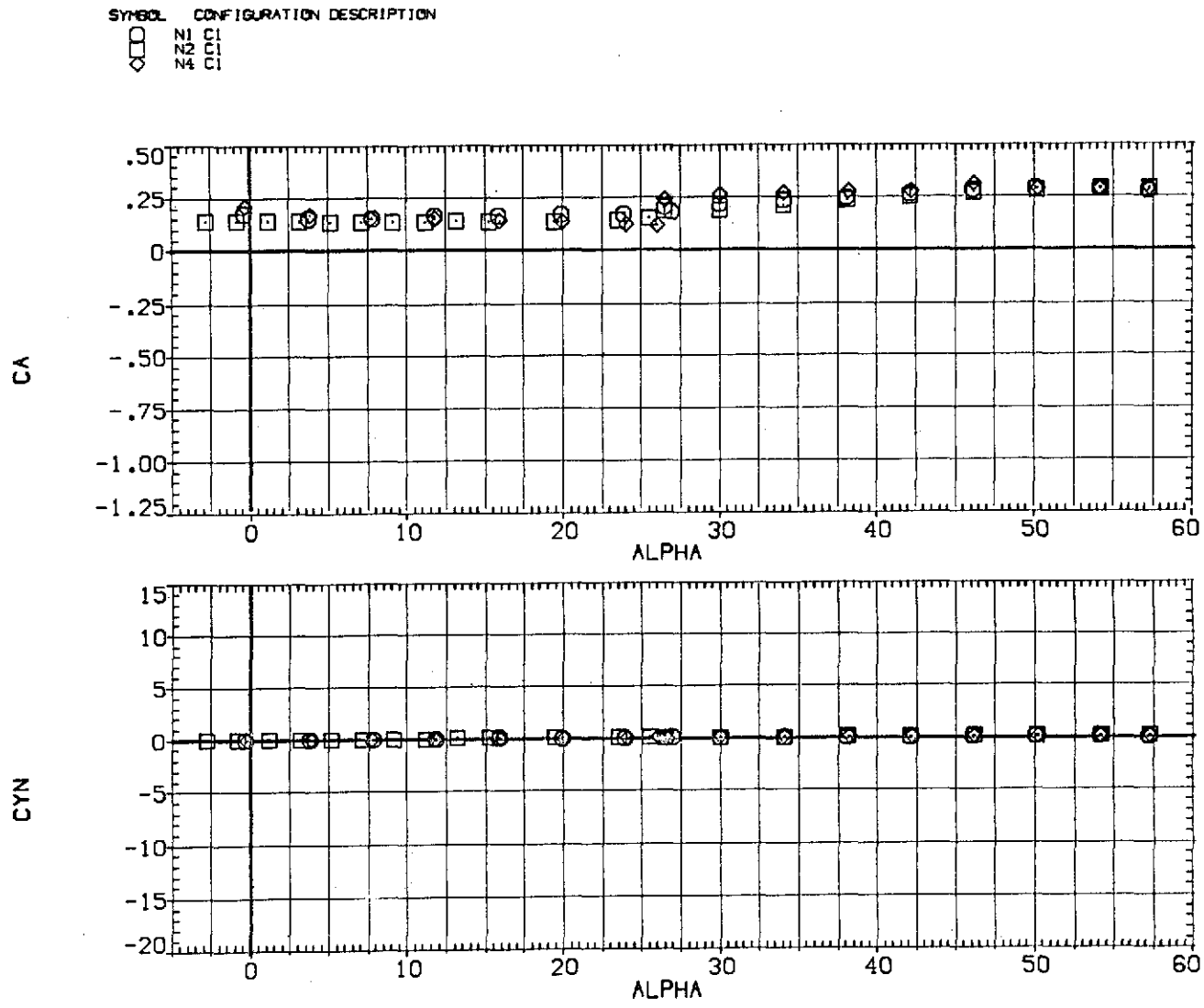

(c) C_A and C_n versus α.

Figure 14.– Concluded.

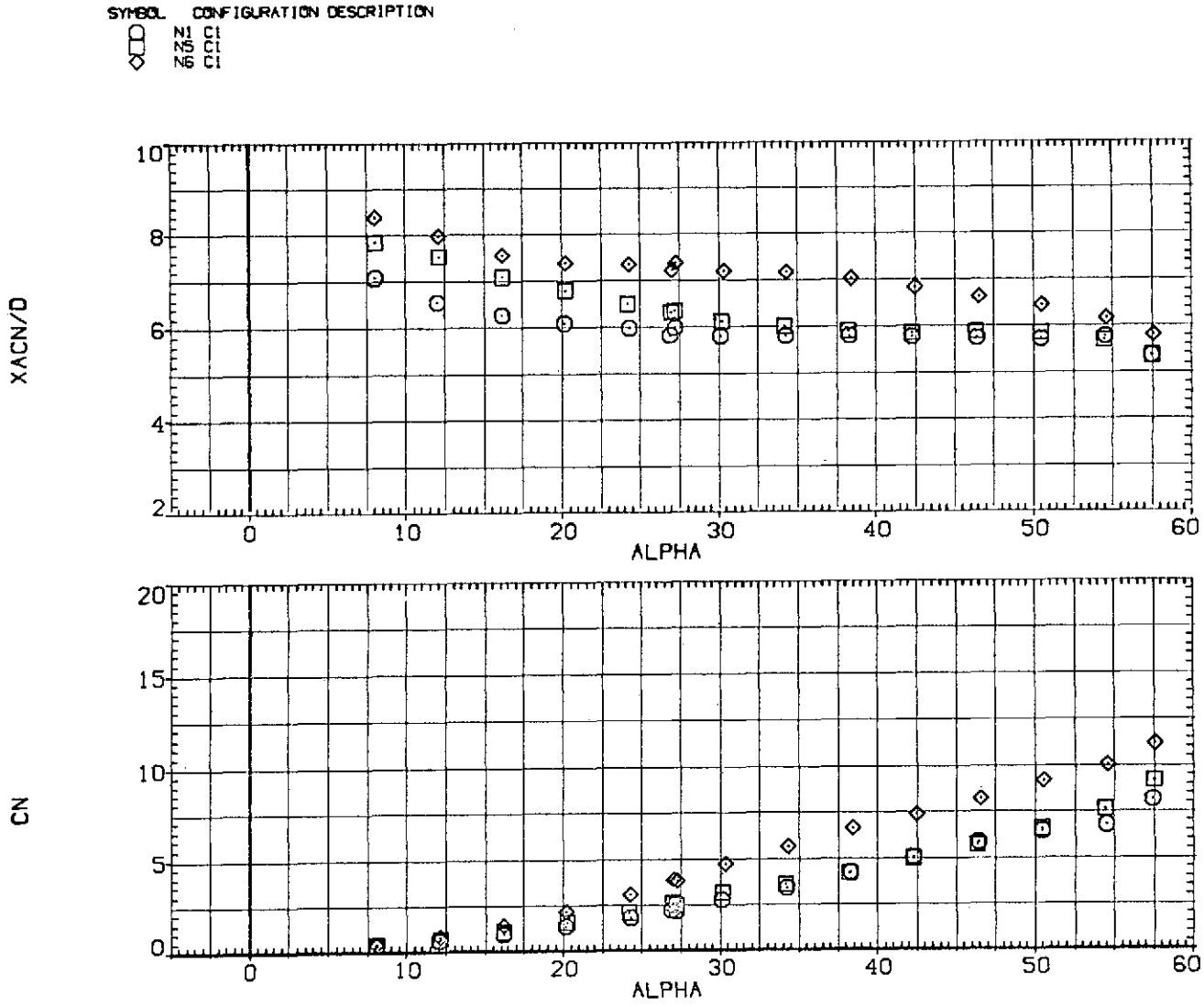

(a) x_{ac_N}/d and C_N versus α.

Figure 15.– Effect of nose strakes; $M = 0.6$, $Re = 6.5 \times 10^5$.

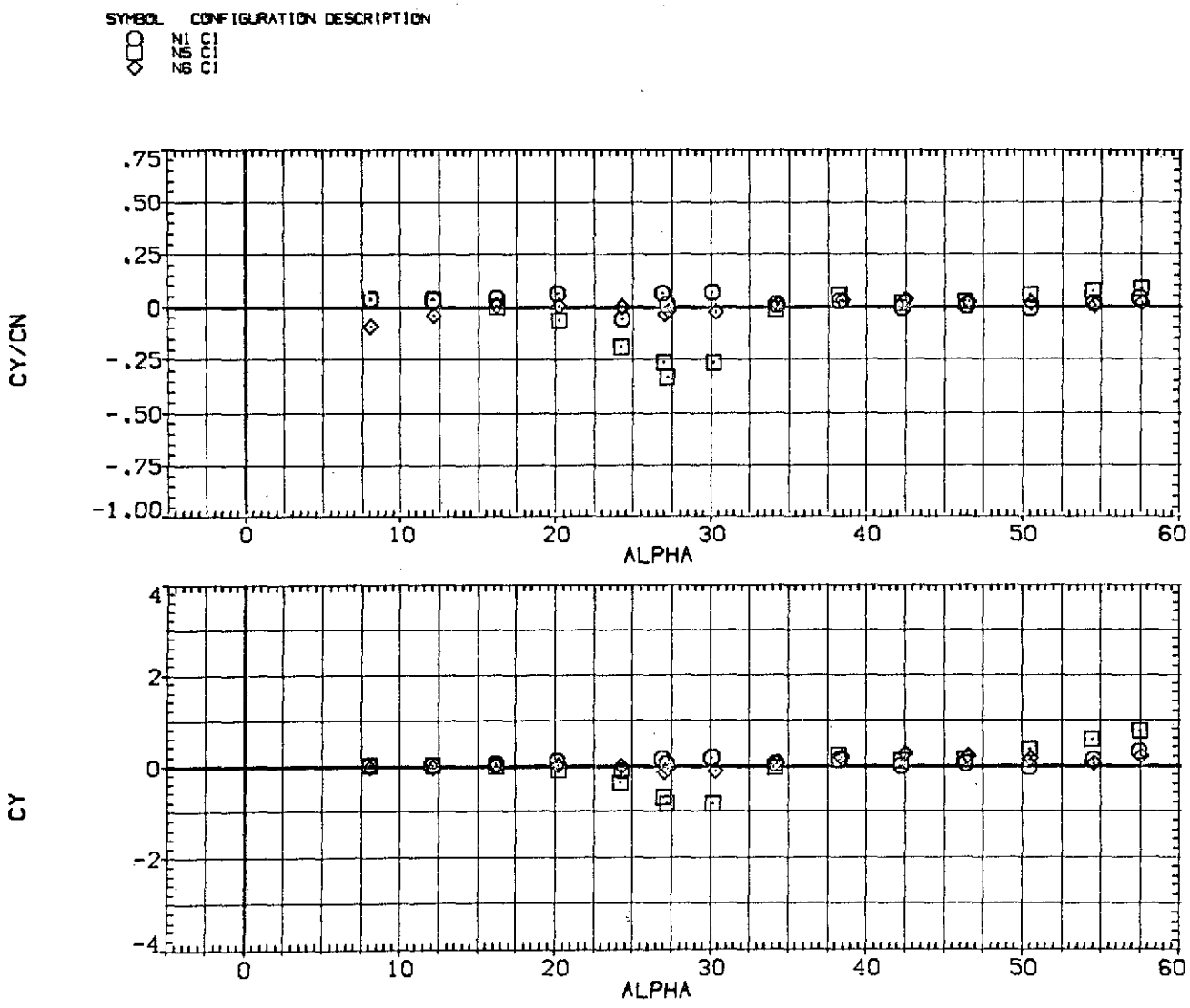

(b) C_Y/C_N and C_Y versus α.

Figure 15.– Continued.

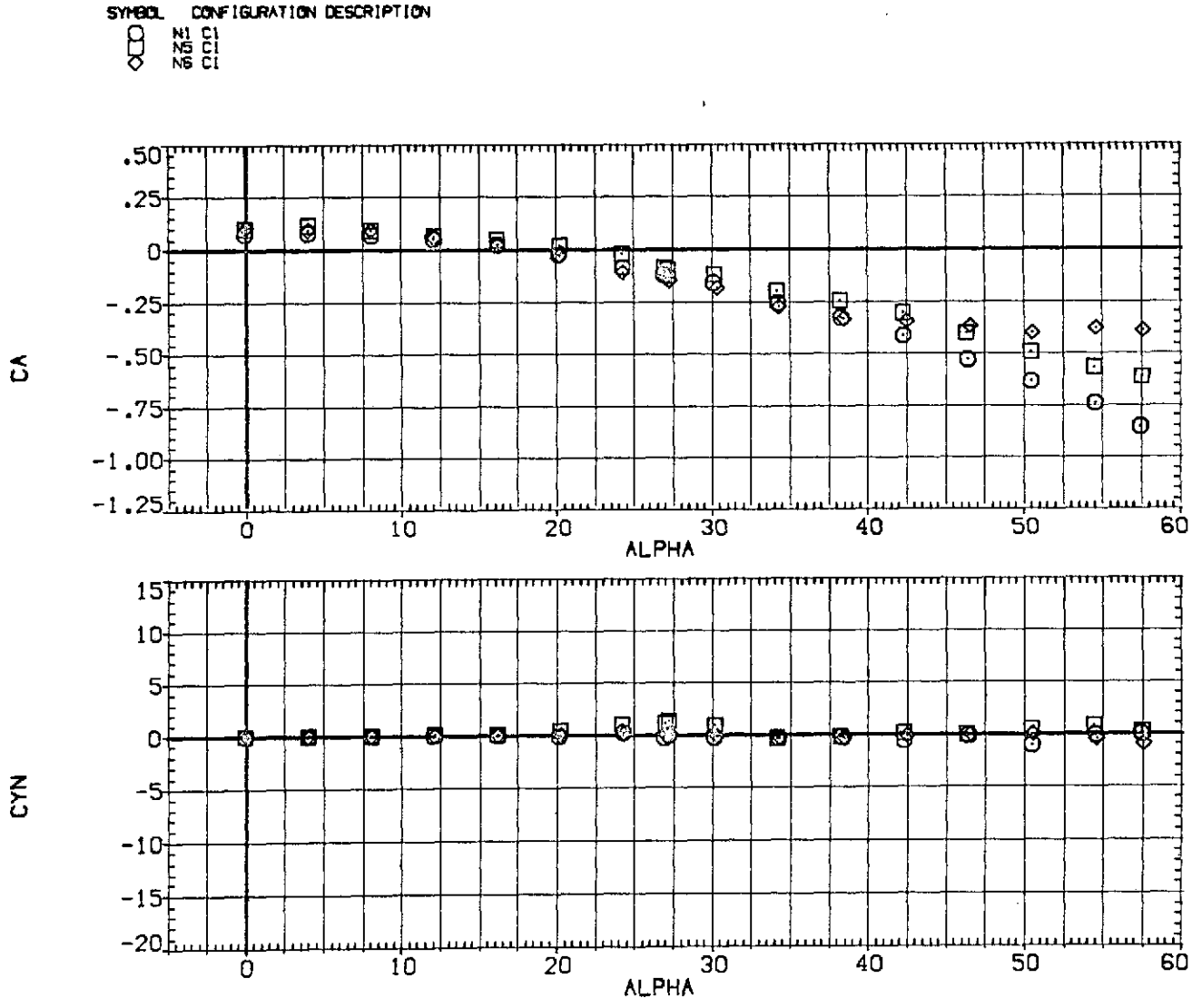

(c) C_A and C_n versus α.

Figure 15.– Concluded.

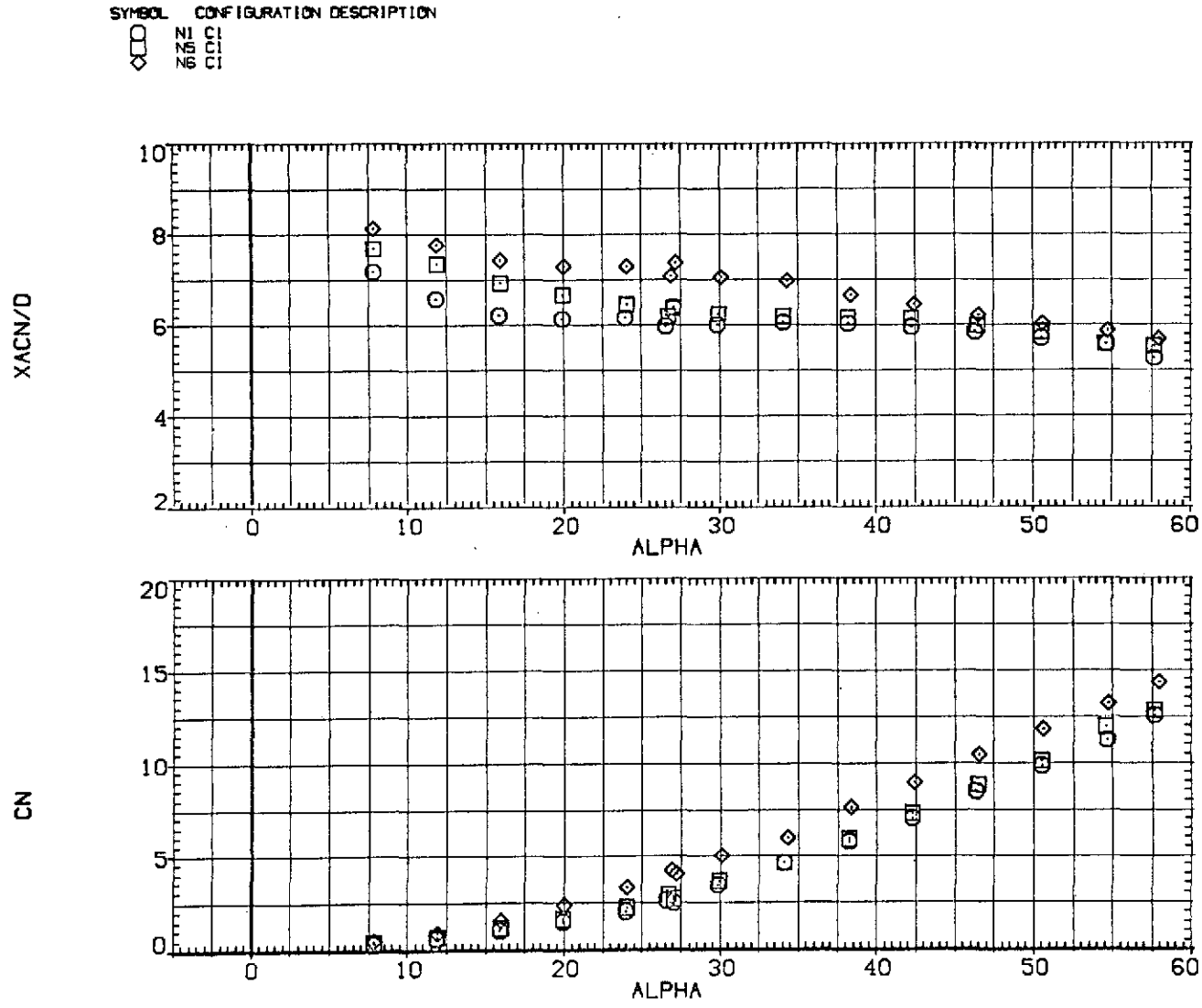

(a) x_{ac_N}/d and C_N versus α.

Figure 16.– Effect of nose strakes; $M = 0.9$, $Re = 6.5 \times 10^5$.

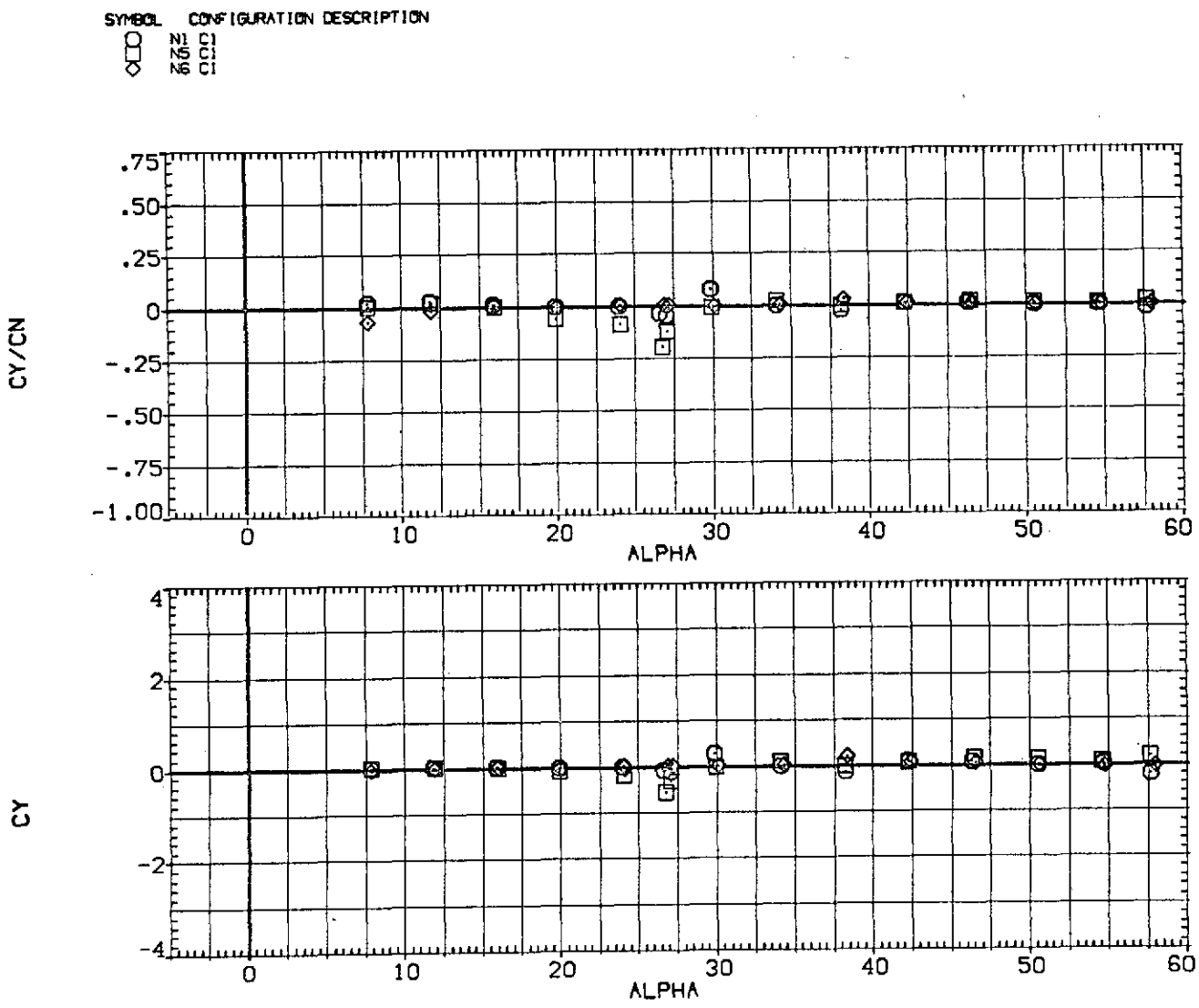

(b) C_Y/C_N and C_Y versus α.

Figure 16.– Continued.

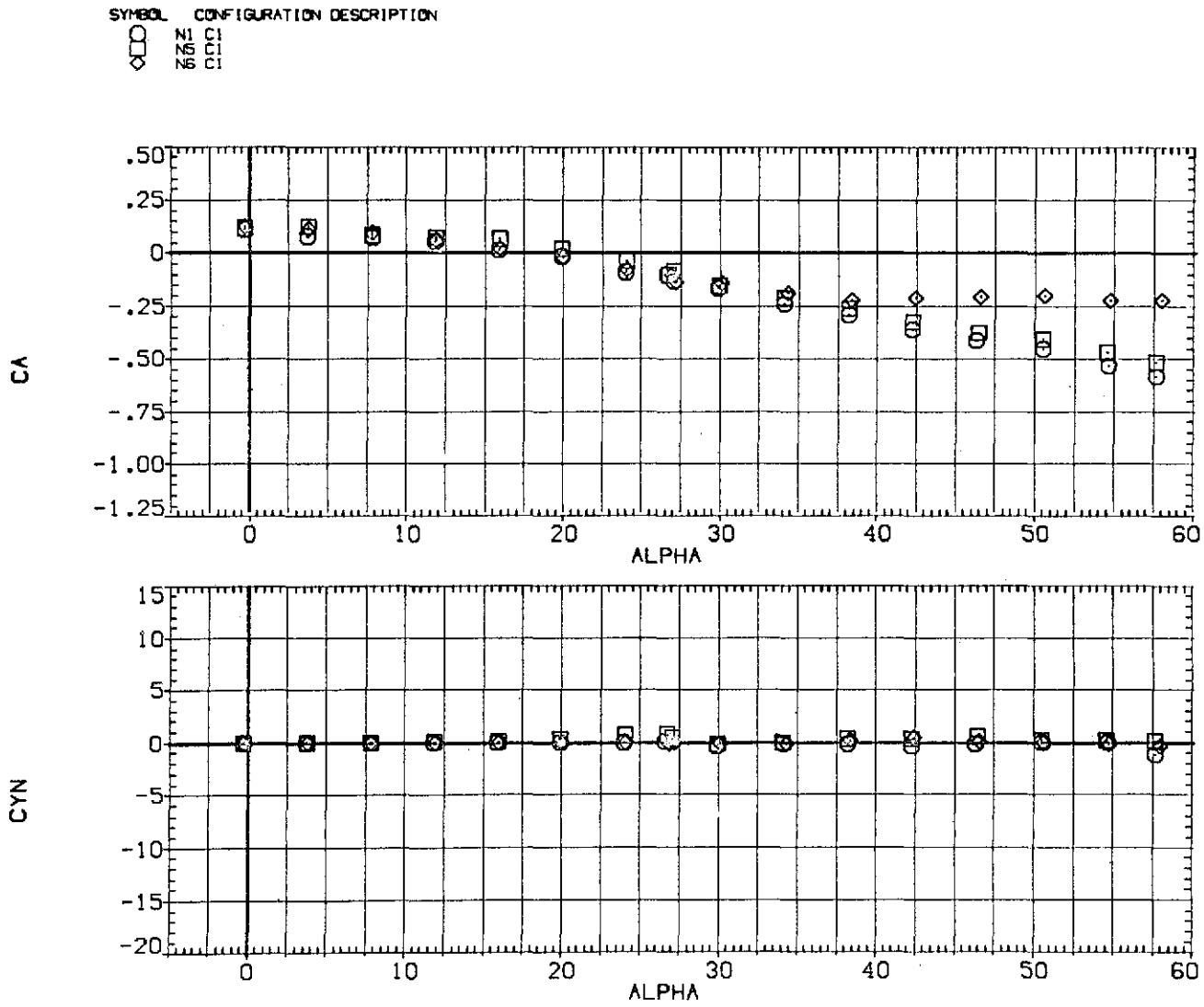

(c) C_A and C_n versus α.

Figure 16.– Concluded.

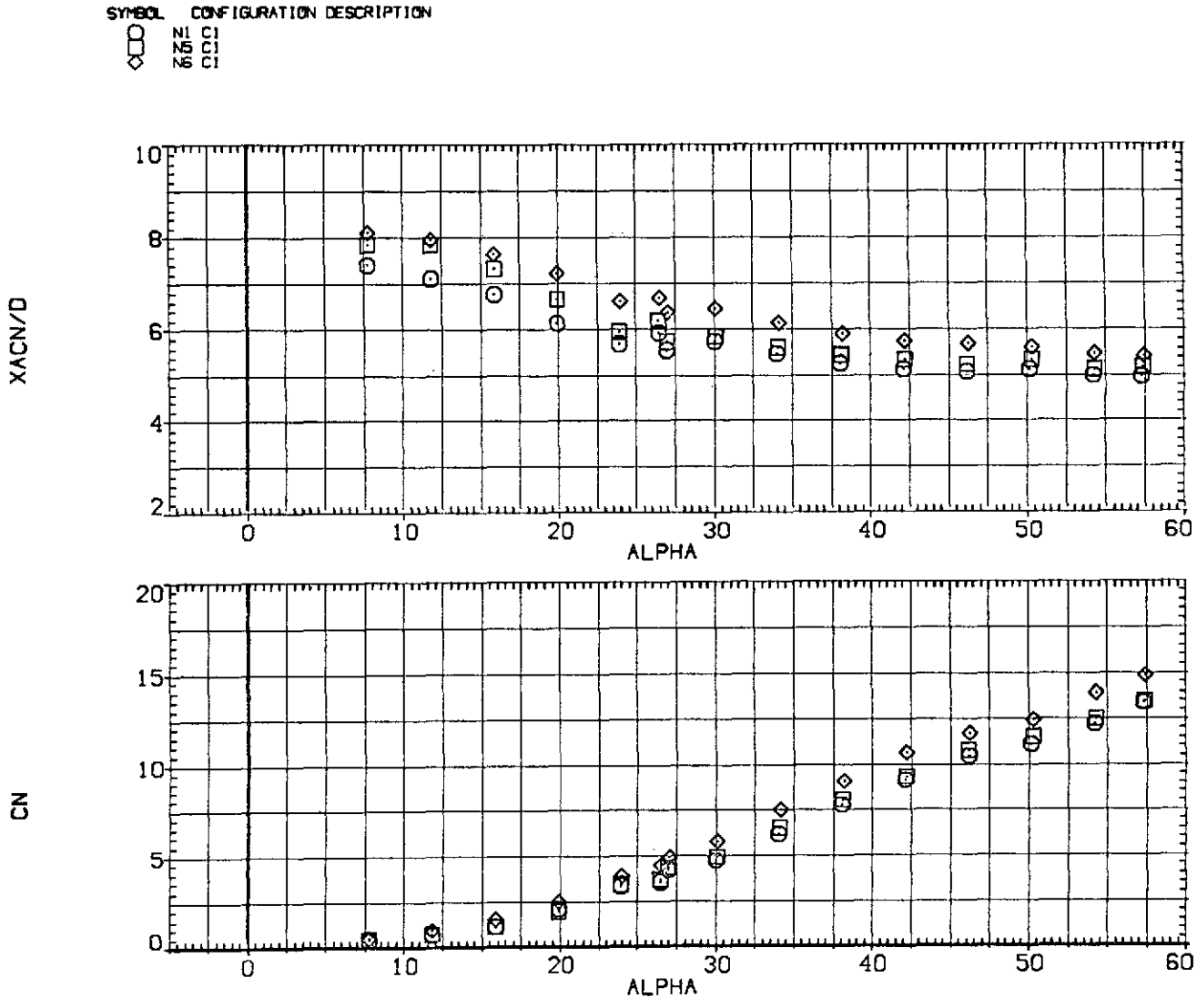

(a) x_{ac_N}/d and C_N versus α.

Figure 17.– Effect of nose strakes; $M = 1.2$, $Re = 3.8 \times 10^5$.

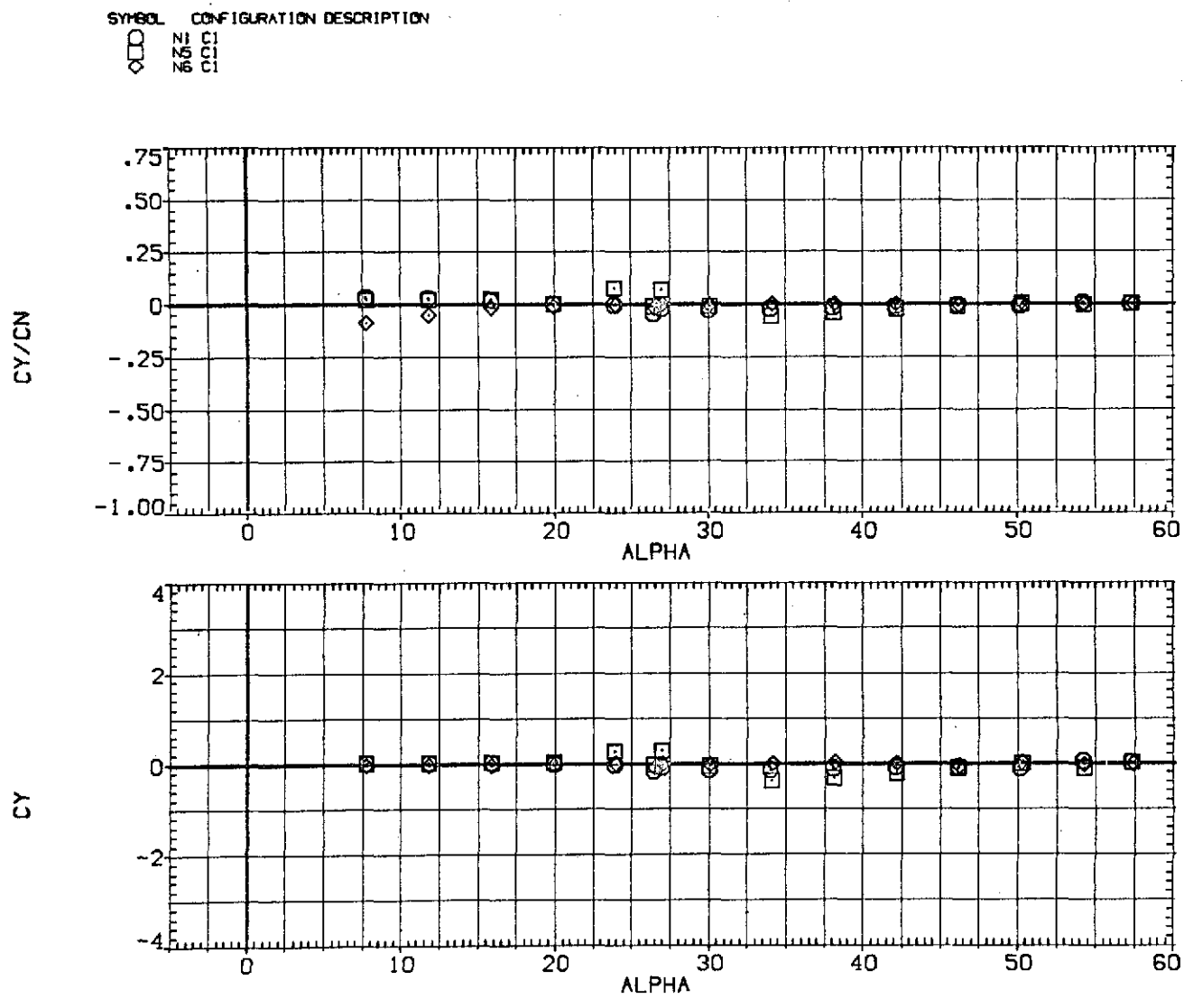

(b) C_Y/C_N and C_Y versus α.

Figure 17.– Continued.

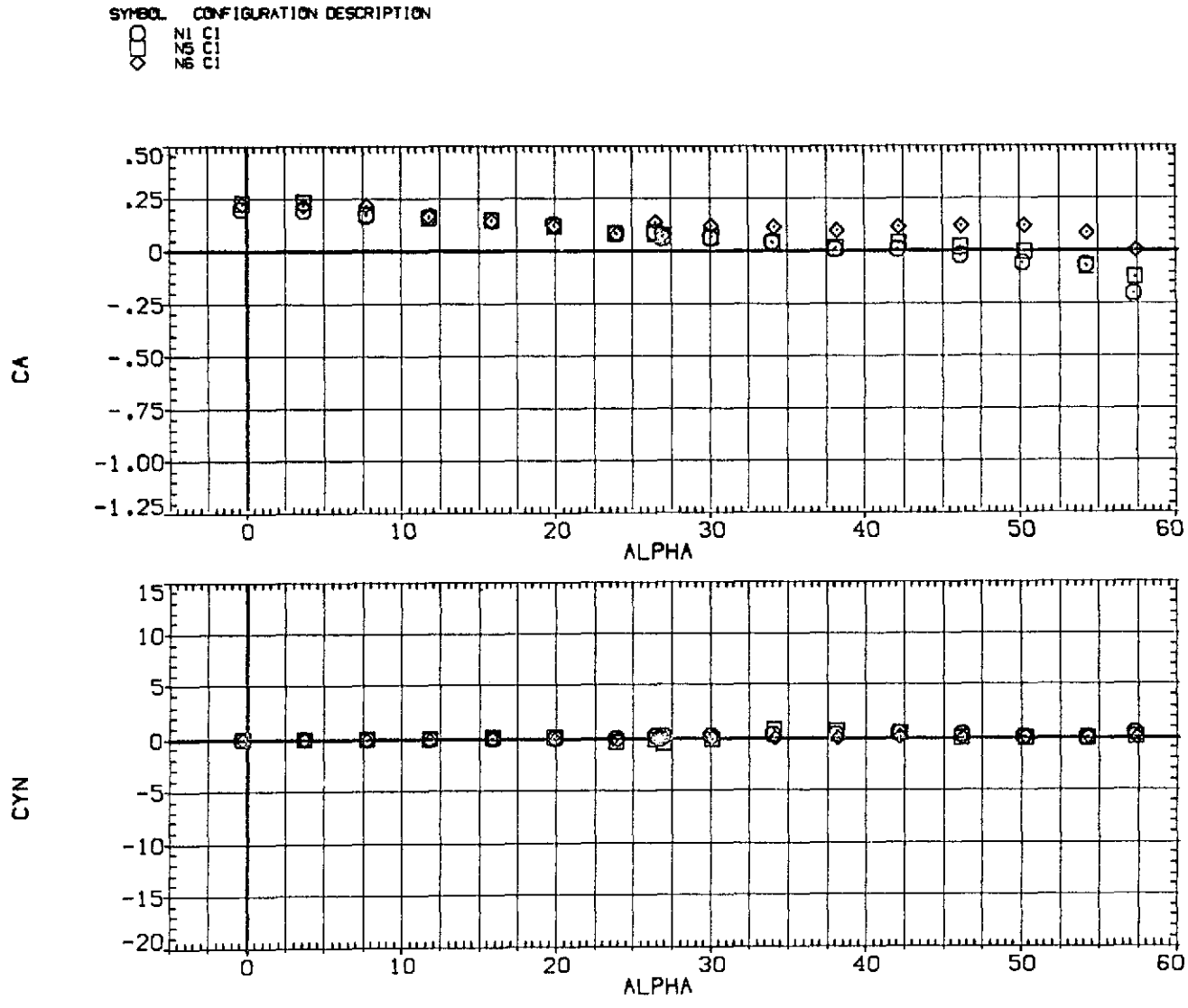

(c) C_A and C_n versus α.

Figure 17.-- Concluded.

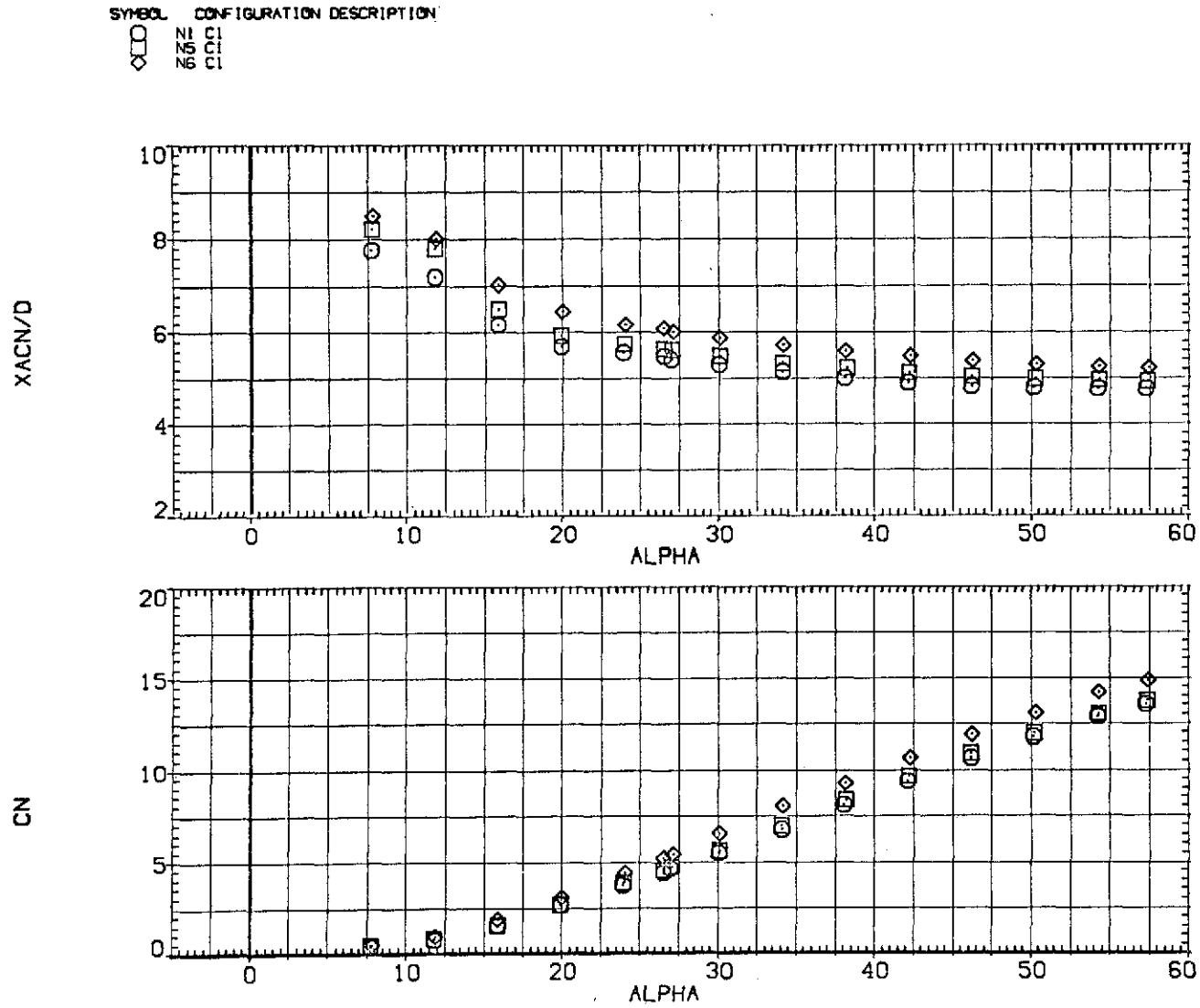

(a) x_{ac_N}/d and C_N versus α.

Figure 18.– Effect of nose strakes; $M = 1.5$, $Re = 3.8 \times 10^5$.

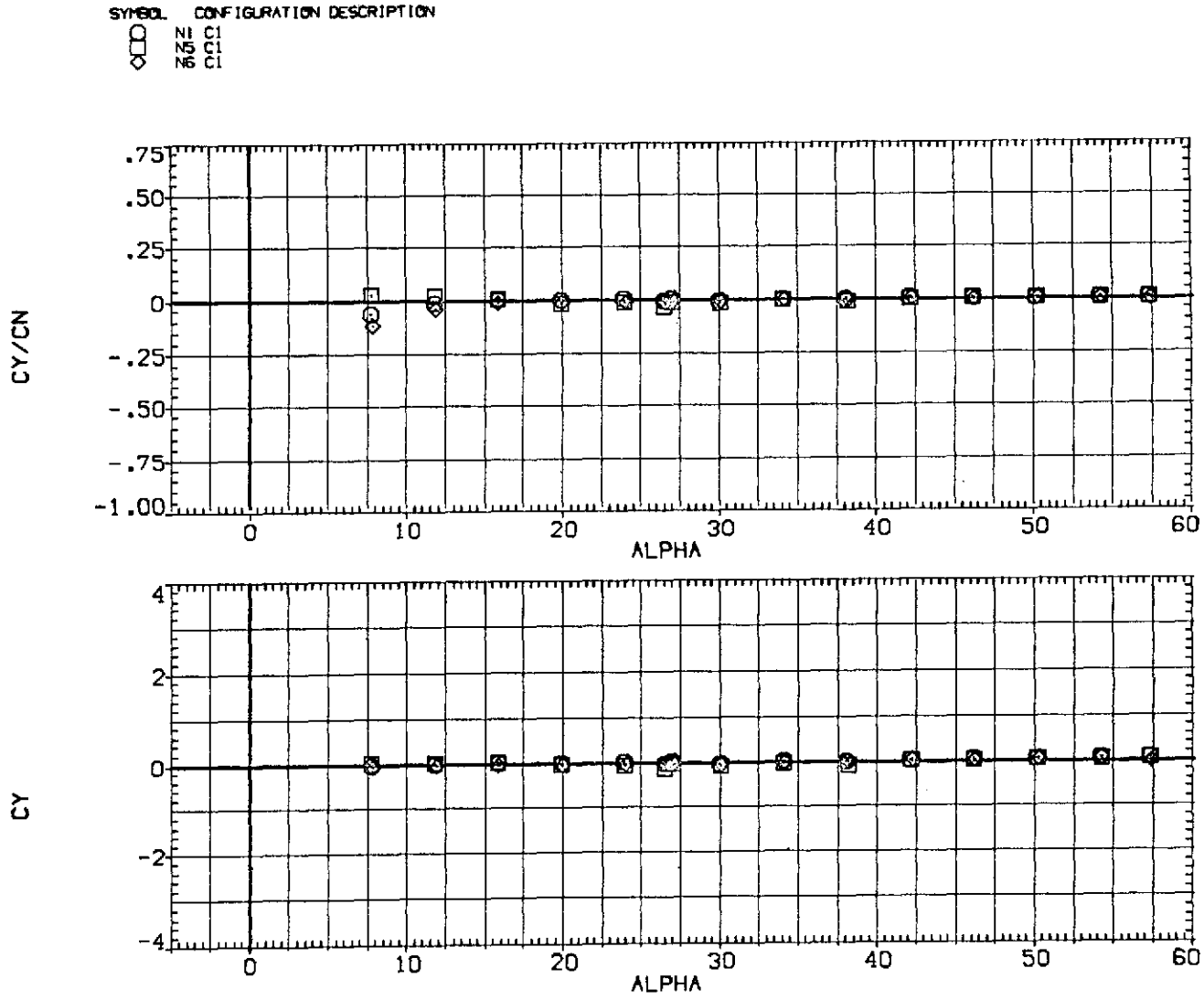

(b) C_Y/C_N and C_Y versus α.

Figure 18.– Continued.

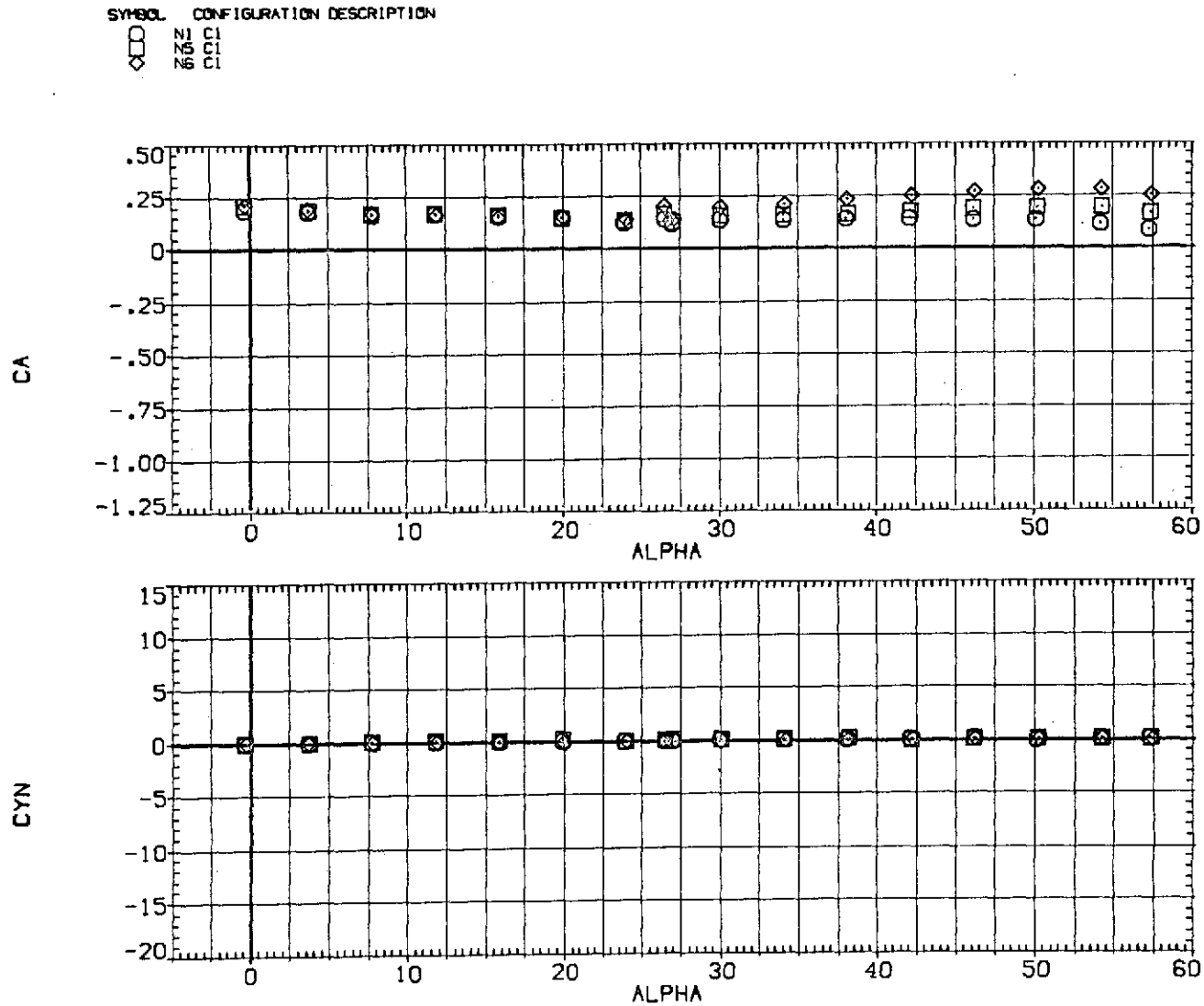

(c) C_A and C_n versus α.

Figure 18.– Concluded.

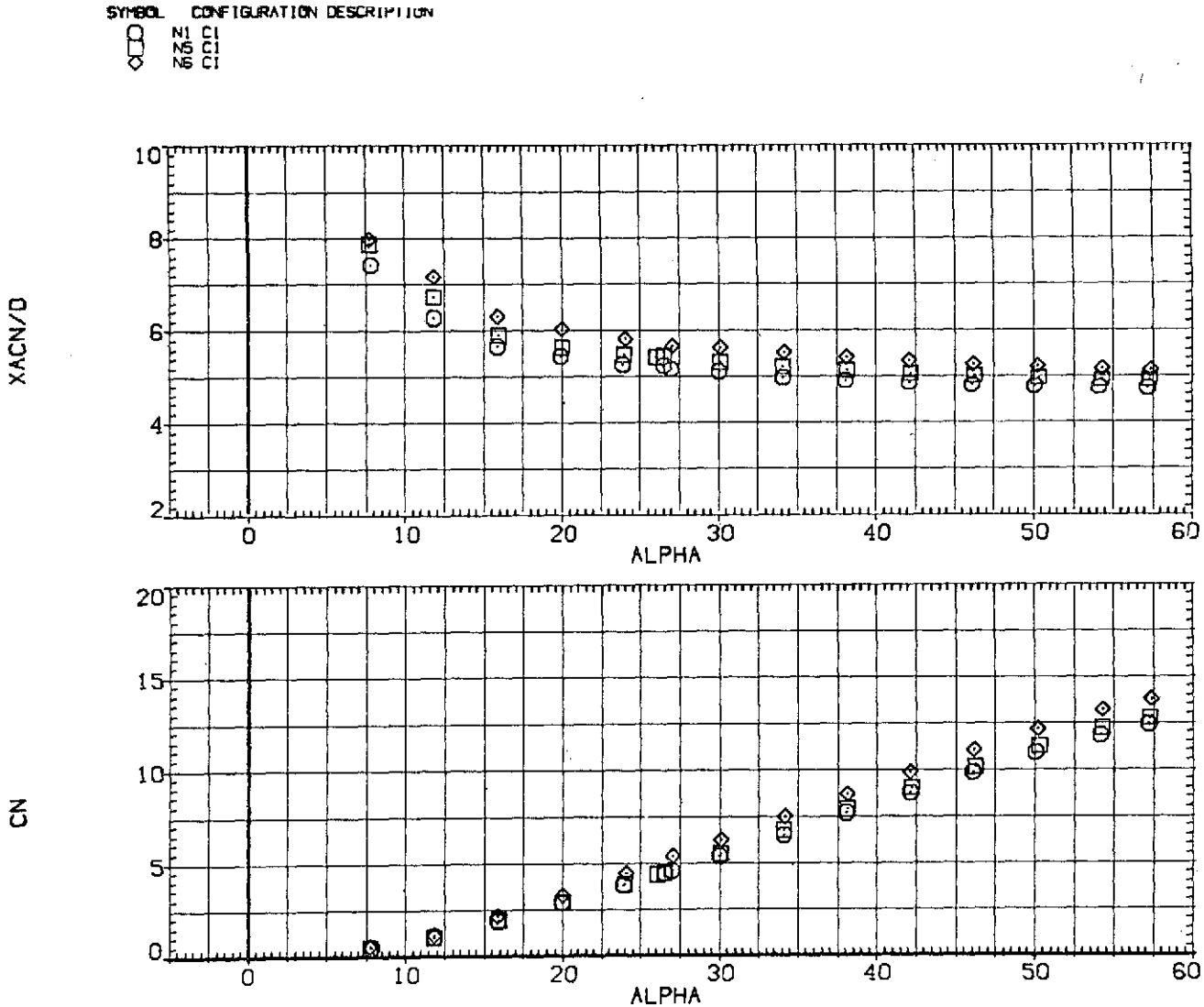

(a) x_{ac_N}/d and C_N versus α.

Figure 19.– Effect of nose strakes; $M = 2.0$, $Re = 3.8 \times 10^5$.

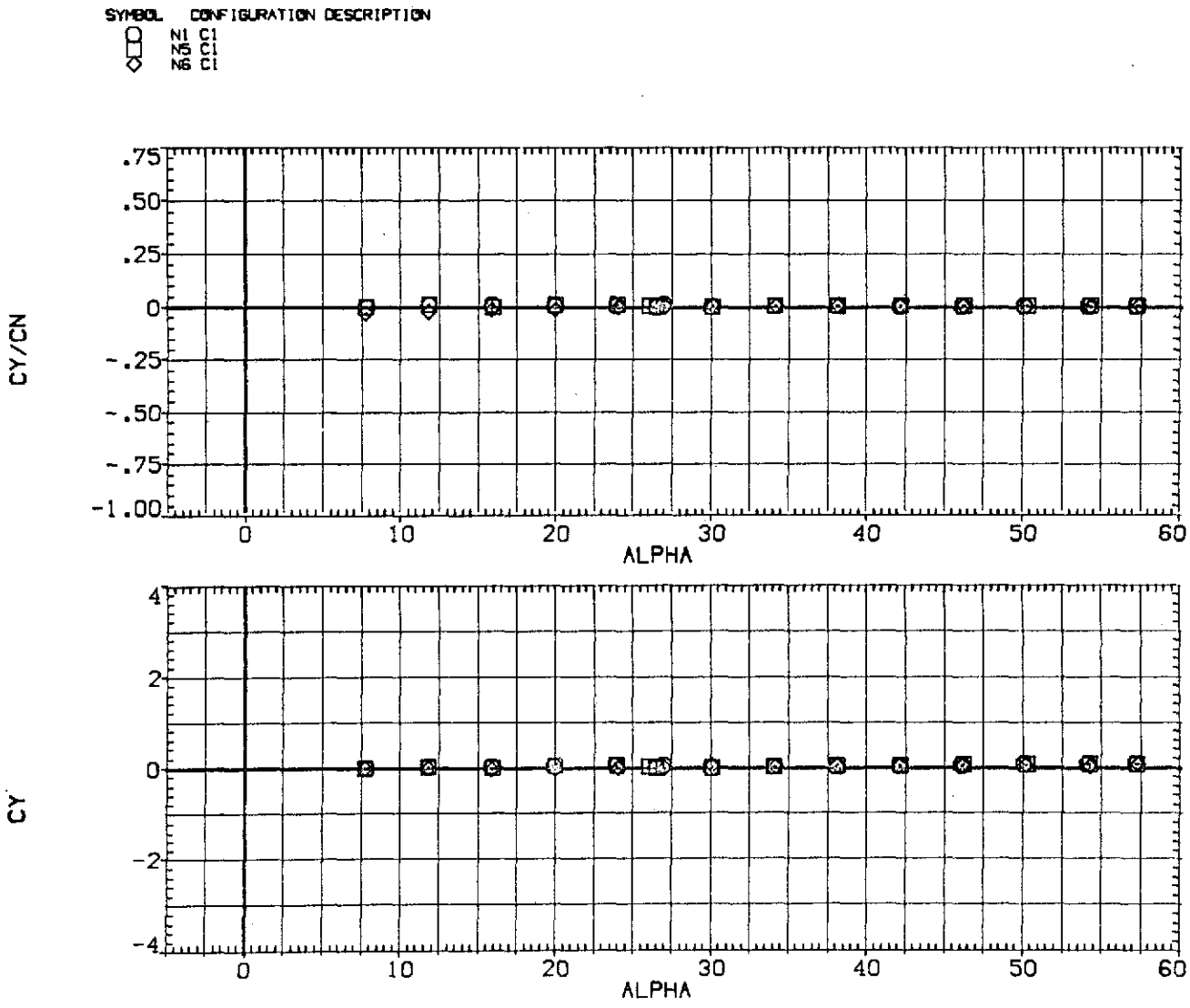

(b) C_Y/C_N and C_Y versus α.

Figure 19.– Continued.

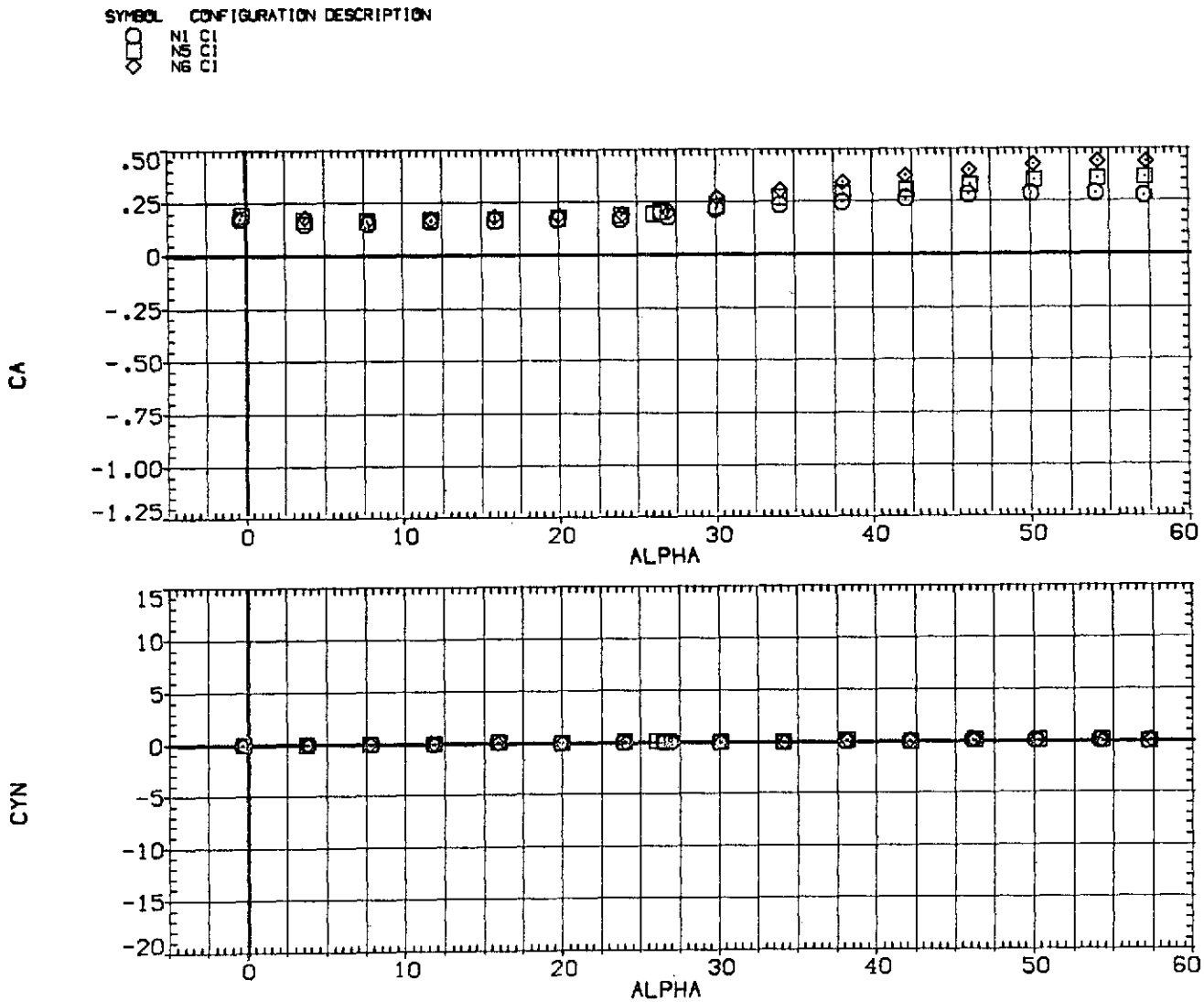

(c) C_A and C_n versus α.

Figure 19.– Concluded.

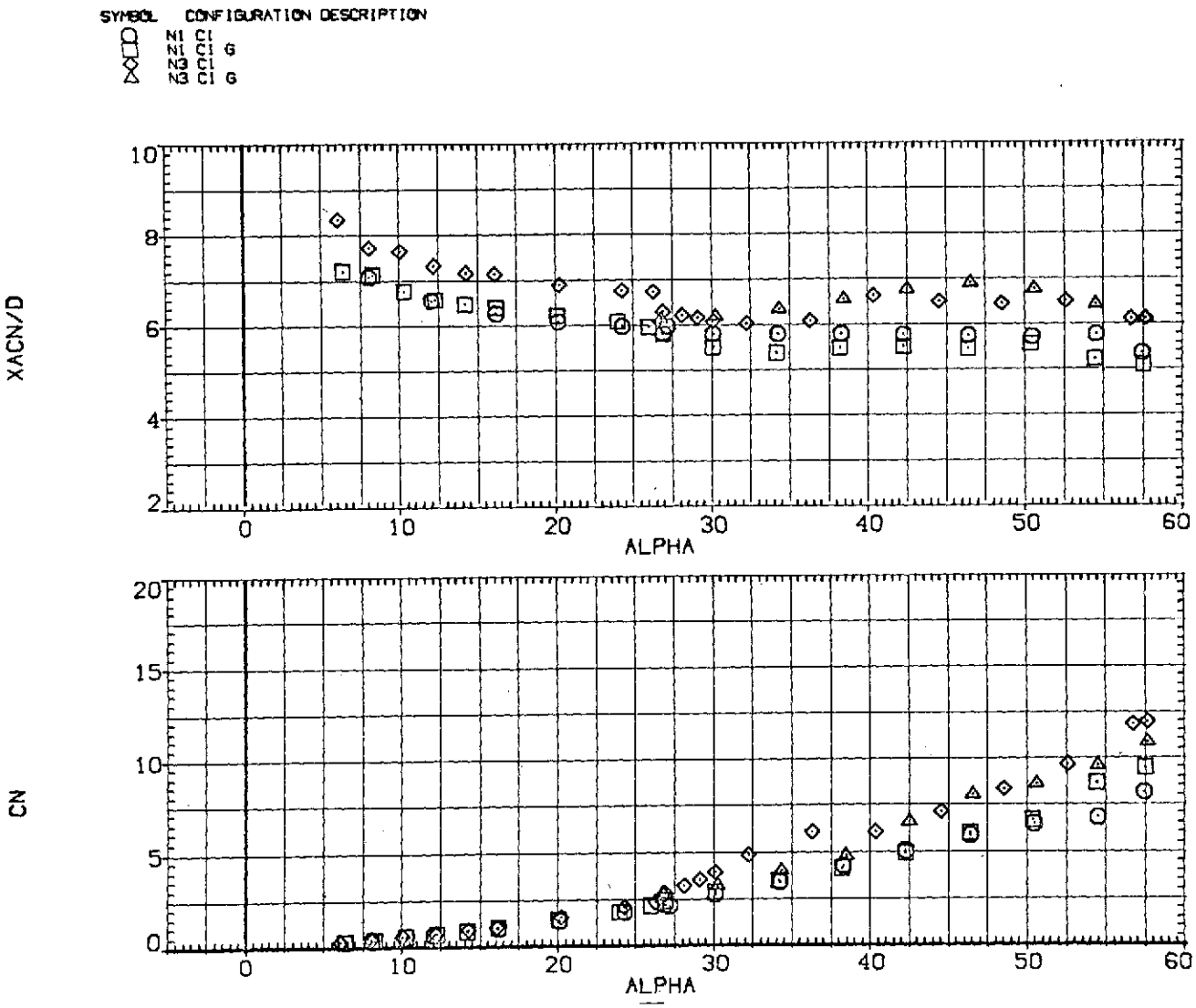

(a) x_{ac_N}/d and C_N versus α.

Figure 20.– Effect of grit ring around nose; $M = 0.6$, $Re = 6.5 \times 10^5$.

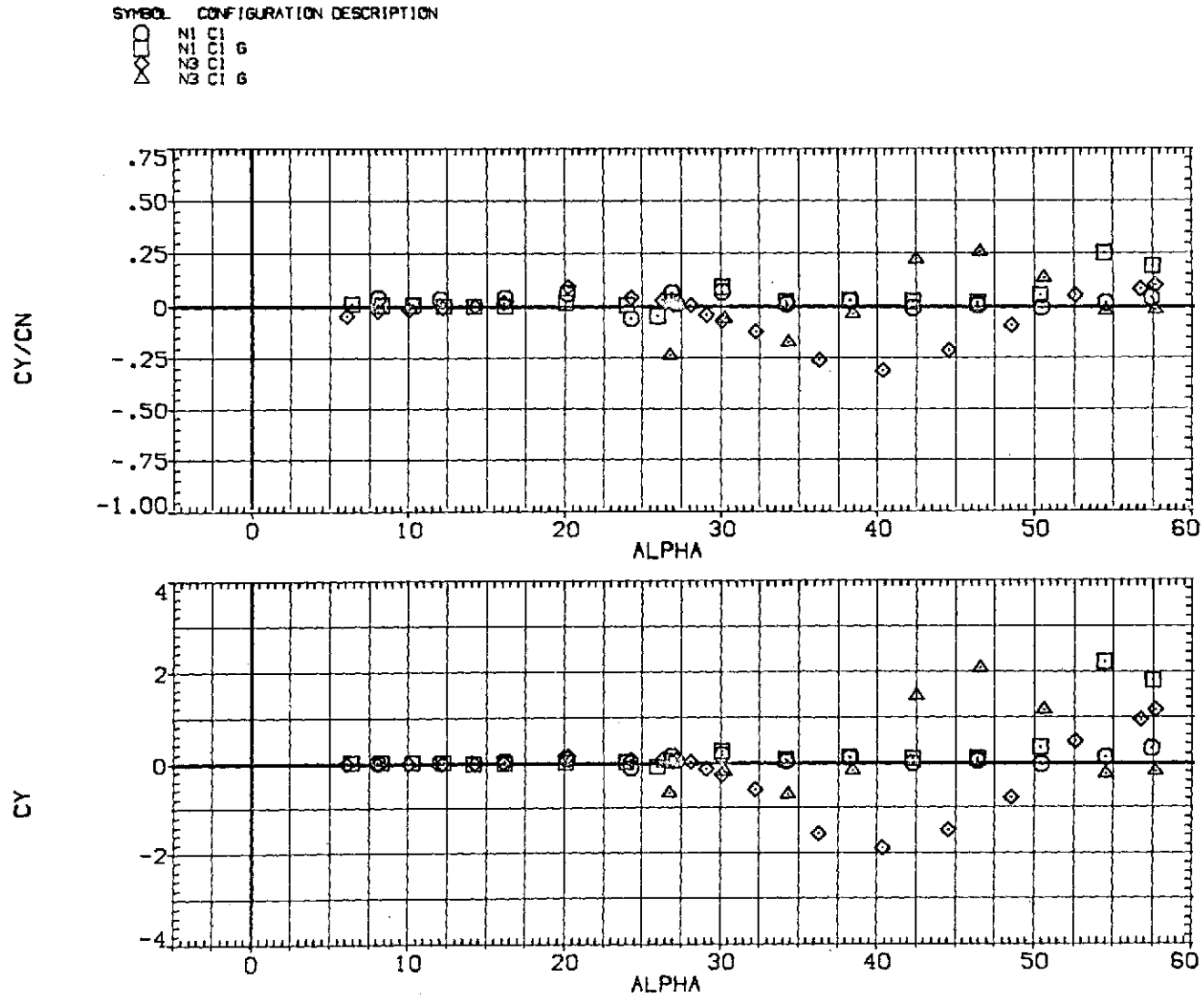

(b) C_Y/C_N and C_Y versus α.

Figure 20.– Continued.

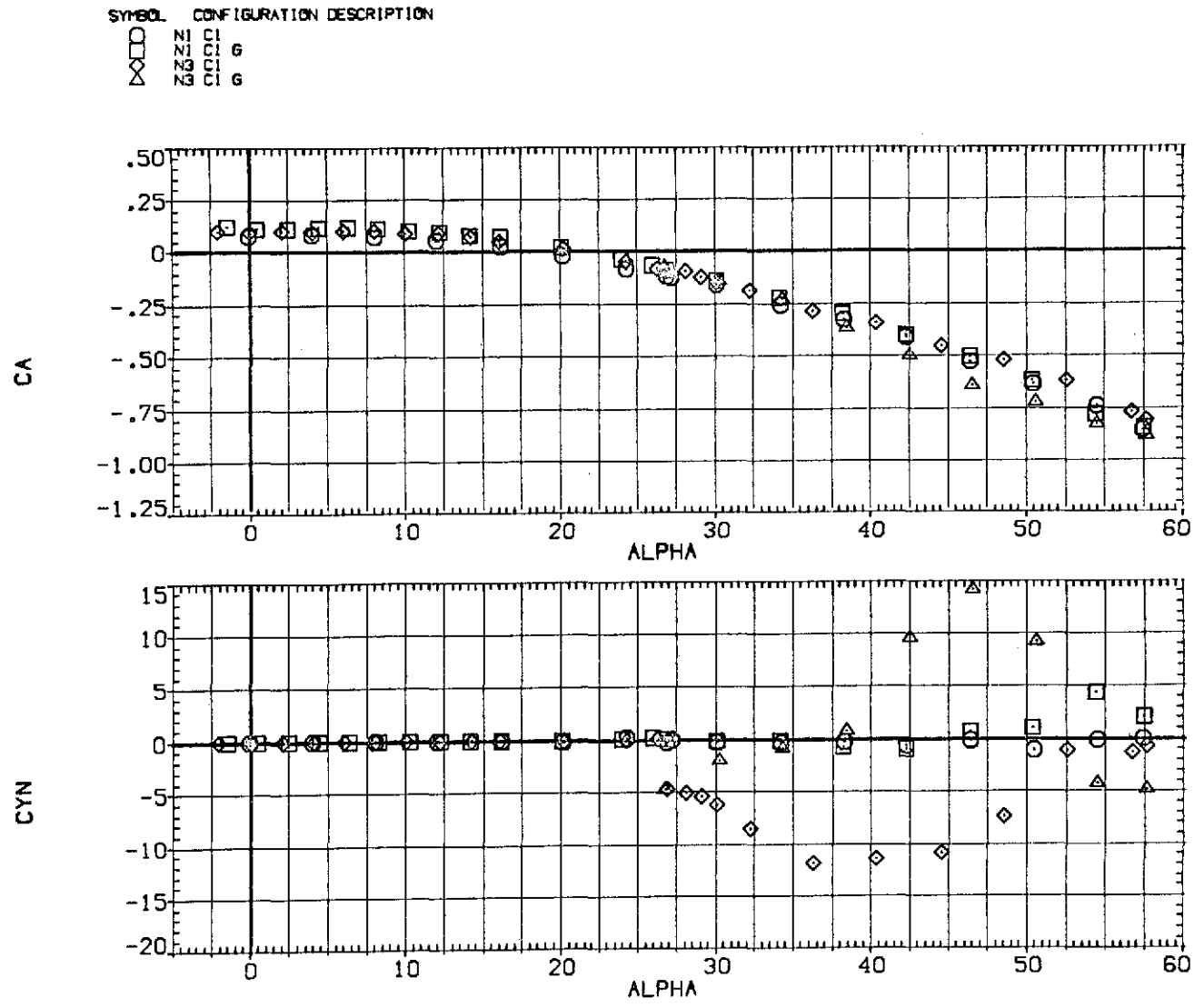

(c) C_A and C_n versus α.

Figure 20.– Concluded.

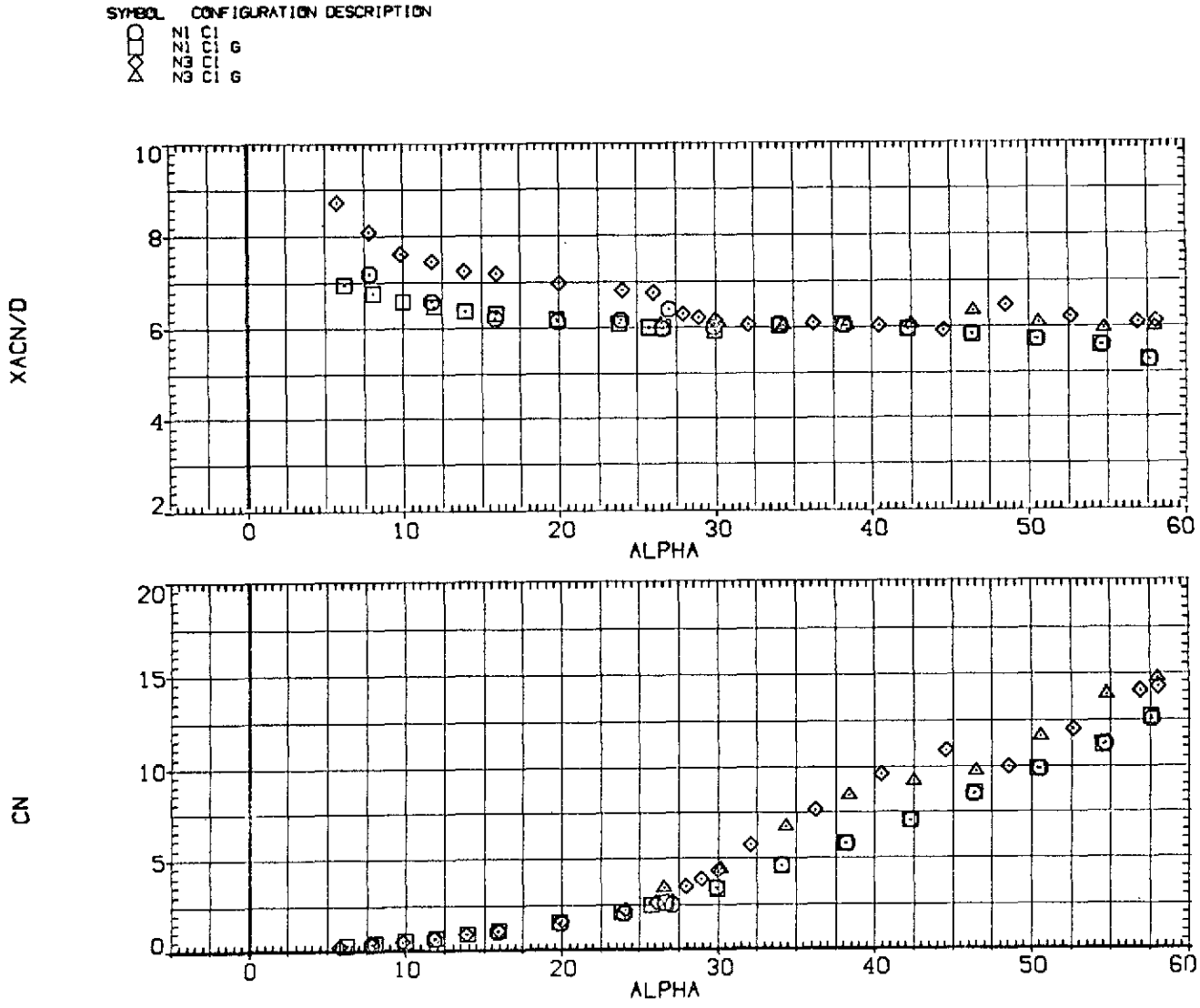

(a) x_{ac_N}/d and C_N versus α.

Figure 21.– Effect of grit ring around nose; $M = 0.9$, $Re = 6.5 \times 10^5$.

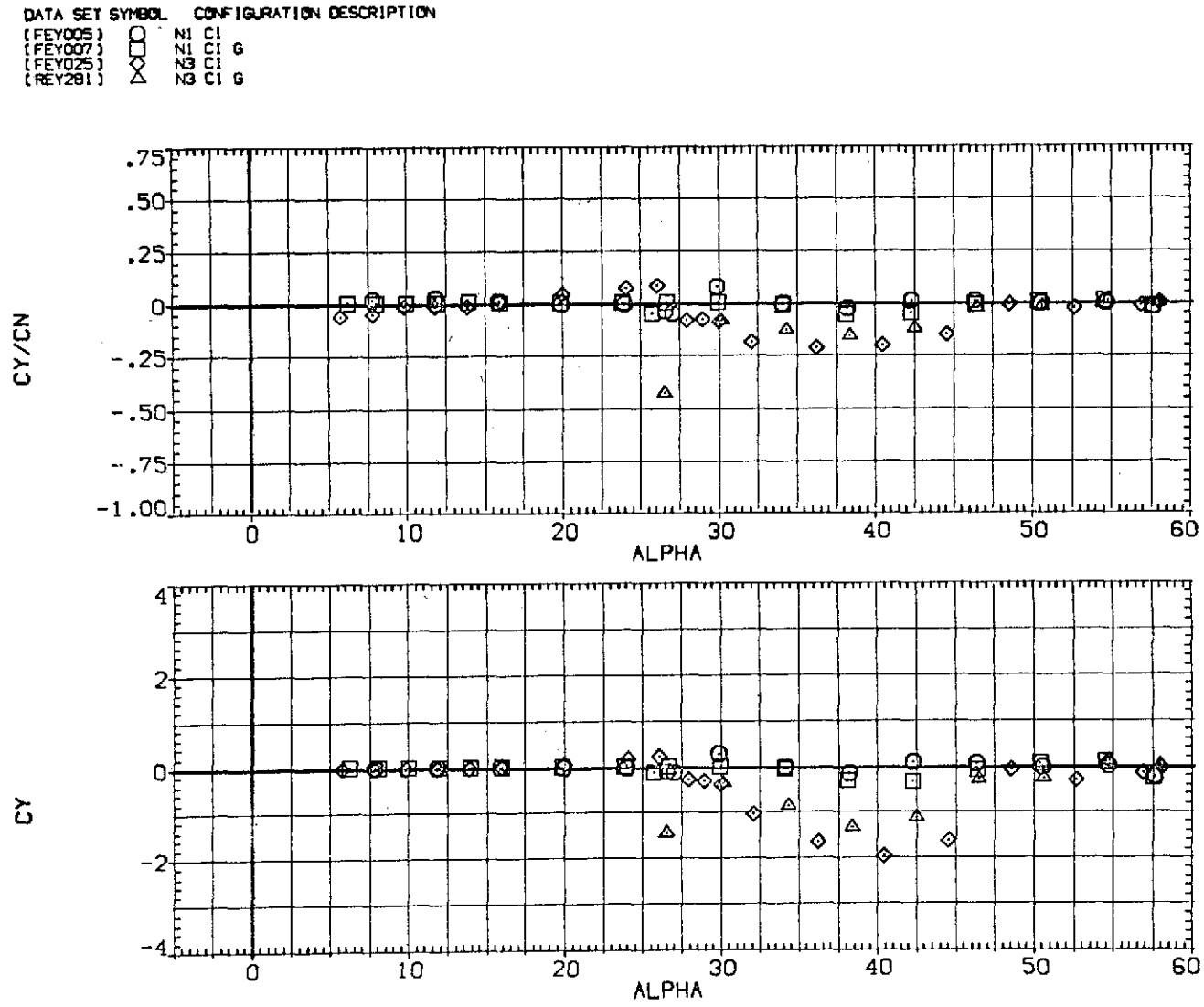

(b) C_Y/C_N and C_Y versus α.

Figure 21.– Continued.

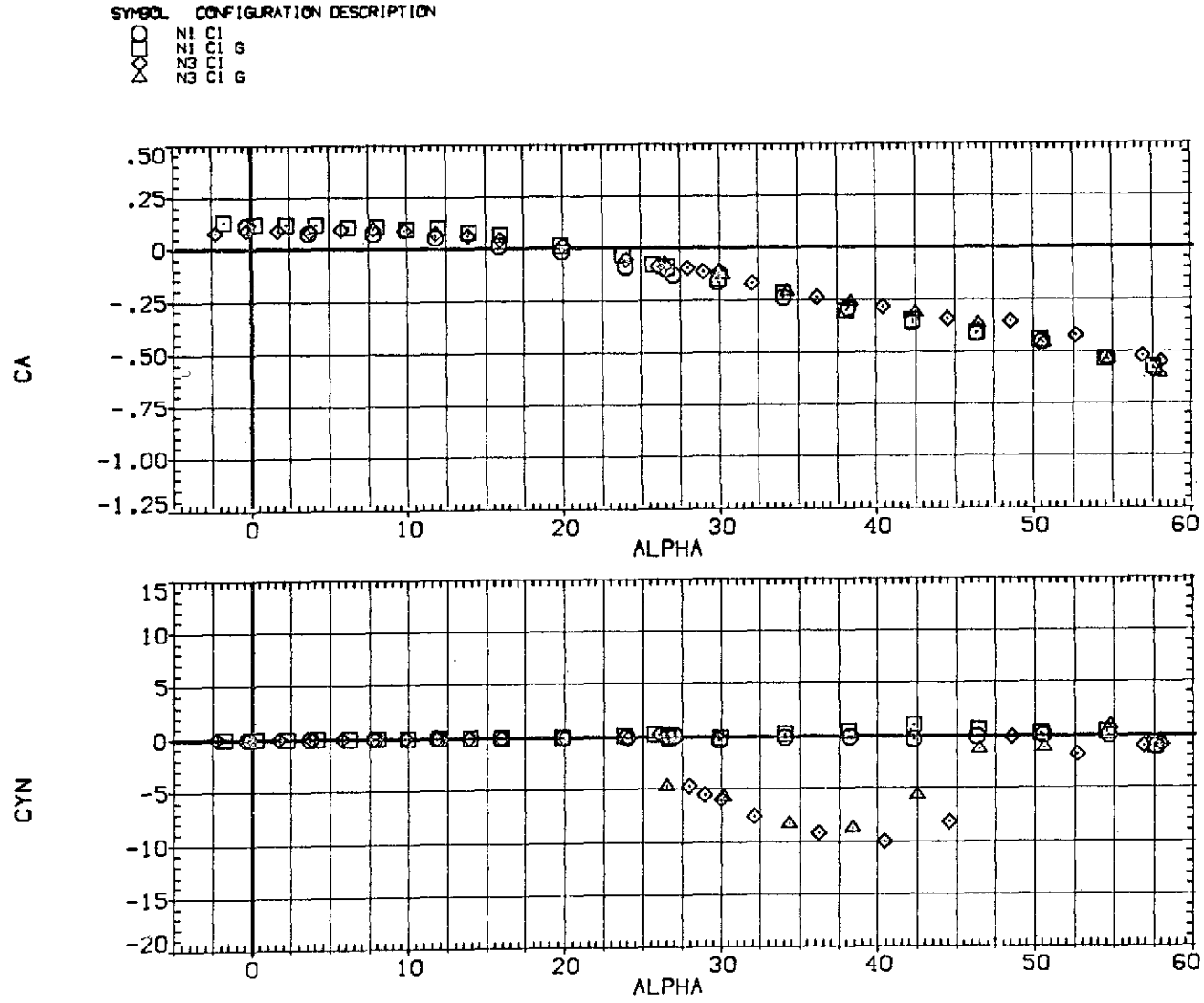

(c) C_A and C_n versus α.

Figure 21.– Concluded.

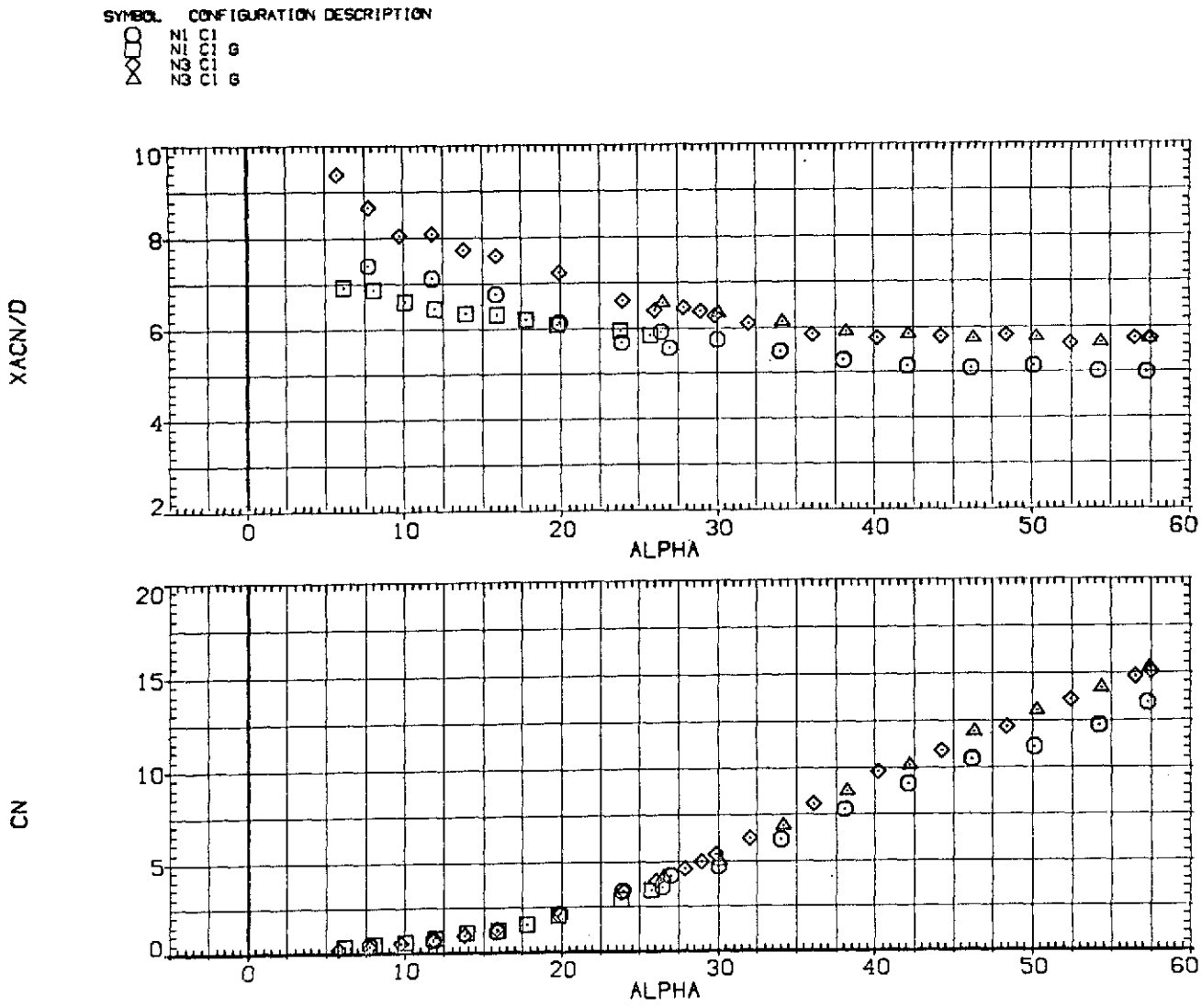

(a) x_{ac_N}/d and C_N versus α.

Figure 22.– Effect of grit ring around nose; $M = 1.2$, $Re = 3.8 \times 10^5$.

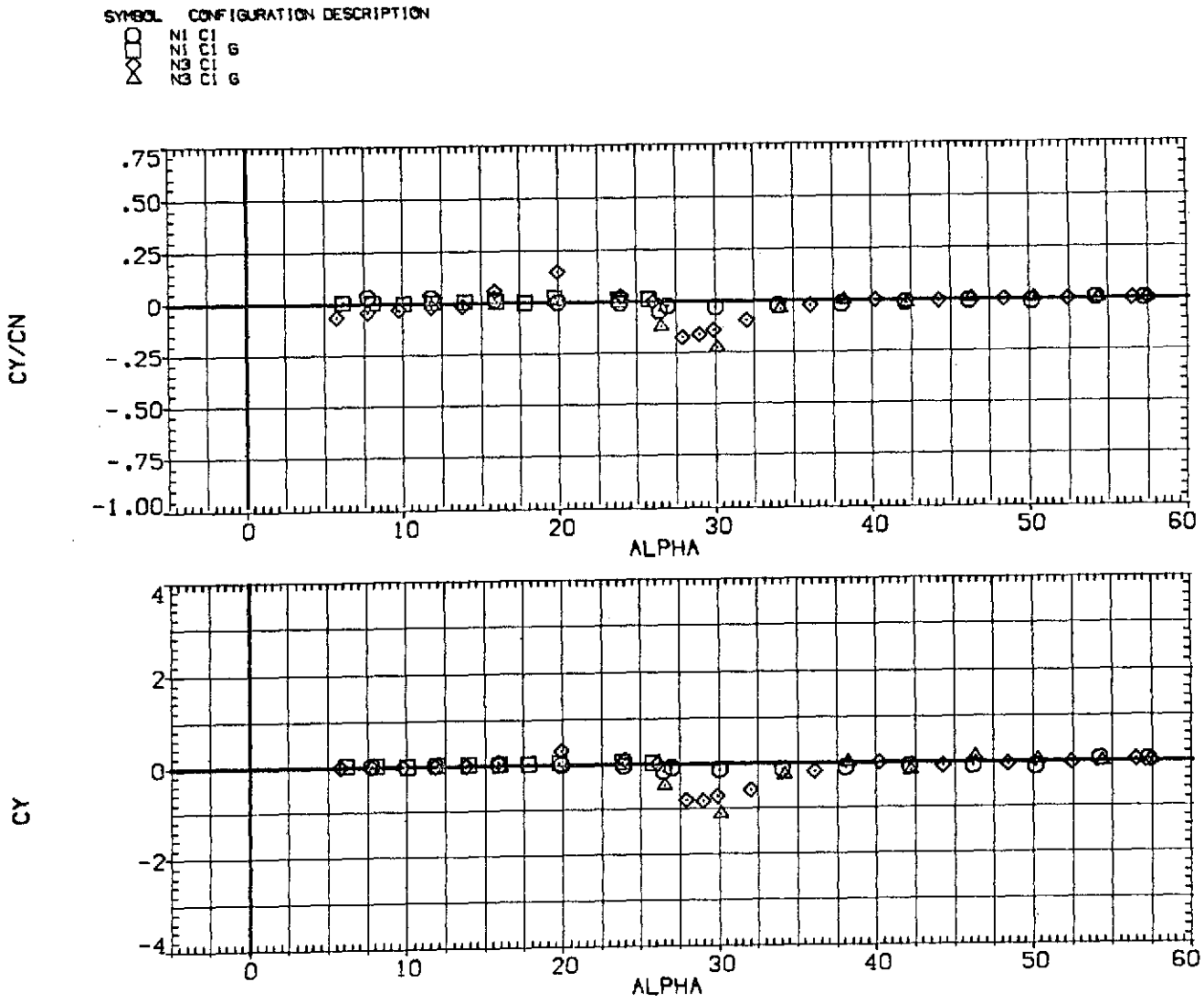

(b) C_Y/C_N and C_Y versus α.

Figure 22.– Continued.

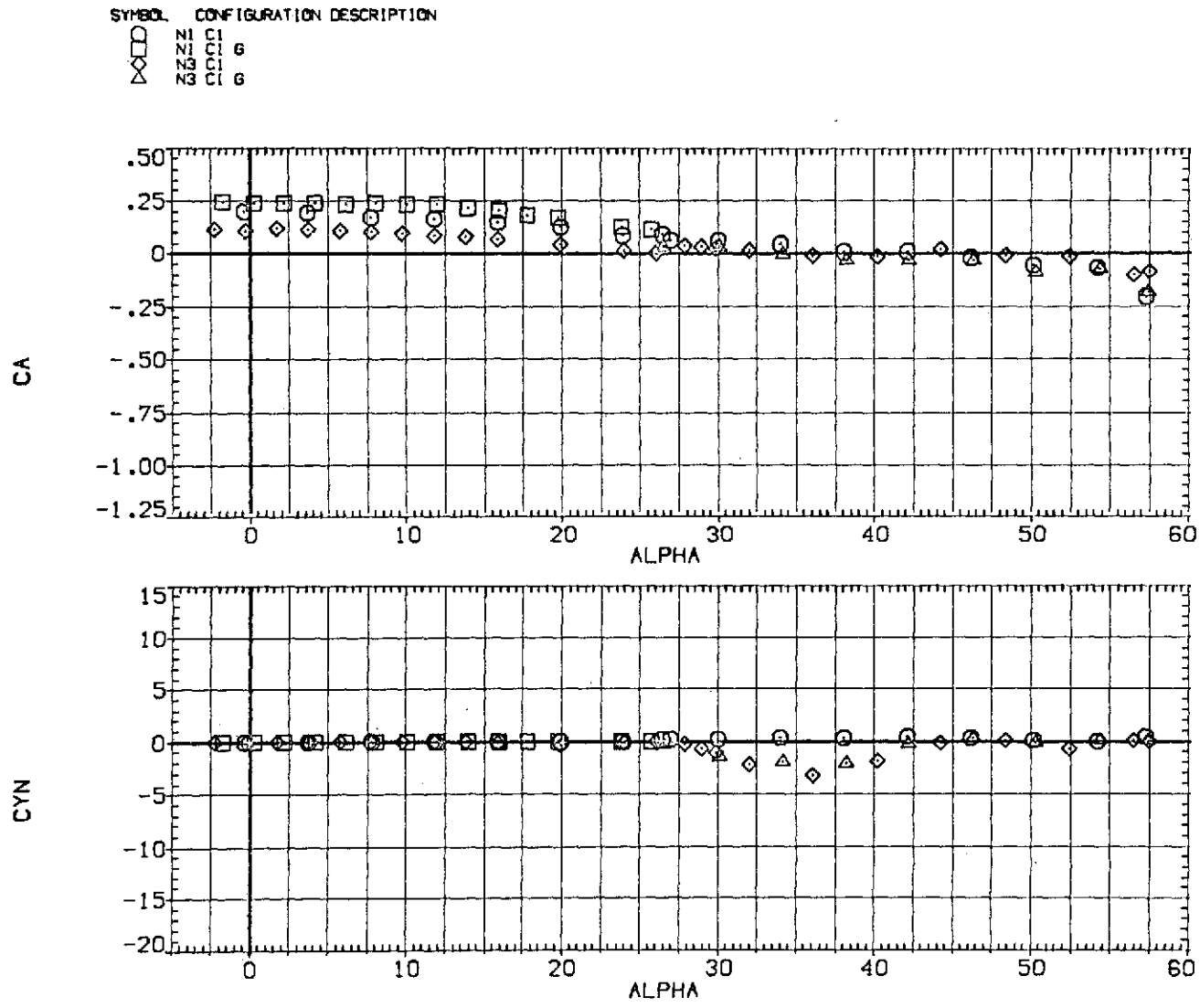

(c) C_A and C_n versus α.

Figure 22.– Concluded.

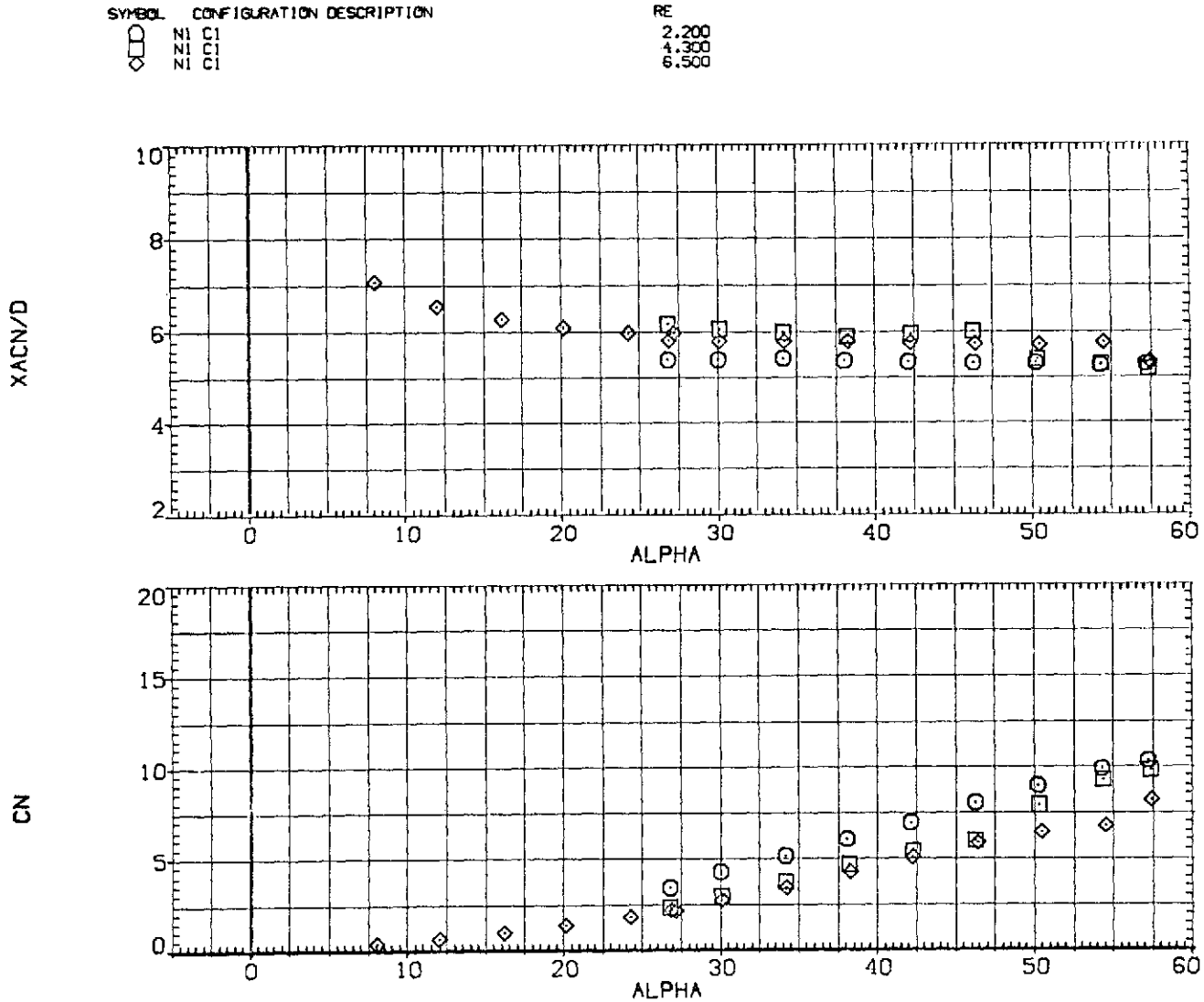

(a) x_{ac_N}/d and C_N versus α.

Figure 23.– Effect of Reynolds number for $N_1 C_1$; $M = 0.6$.

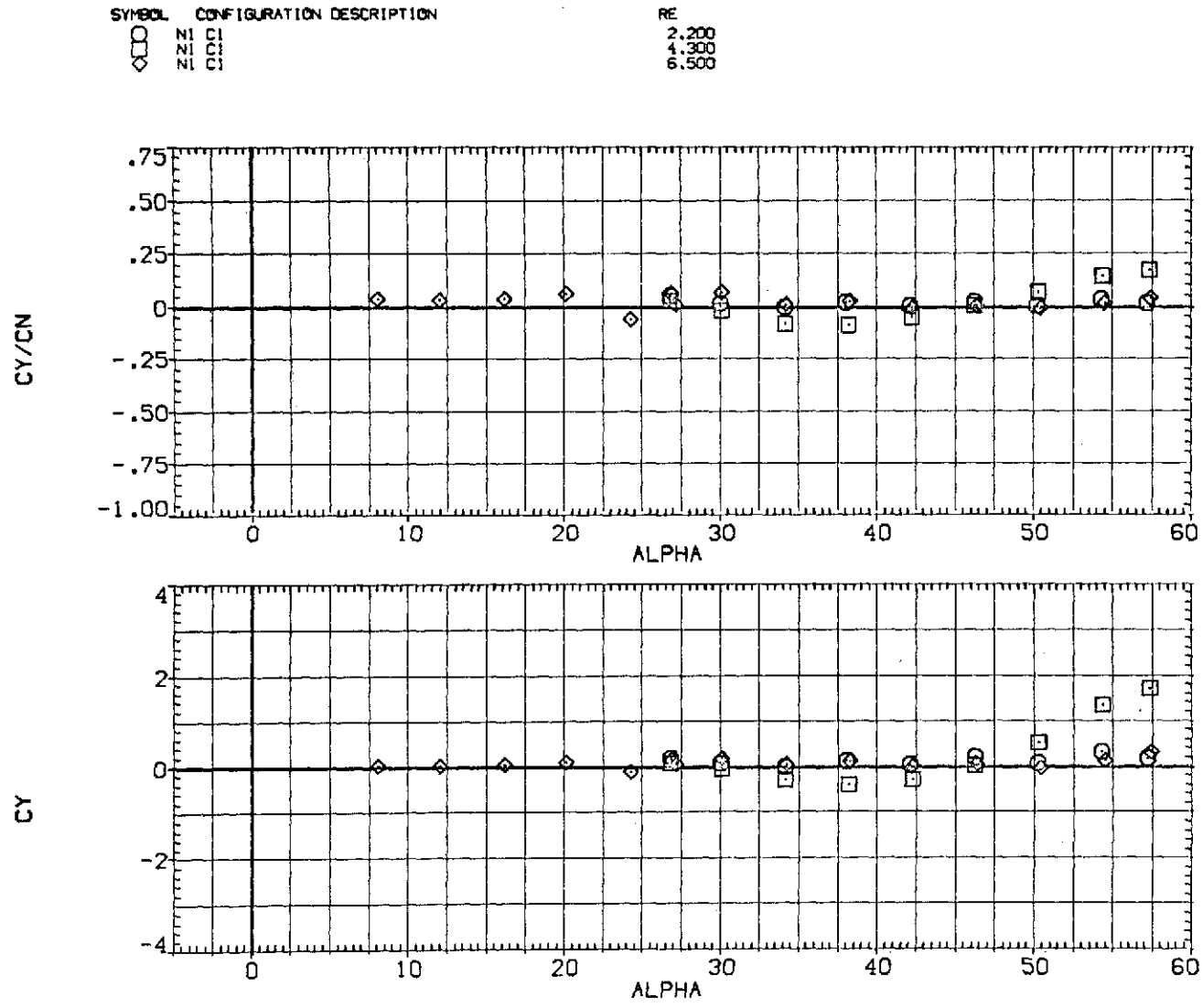

(b) C_Y/C_N and C_Y versus α.

Figure 23.-- Continued.

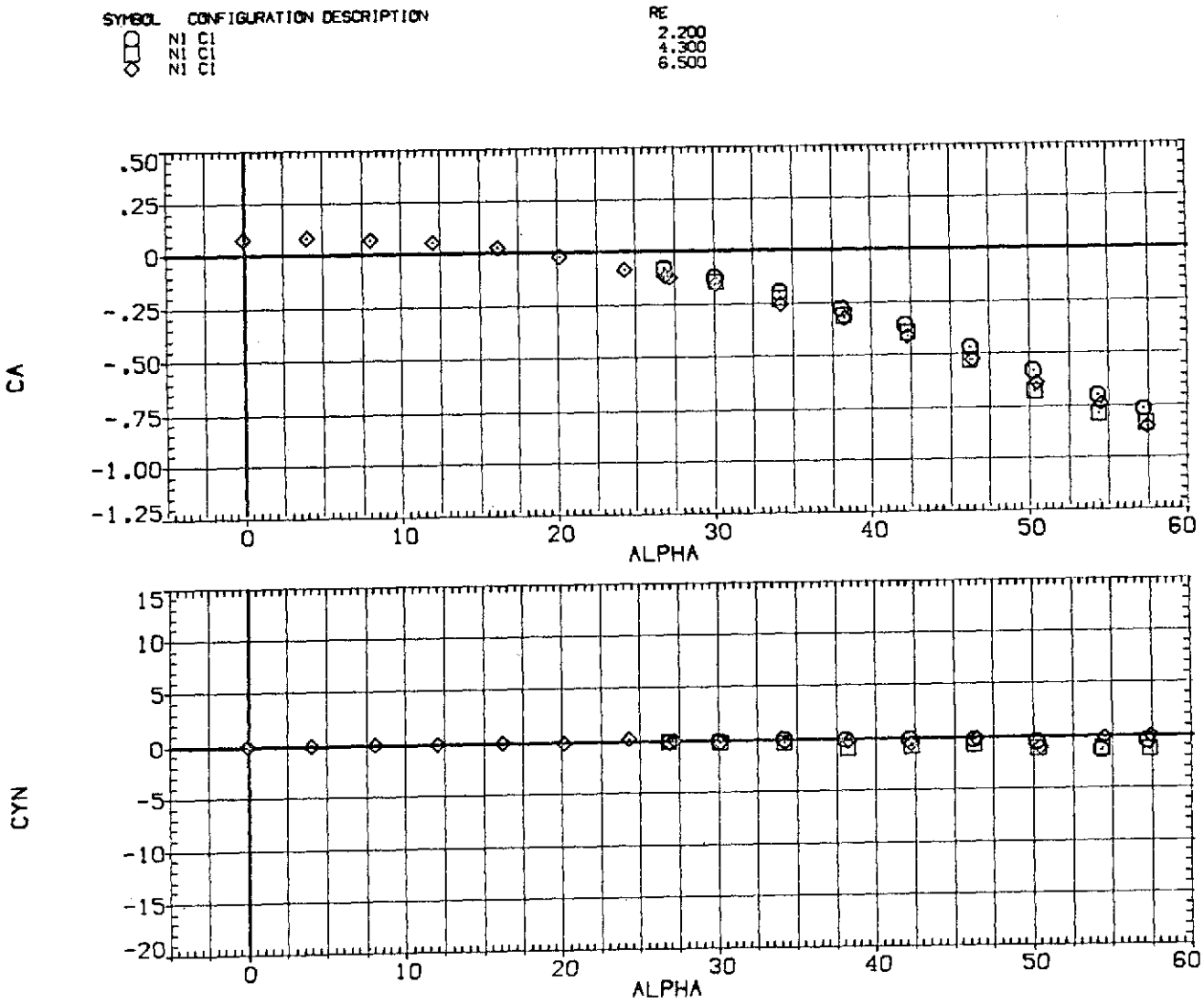

(c) C_A and C_n versus α.

Figure 23.– Concluded.

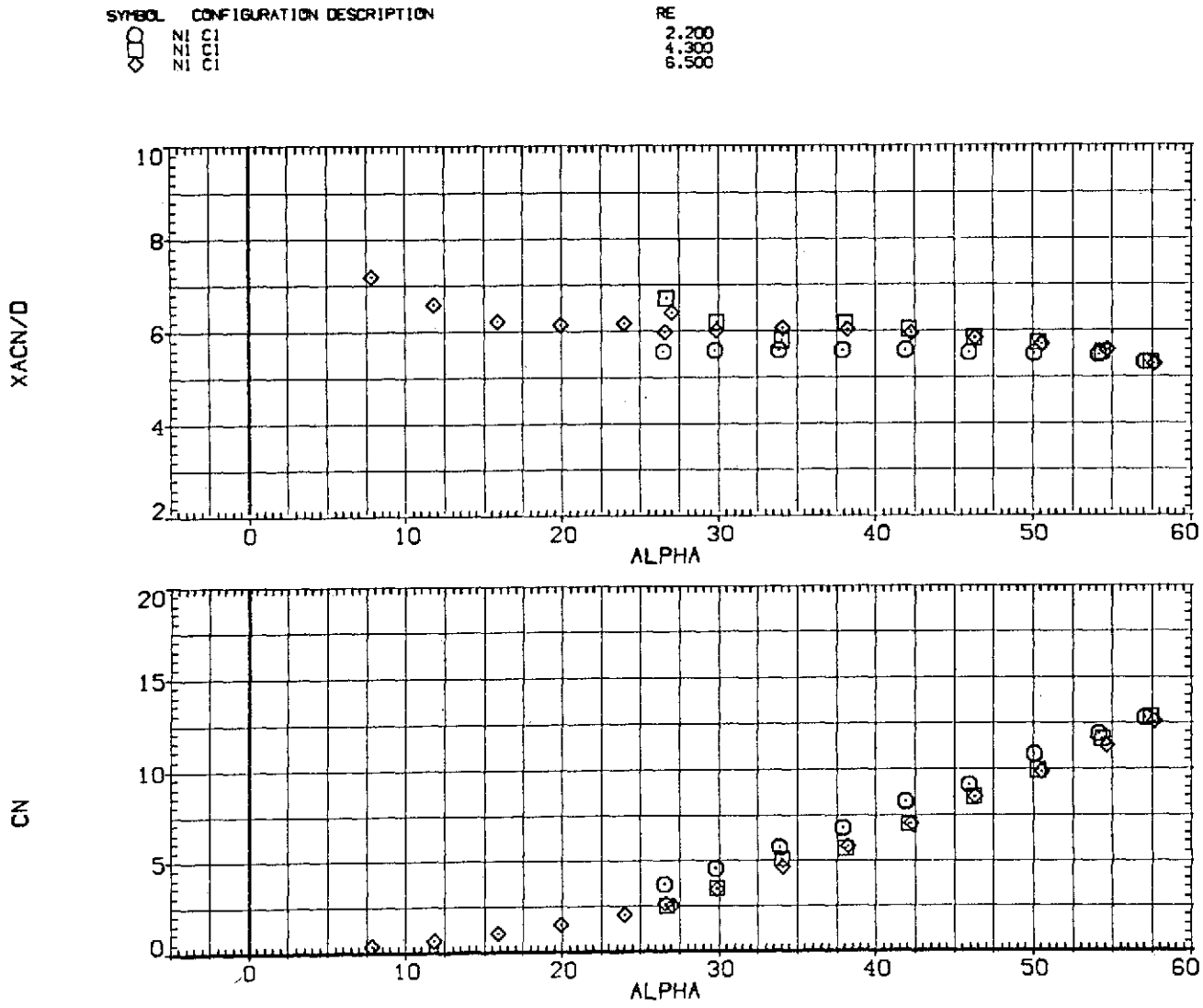

(a) x_{ac_N}/d and C_N versus α.

Figure 24.– Effect of Reynolds number for $N_1 C_1$; $M = 0.9$.

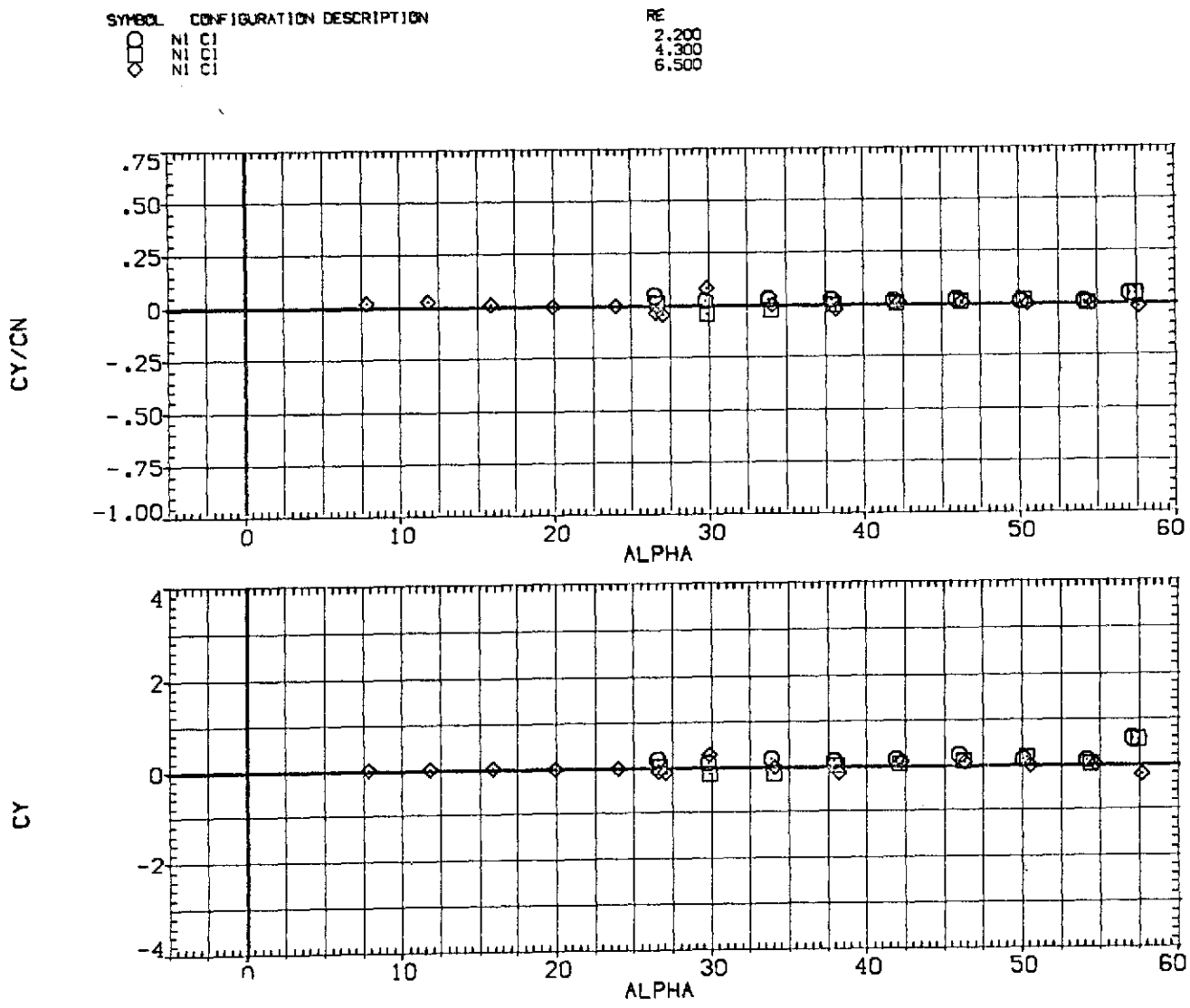

(b) C_Y/C_N and C_Y versus α.

Figure 24.– Continued.

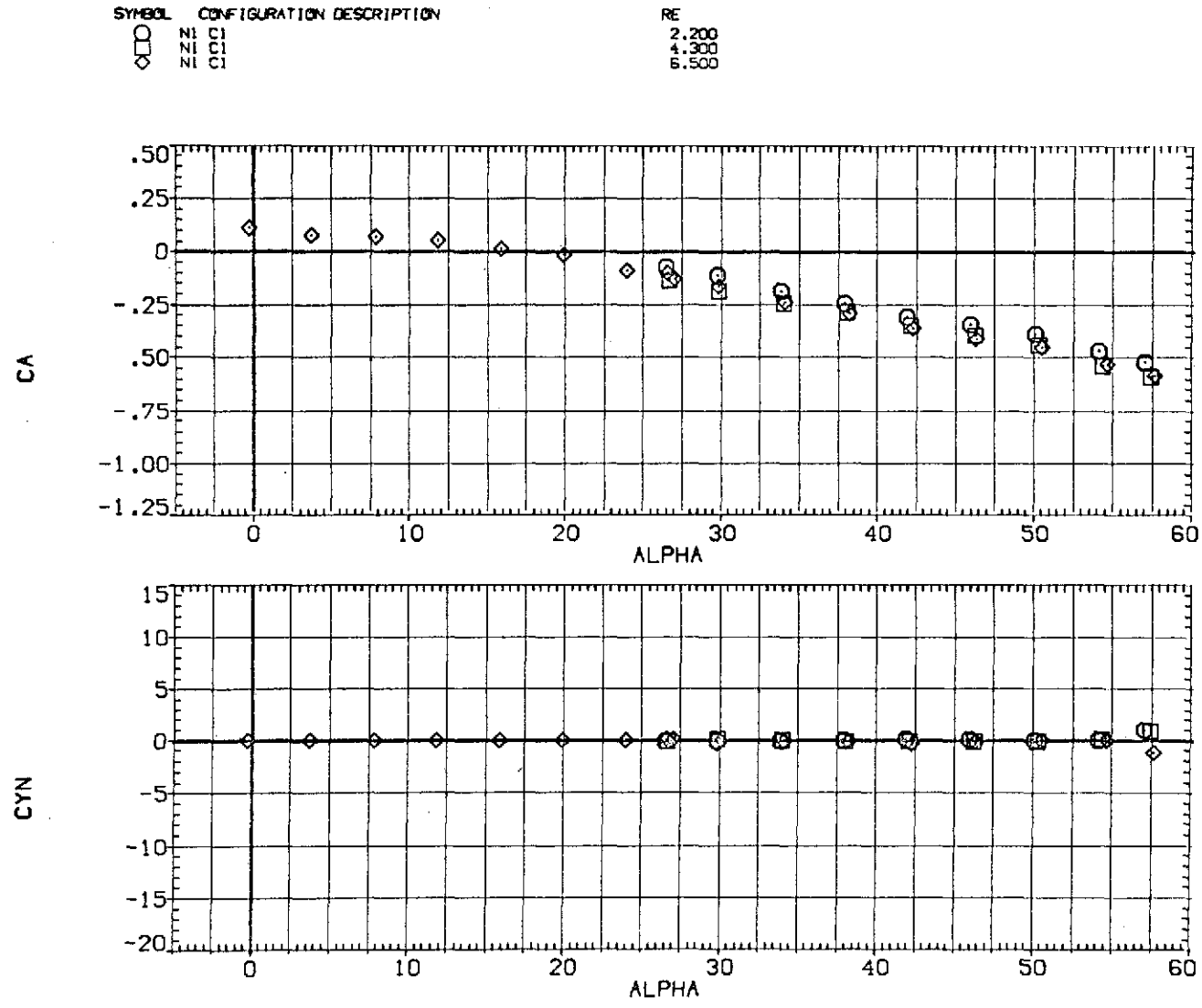

(c) C_A and C_n versus α.

Figure 24.– Concluded.

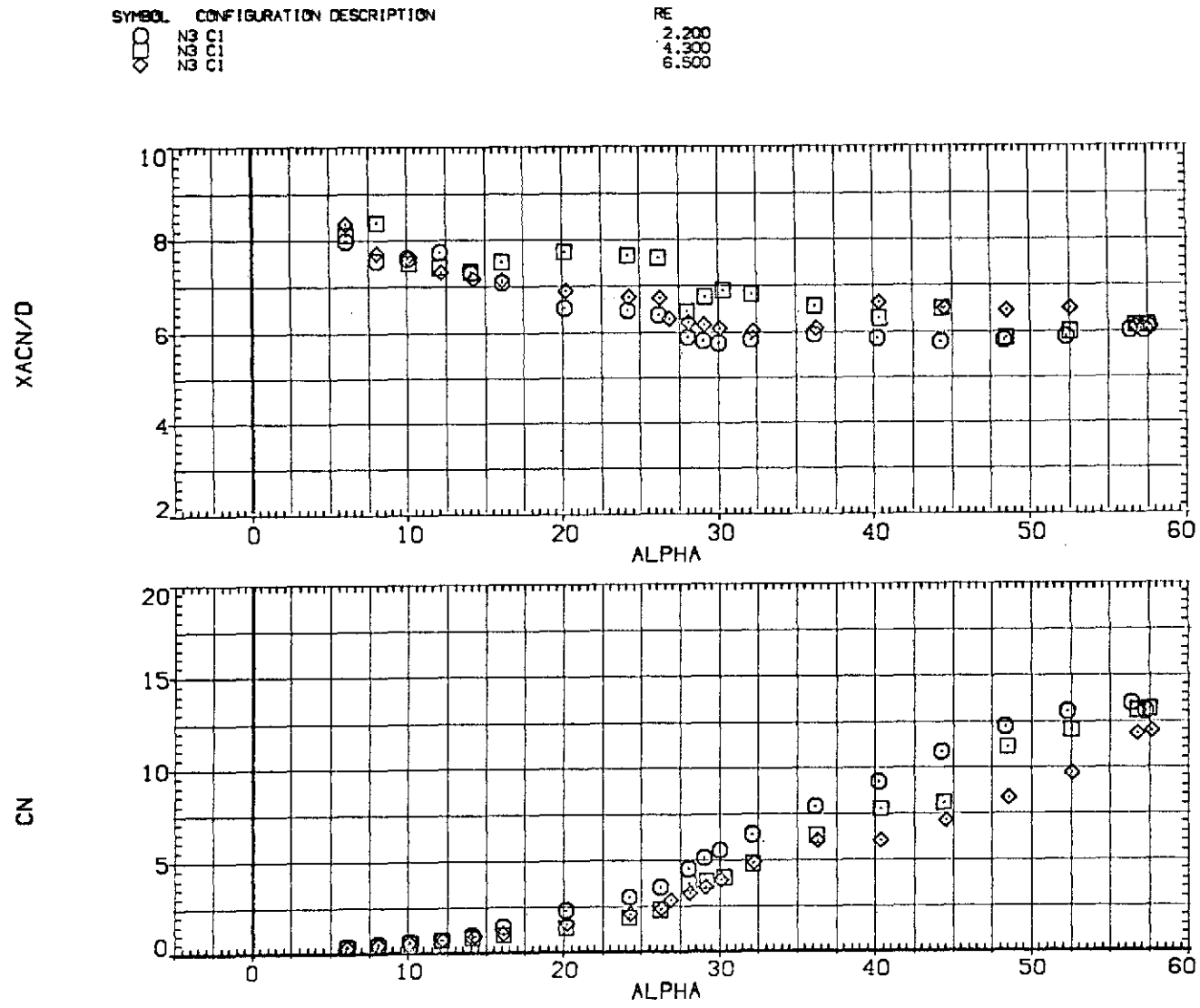

(a) x_{ac_N}/d and C_N versus α.

Figure 25.– Effect of Reynolds number for N_3C_1; $M = 0.6$.

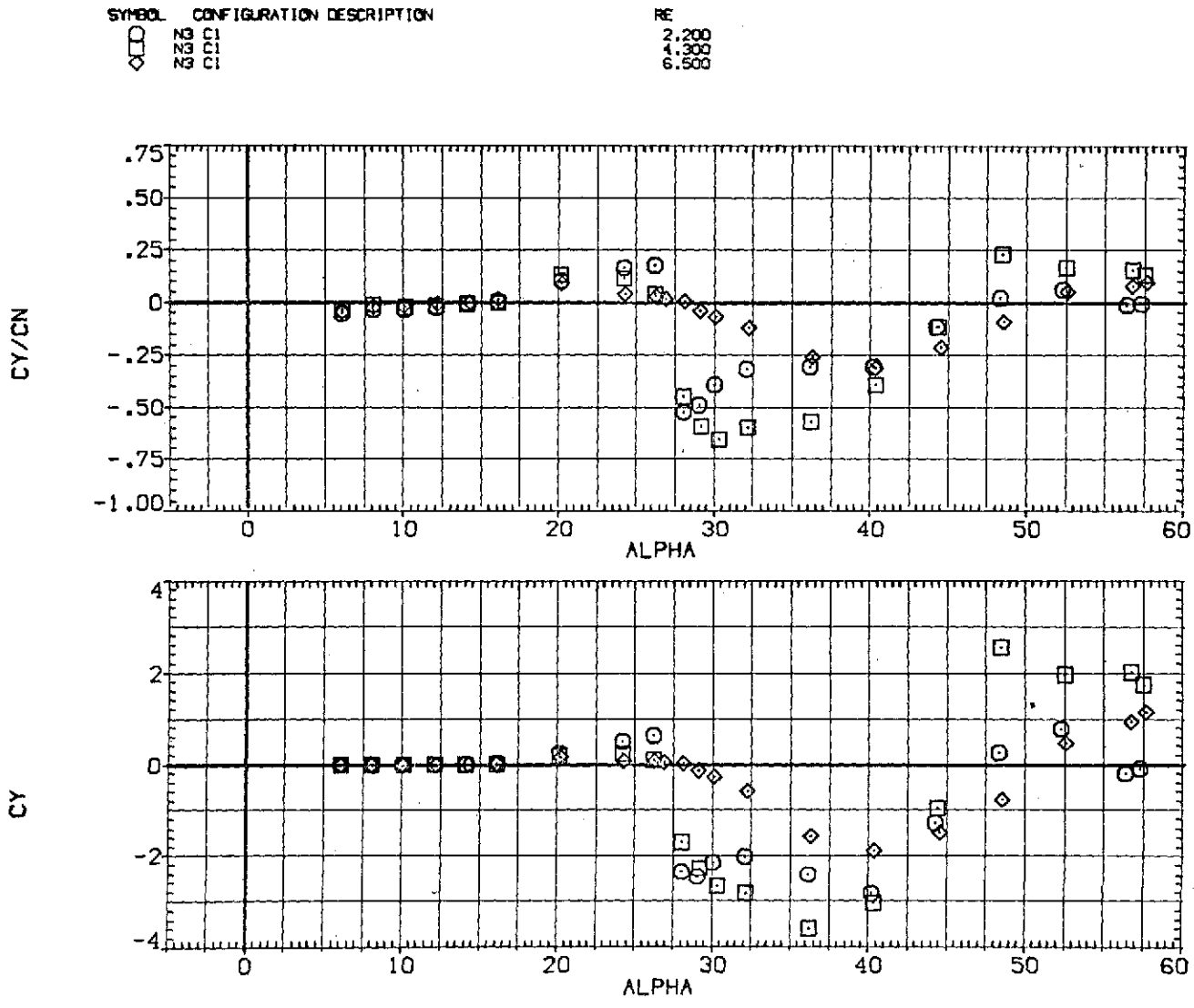

(b) C_Y/C_N and C_Y versus α.

Figure 25.-- Continued.

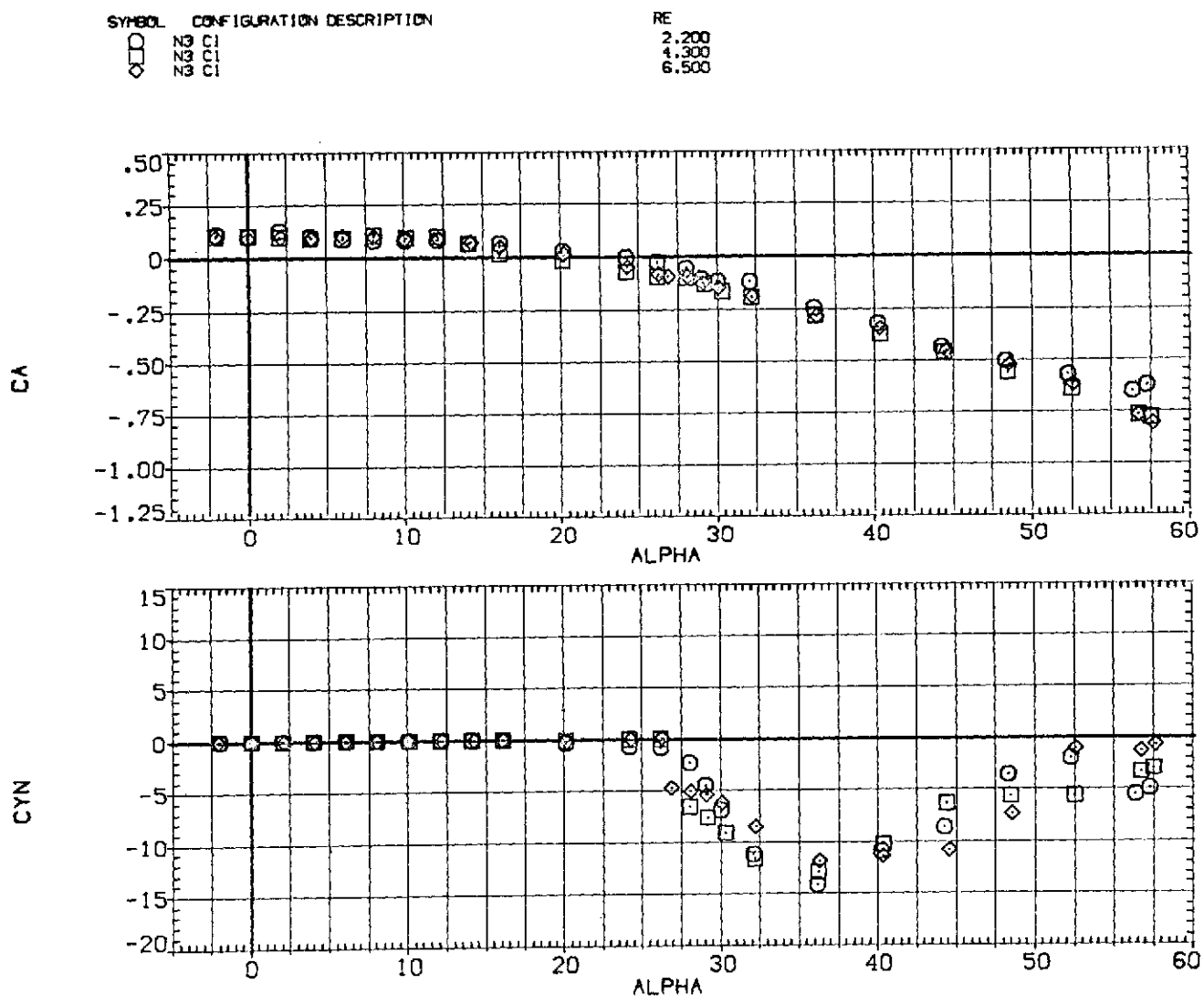

(c) C_A and C_n versus α.

Figure 25.– Concluded.

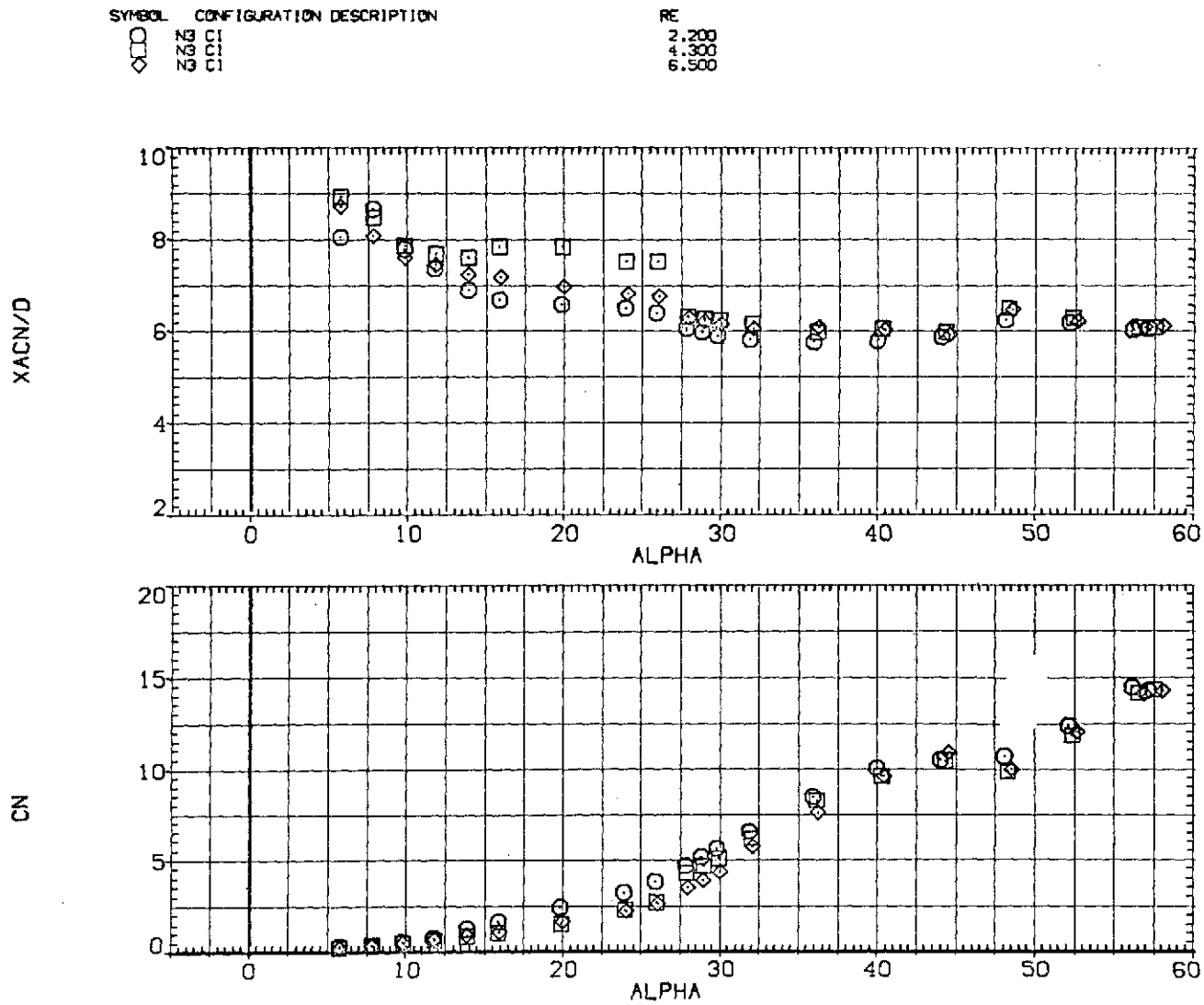

(a) x_{ac_N}/d and C_N versus α.

Figure 26.– Effect of Reynolds number for N_3C_1; $M = 0.9$.

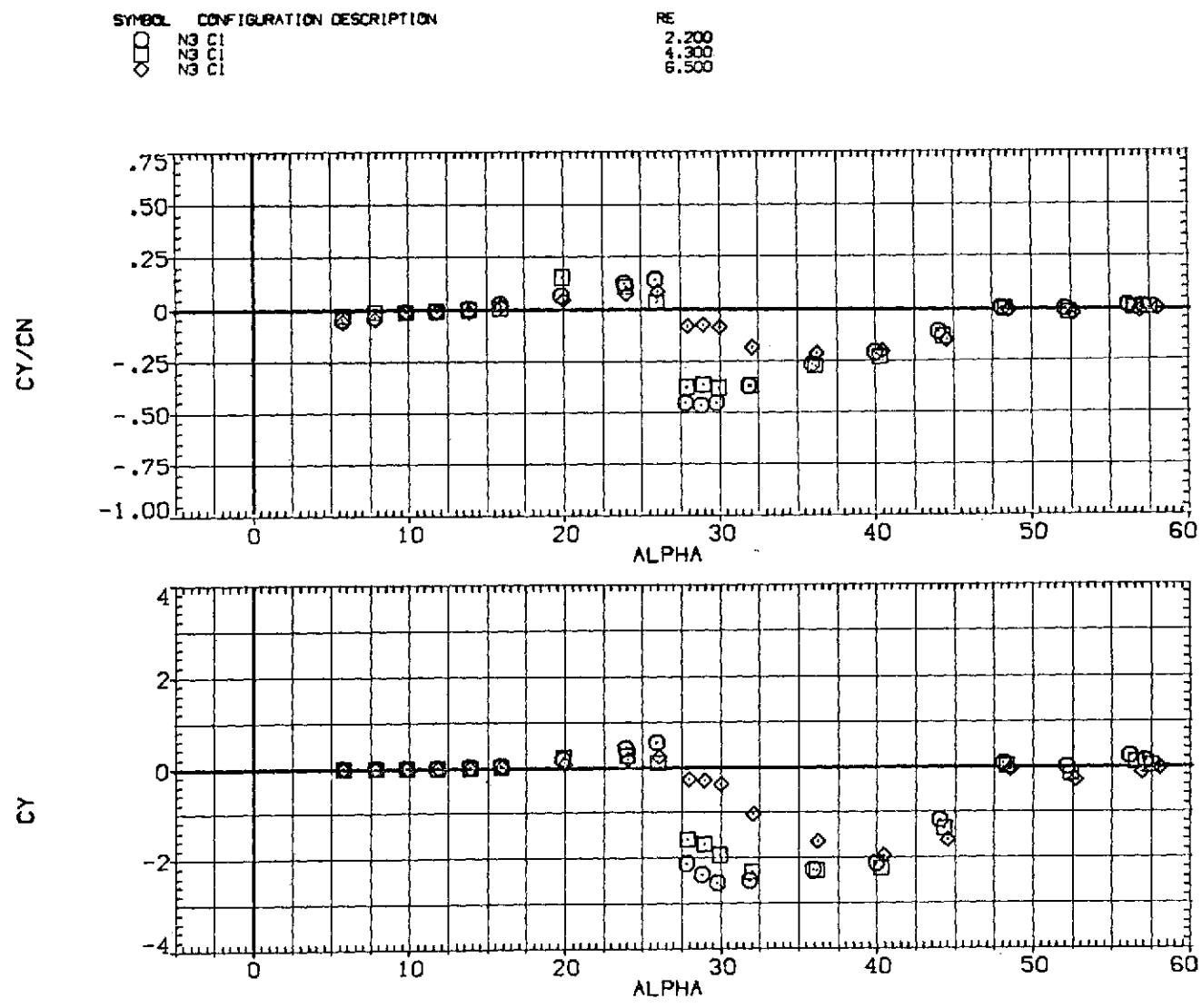

(b) C_Y/C_N and C_Y versus α.

Figure 26.– Continued.

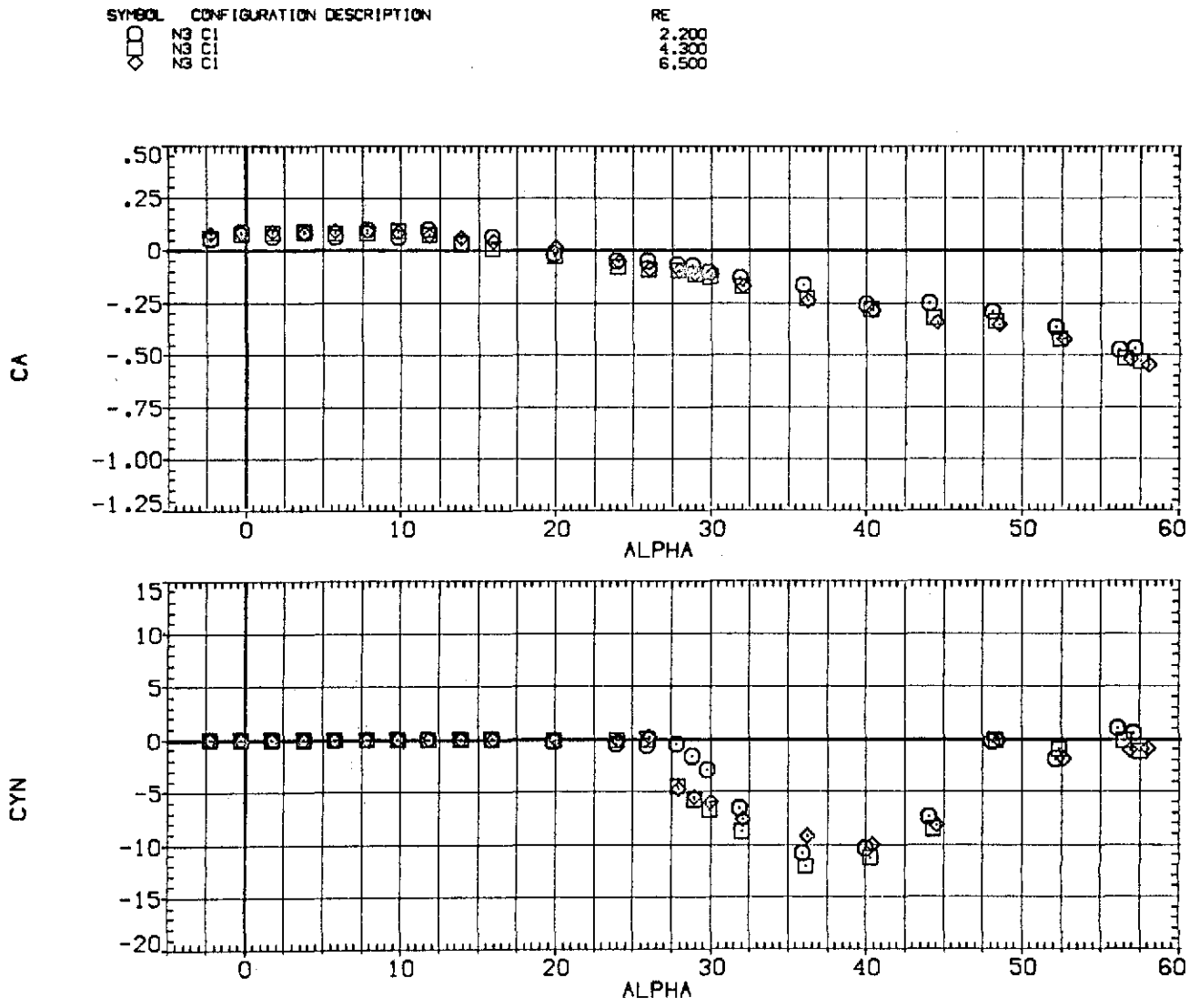

(c) C_A and C_n versus α.

Figure 26.– Concluded.

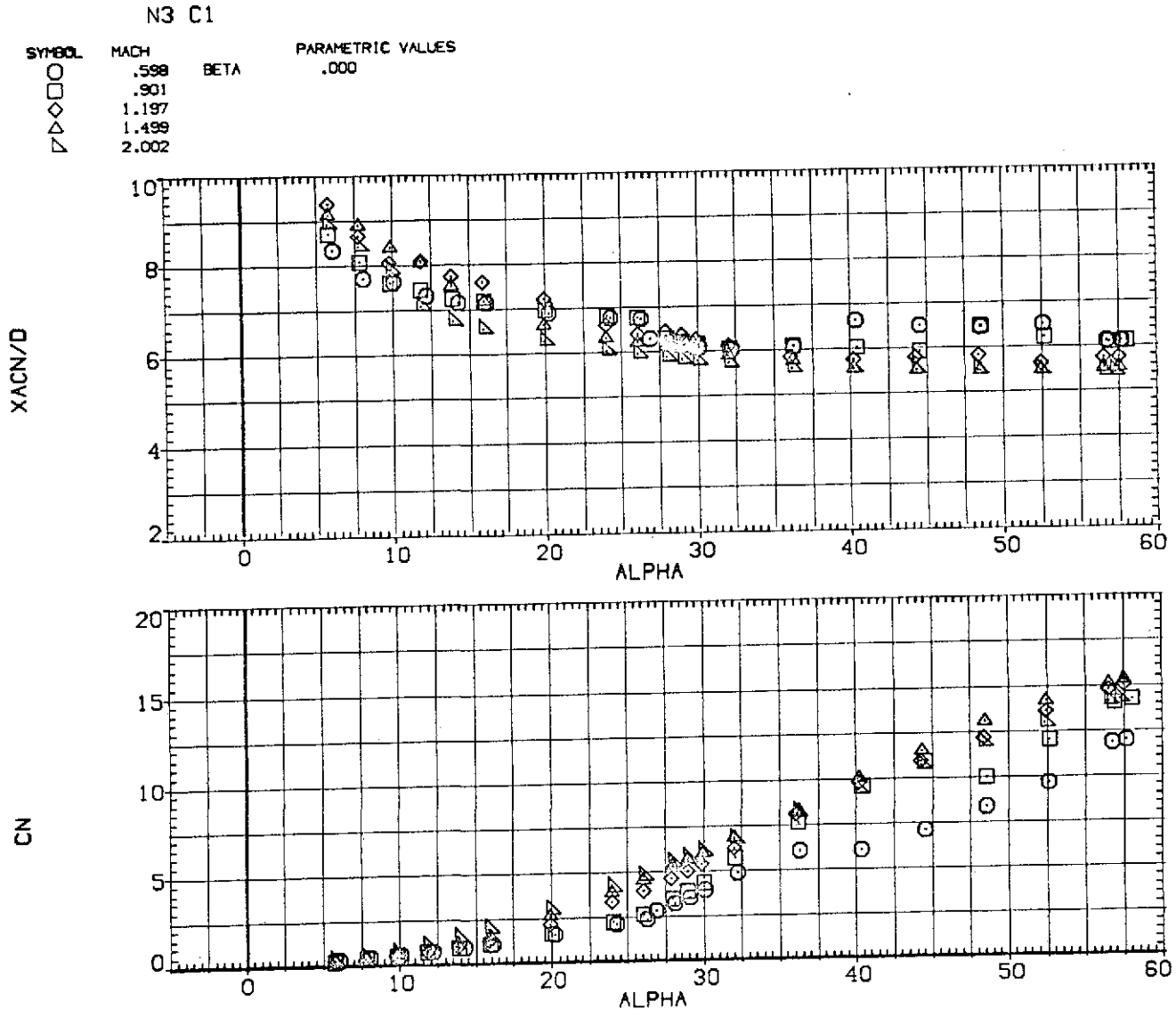

(a) x_{ac_N}/d and C_N versus α.

Figure 27.– Effect of Mach number for N_3C_1.

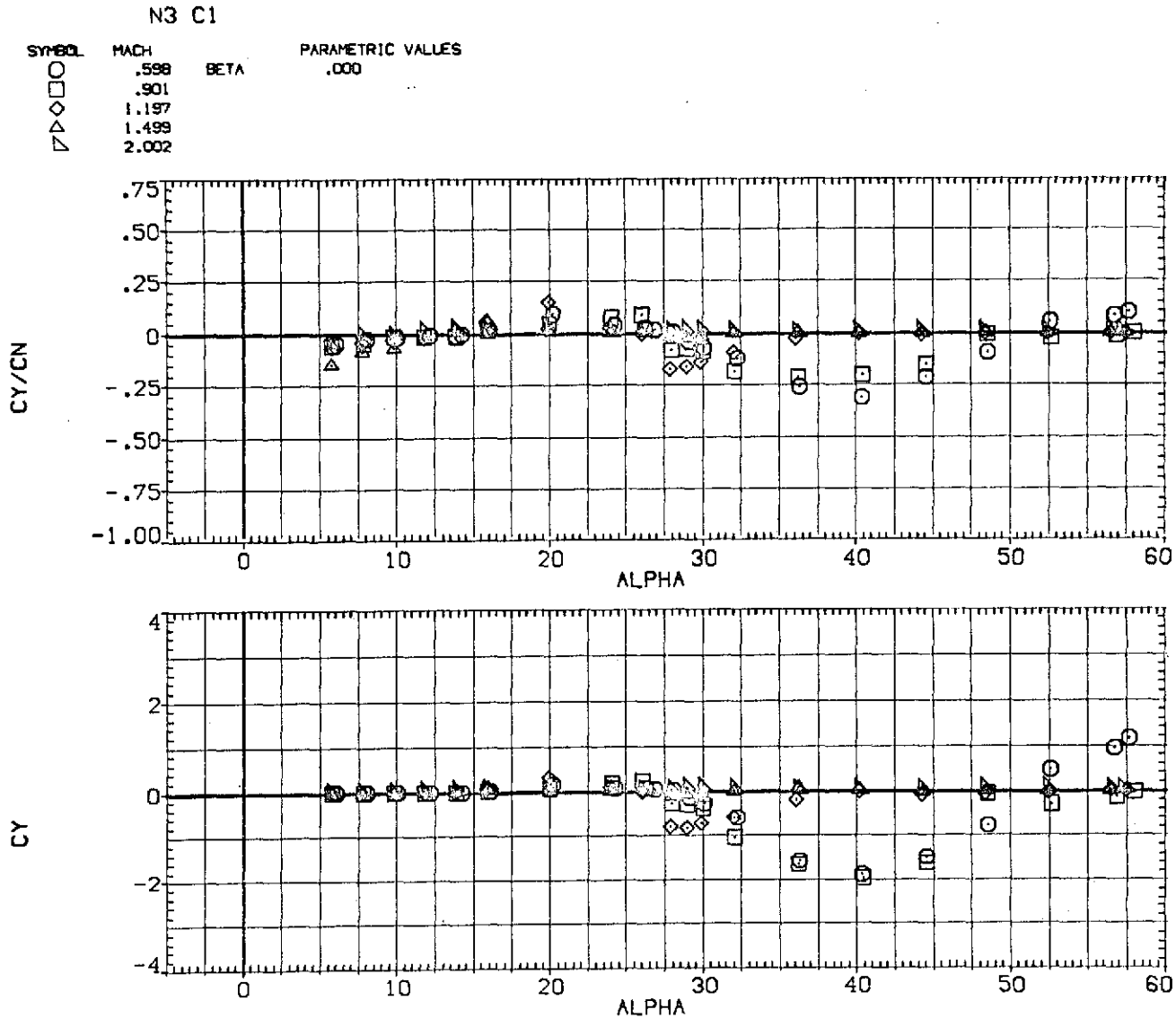

(b) C_Y/C_N and C_Y versus α.

Figure 27.– Continued.

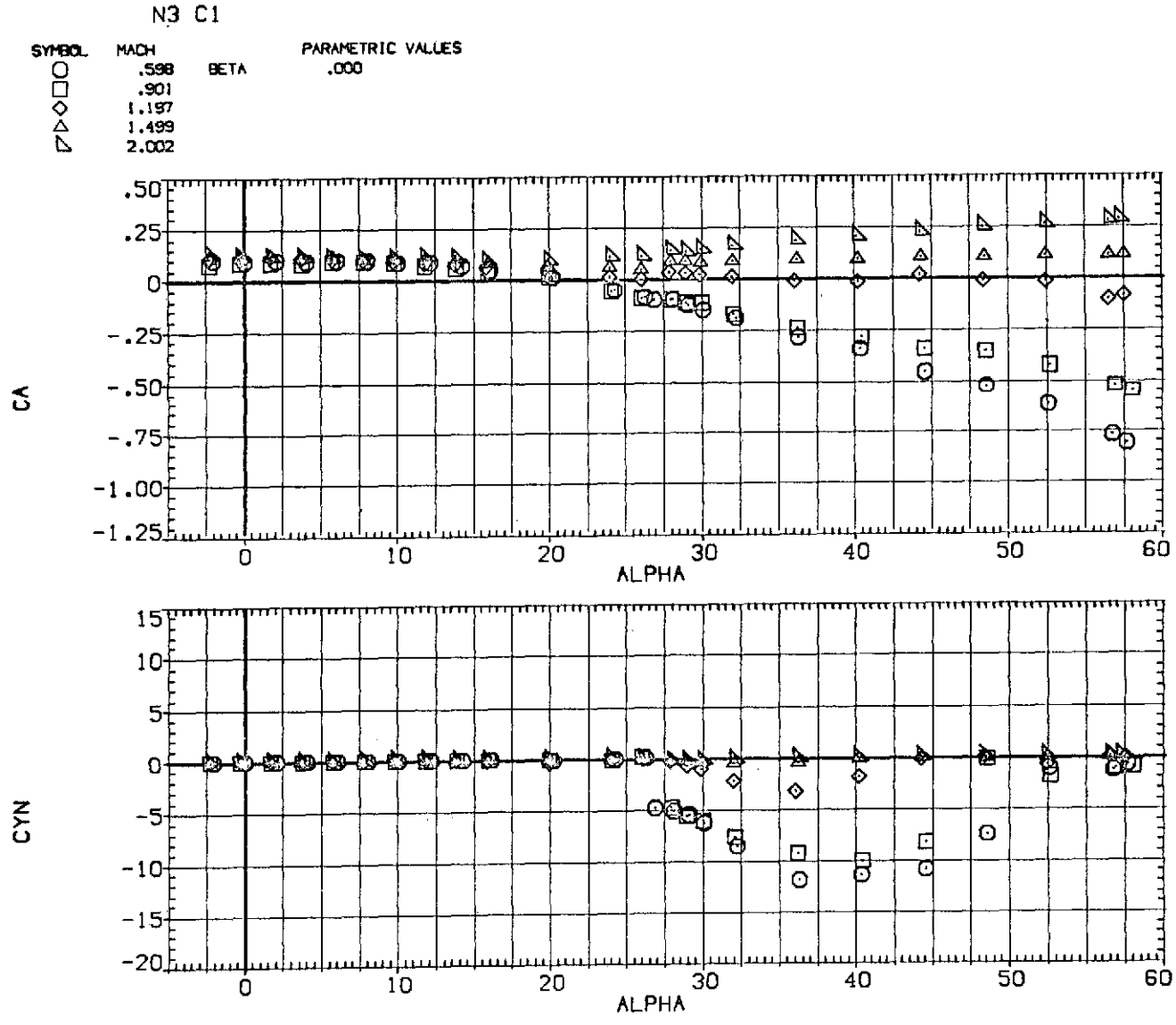

(c) C_A and C_n versus α.

Figure 27.– Concluded.